

The effect of adenylate kinase on the
glycolytic oscillations of *Saccharomyces*
cerevisiae

by

Morne van Wyk



*Thesis presented in partial fulfilment of the requirements for
the degree of Master of Science (Biochemistry) in the Faculty
of Science at Stellenbosch University*

Supervisor: Prof. J.L. Snoep
Co-supervisor: Dr. D.D. van Niekerk,
Dr. T. Kouril

April 2019

Declaration

By submitting this thesis electronically, I declare that the entirety of the work contained therein is my own, original work, that I am the sole author thereof (save to the extent explicitly otherwise stated), that reproduction and publication thereof by Stellenbosch University will not infringe any third party rights and that I have not previously in its entirety or in part submitted it for obtaining any qualification.

Date: 2019/01/15

Copyright © 2019 Stellenbosch University
All rights reserved.

Abstract

The effect of adenylate kinase on the glycolytic oscillations of *Saccharomyces cerevisiae*

M. van Wyk

*Department of Biochemistry,
University of Stellenbosch,
Private Bag X1, Matieland 7602, South Africa.*

Thesis: MSc (Biochemistry)

January 2019

The regulation of phosphofructokinase (PFK) by ATP and AMP is a necessary feature for glycolytic oscillations. The enzyme adenylate kinase (AK) is responsible for the interconversion of $\text{ATP} + \text{AMP} \rightleftharpoons 2 \text{ADP}$, and so influences the regulation of PFK. We present here, both experimentally and through model simulations, that a decrease in AK activity results in an increase in period time of the glycolytic oscillations. We show, for the first time, that AK is a necessary component of these oscillations and an absence of AK activity results in no oscillations. Using an existing model for glycolytic oscillations, we incorporate a mechanistic equation for AK activity with parameters determined from fits to enzyme kinetic data. In the subsequent model simulations we piece apart the individual contributions of ATP and AMP towards these oscillations and find that a reduction in AK activity leads to changes in both ATP and AMP oscillation phase and amplitude. This causes changes in PFK T and R state switching, increasing the period time of the oscillations.

Uittreksel

Die effek van adenylaatkinaſe op die glikolitiese ossillasies van *Saccharomyces cerevisiae*

M. van Wyk

*Departement Biochemie,
Universiteit van Stellenbosch,
Privaatsak X1, Matieland 7602, Suid Afrika.*

Tesis: MSc (Biochemie)

Januarie 2019

Die regulering van fosfofruktokinaſe (PFK) deur ATP en AMP is 'n noodsaaklike kenmerk vir glikolitiese ossillasies. Die ensiem adenylaatkinaſe (AK) is verantwoordelik vir die interkonversie van $ATP + AMP \rightleftharpoons 2 ADP$, en beïnvloed ook die regulering van PFK. Ons bied hier, beide eksperimenteel en deur middel van simulaties, aan dat 'n afname in AK-aktiwiteit 'n toename in die tydperk van die glikolitiese ossillasies tot gevolg het. Ons wys vir die eerste keer dat AK 'n noodsaaklike komponent van hierdie ossillasies is en dat 'n afwesigheid van AK-aktiwiteit geen ossillasies tot gevolg het nie. Deur 'n bestaande model vir glikolitiese ossillasies te gebruik, inkorporeer ons 'n meganistiese vergelyking vir AK-aktiwiteit met parameters wat bepaal word uit pasings tot ensiemkinetiese data. In die daaropvolgende model simulaties onderskei ons die individuele bydraes van ATP en AMP na hierdie ossillasies en vind dat 'n vermindering in AK aktiwiteit lei tot veranderinge in beide ATP- en AMP-ossillasiefase en amplitude. Dit veroorsaak veranderinge in PFK T en R staatskakelaars, wat die tydperkstyd van die ossillasies verhoog.

Acknowledgements

I would like to express my sincere gratitude to the following people and organisations. A special thank you to my supervisors, Prof Snoep, Dr. van Niekerk and Dr. Kuoril whose guidance and expertise was invaluable. A special thank you to Mr. Arends for always keeping the lab running smoothly and to my fellow students at the JJJ lab. Thank you to the University of Stellenbosch and the NRF. And lastly, thank you to my family and friends for their support.

Dedications

This thesis is dedicated to my family.

Contents

Declaration	i
Abstract	ii
Uittreksel	iii
Acknowledgements	iv
Dedications	v
Contents	vi
List of Figures	viii
List of Tables	x
1 General Introduction	1
2 Literature Review	3
2.1 Introduction	3
2.2 Thermodynamics of dissipative structures	3
2.3 Oscillations in nature	8
2.4 Glycolytic oscillations	10
2.4.1 Whole cells	12
2.4.2 Cell extracts	14
2.4.3 Phosphofructokinase as an osillophore	19
2.4.4 Adenylate kinase and its role in glycolytic oscillations . .	21
2.5 Systems biology	22
2.5.1 Deriving rate equations of enzymes	23
2.5.2 The dupreez6 mathematical model of glycolytic oscillations in yeast cell free extracts	25
2.5.3 Epilogue	26
3 Methods	27
3.1 Introduction	27

3.2	Experimental induction of glycolytic oscillations and the inhibition of adenylate kinase	27
3.3	Protein and Enzymatic Assays	29
3.4	Mathematical modelling	30
4	Results	31
4.1	Introduction	31
4.2	Adenylate kinase kinetics	31
4.2.1	Random order Bi-Bi mechanism	33
4.2.2	Iso-random Bi-Bi mechanism	36
4.2.3	Spatio-temporal Bi-Bi mechanism	38
4.2.4	Combination of the Iso-random and spatio-temporal Bi-Bi adenylate kinase mechanisms	41
4.3	Experimental induction and analysis of glycolytic oscillations in yeast cell free extracts	44
4.3.1	Inducing and controlling glycolytic oscillations	45
4.3.2	Inhibiting adenylate kinase during glycolytic oscillations	47
4.4	Model predictions of the effect of adenylate kinase on glycolytic oscillations	48
4.4.1	Analysing the dupreez6 model	48
4.4.2	Including a mechanistic description of adenylate kinase into the dupreez6 model	52
5	General Discussion and Conclusion	55
5.1	Adenylate kinase kinetics	55
5.2	Experimental oscillations and model analysis	57
5.3	Conclusion	65
5.3.1	Epilogue	65
	Appendices	67
A		68
A.1	Adenylate kinase rate equation derivations	68
A.1.1	Iso random bi-bi mechanism	68
A.1.2	Spatio-temporal mechanism	70
A.1.3	Iso-random spatio-temporal combination mechanism	72
	List of References	75

List of Figures

2.1	Thermodynamic reversible process	5
2.2	Example phase diagram	9
2.3	Example oscillations	9
2.4	Extended glycolytic pathway	13
2.5	Phase relationships between between the glycolytic intermediates during glycolytic oscillations	14
2.6	Crossover plot of the glycolytic intermediates	18
2.7	PFK reaction mechanism	20
4.1	PK-LDH assay couple	32
4.2	HK-G6PDH assay couple	32
4.3	Random order bi-bi mechanism of adenylate kinase	34
4.4	Fitted random order bi-bi rate equation	37
	(a) Adenylate kinase rate against the concentration of the substrate ADP	37
	(b) Adenylate kinase rate against the concentration of the substrate AMP	37
	(c) Adenylate kinase rate against concentration of the sub- strate ATP	37
	(d) Adenylate kinase rate against the concentration of the in- hibitor Ap5A	37
4.5	Iso-random ordered bi-bi mechanism of adenylate kinase	38
4.6	Fitted iso random bi-bi rate equation	39
	(a) Adenylate kinase rate against the concentration of the substrate ADP	39
	(b) Adenylate kinase rate against the concentration of the substrate AMP	39
	(c) Adenylate kinase rate against the concentration of the substrate ATP	39
	(d) Adenylate kinase rate against the concentration of the in- hibitor Ap5A	39
4.7	Spatio-temporal order bi-bi mechanism of adenylate kinase	40
4.8	Fitted spatio-temporal rate equation	41

(a)	Adenylate kinase rate against the concentration of the substrate ADP	41
(b)	Adenylate kinase rate against the concentration of the substrate AMP	41
(c)	Adenylate kinase rate against the concentration of the substrate ATP	41
(d)	Adenylate kinase rate against the concentration of the inhibitor Ap5A	41
4.9	Combination mechanism of adenylate kinase	42
4.10	Fitted combination rate equation	43
(a)	Adenylate kinase rate against the concentration of the substrate ADP	43
(b)	Adenylate kinase rate against the concentration of the substrate AMP	43
(c)	Adenylate kinase rate against the concentration of the substrate ATP	43
(d)	Adenylate kinase rate against the concentration of the inhibitor Ap5A	43
4.11	Experimentally induced oscillations using trehalose	46
4.12	Experimentally induced oscillations using glycolgen	47
4.13	Adenylate kinase inhibitor (Ap5A) titration on glycolytic oscillations	49
4.14	Data showing the % increase in period time in relation to the % adenylate kinase activity	50
4.15	%AK and %frequency vs inhibitor Ap5A	51
4.16	Simulation of the dupreez6 model of glycolytic oscillations	52
4.17	Simulation of the vanwyk1 model	54
5.1	vanwyk1 WT model simulation of ATP, AMP and $R/(T+R)$	59
5.2	vanwyk1 inhibited model simulation of ATP, AMP and $R/(T+R)$	60
5.3	Effect of AMP phase shift of T and R state switching	62
5.4	Effect of ATP and AMP amplitude on the T and R state switching of PFK	63
5.5	vanwyk1 model simulation of AMP with WT and inhibited T and R state switching	64
5.6	vanwyk1 model simulation of ATP with WT and inhibited T and R state switching	64

List of Tables

2.1	Table of cellular oscillators	11
4.1	Table of fitted parameters	44
4.2	Fitted parameters statistics	44

Chapter 1

General Introduction

During the breakdown of glucose via glycolysis, under certain conditions the concentrations of glycolytic intermediates repeatedly fluctuate over time. These continuous fluctuations are glycolytic oscillations [1], which are a property of the pathway as a whole, but occur mainly because of the regulation of the phosphofructokinase enzyme (PFK) [2]. PFK is responsible for the conversion of fructose 6-phosphate and ATP to fructose 1,6-bisphosphate and ADP, and its activity is sensitive to the relative ATP/AMP ratio of its environment. At low ATP/AMP ratios PFK is more active, and at high ATP/AMP ratios it is inhibited, and this mechanism is responsible for glycolytic oscillations. During glycolytic oscillations, one complete cycle proceeds as follows: As ATP is utilised in the upper part of glycolysis the ATP/AMP ratio decreases and PFK activity increases which increases the carbon flux through glycolysis. This increased flux through glycolysis leads to the production of ATP and an increase in the ATP/AMP ratio, thereby decreasing PFK activity and decreasing the flux through glycolysis. The cycle then starts again as ATP is utilised in the upper part of glycolysis, decreasing the ATP/AMP ratio and once again increasing the rate of PFK and the flux through glycolysis. The ATP/AMP ratio is important for the control of these oscillations. This presents an interesting question: what are the individual contributions of ATP and AMP toward these glycolytic oscillations? No adequate answers have yet been published on this topic.

To answer this question we need to piece apart the individual contributions of ATP and AMP in glycolytic oscillations. This is difficult due to the adenylate kinase enzyme (AK) which is responsible for the interconversion of 2ADP to ATP and AMP. AK is also the primary source of AMP for glycolysis. AK has fast kinetics and it is generally assumed to be operating close to equilibrium. In addition, ATP, ADP and AMP form a moiety conserved cycle. This means that the sum of the concentrations of ATP, ADP and AMP, within a closed system, remains constant. Because of this moiety conserved cycle as well as AK's fast kinetics, ATP and AMP are always linked, making it difficult to separate the individual contributions of ATP and AMP toward the

glycolytic oscillations. A perturbation in either ATP, ADP or AMP concentration results only in a change in the sum of adenosine nucleotide phosphates as they return to their equilibrium ratios. To get a better understanding of the underlying control of ATP and AMP on glycolytic oscillations we first need to study how AK affects glycolytic oscillations.

The aim of this thesis is to answer the following research questions:

1. How does adenylate kinase affect the glycolytic oscillations of *Saccharomyces cerevisiae*?
2. What are the individual contributions of ATP and AMP towards these glycolytic oscillations?

With the aforementioned research questions, glycolytic oscillations were induced in cell free extracts and the adenylate kinase enzyme subsequently inhibited. The kinetic mechanism of adenylate kinase was derived and included into an already existing model of glycolytic oscillations. The simulations from the model were then compared to the experimental data. The new model was then used to investigate the ability of AMP to activate PFK.

Chapter 2 serves as a comprehensive literature review on the important topics related to this thesis. Chapter 3 lists the various methodologies used during the experiments of this thesis and the results of these experiments are presented in Chapter 4. In Chapter 4, first the results of the kinetic characterisation of AK are presented and subsequently the experimental oscillations, and AK inhibition are shown. This is followed by the model analysis, which makes use of both the AK kinetics results and experimental oscillations results. We also explore in this chapter the contributions of AMP and ATP toward the oscillations. Finally, Chapter 5 is a general discussion of these results, and conclusion.

Chapter 2

Literature Review

2.1 Introduction

This chapter serves as a comprehensive literature review of the relevant topics that concern this study. It begins with a brief introduction to the thermodynamics involved in dynamic systems which are far from equilibrium such as glycolytic oscillations. This serves as a good starting point to understand the importance of these types of non-equilibrium structures which are found throughout nature. The nature of these non-linear non-equilibrium structures forms the basis of all living systems as dissipative structures. A couple of non-equilibrium or oscillatory systems are briefly discussed to illustrate how often these types of systems arise in nature. A large portion of this chapter directly involves glycolytic oscillations and the individual enzymes that are crucial for these oscillations to occur such as phosphofructokinase and adenylate kinase and how these enzymes influence these oscillations. Glycolytic oscillations are often studied in yeast cells, however they occur in many cell types including muscle cells and β -pancreatic cells. These oscillations are also observed in the *extracts* of yeast cells which is what is dealt with in this study. Mathematical models of glycolytic oscillations have been developed to further understand the underlying mechanisms of these oscillations and how they are controlled. A short section discusses the development of these models and elaborates on a model of glycolytic oscillations developed in our research group, the *dupreez6* model which can be found on the JWS online model database (<http://jjj.biochem.sun.ac.za/models/dupreez6/>).

2.2 Thermodynamics of dissipative structures

In nature most thermodynamic processes are irreversible [3], but may be reversed with the addition of energy. For example, the transfer of heat from a warm body to a cold body is irreversible, as is the transfer of mechanical energy to heat by the force of friction as one body slides over another. However,

we can consider an example where reversibility is possible. Consider a net flow of particles from one compartment to an adjacent one over a semi-permeable membrane Fig. 2.1. This net flow can be reversed through some change in one or both of the compartments e.g. pressure change, temperature change, concentration change etc. Even in the case of a net movement of particles from one compartment to the adjacent one, individual particles still move in both directions, indicating a constant micro-reversibility. It is the net thermodynamic processes, under a specific set of conditions, that we consider to be irreversible. In the scope of thermodynamics, entropy (S) is a classic example of irreversibility. The entropy of a closed system is always increasing and will continue to increase until it reaches a maximum. At this point of maximum entropy, the change in entropy over time reaches a minimum, and at this minimum the system reaches a point known as thermodynamic equilibrium. So, at thermodynamic equilibrium:

$$\frac{dS}{dt} \approx 0$$

Thermodynamic equilibrium can also be described in terms of Helmholtz's free energy which extends to systems which can transfer energy, but not matter, with the outside world [4]. The equation of Helmholtz's free energy is as follows:

$$F = E - TS$$

where E is the internal energy of the system and T the absolute temperature of the system. The Gibbs free energy, which is more relevant to biological systems, describes a similar energy distribution to that of Helmholtz's. The Gibbs free energy equation is:

$$G = H - TS$$

Where H is the enthalpy of the system which is equal to the internal energy plus the product of its volume and pressure. These relations describe the distribution of free energy within a system. At equilibrium, the entropy is maximised and so the free energy (F and G) reaches a minimum. However, by decreasing the temperature of the system the internal energy (E) or enthalpy (H) would become the dominant contributing factor to the free energy and so more complex structures, which require more energy, would be able to exist. Assuming that the internal energy levels are equally distributed throughout the system, it is possible for complex, low entropy structures such as crystals to spontaneously exist, given that T is sufficiently low. However, for biological structures such as proteins, this seems more unlikely due to the energy requirements and sizes of the molecules. As an example, there are 20 different amino acids so for a protein chain of 100 amino acids long, there exists approximately $20^{100} \approx 10^{130}$ different ways in which the amino acids could

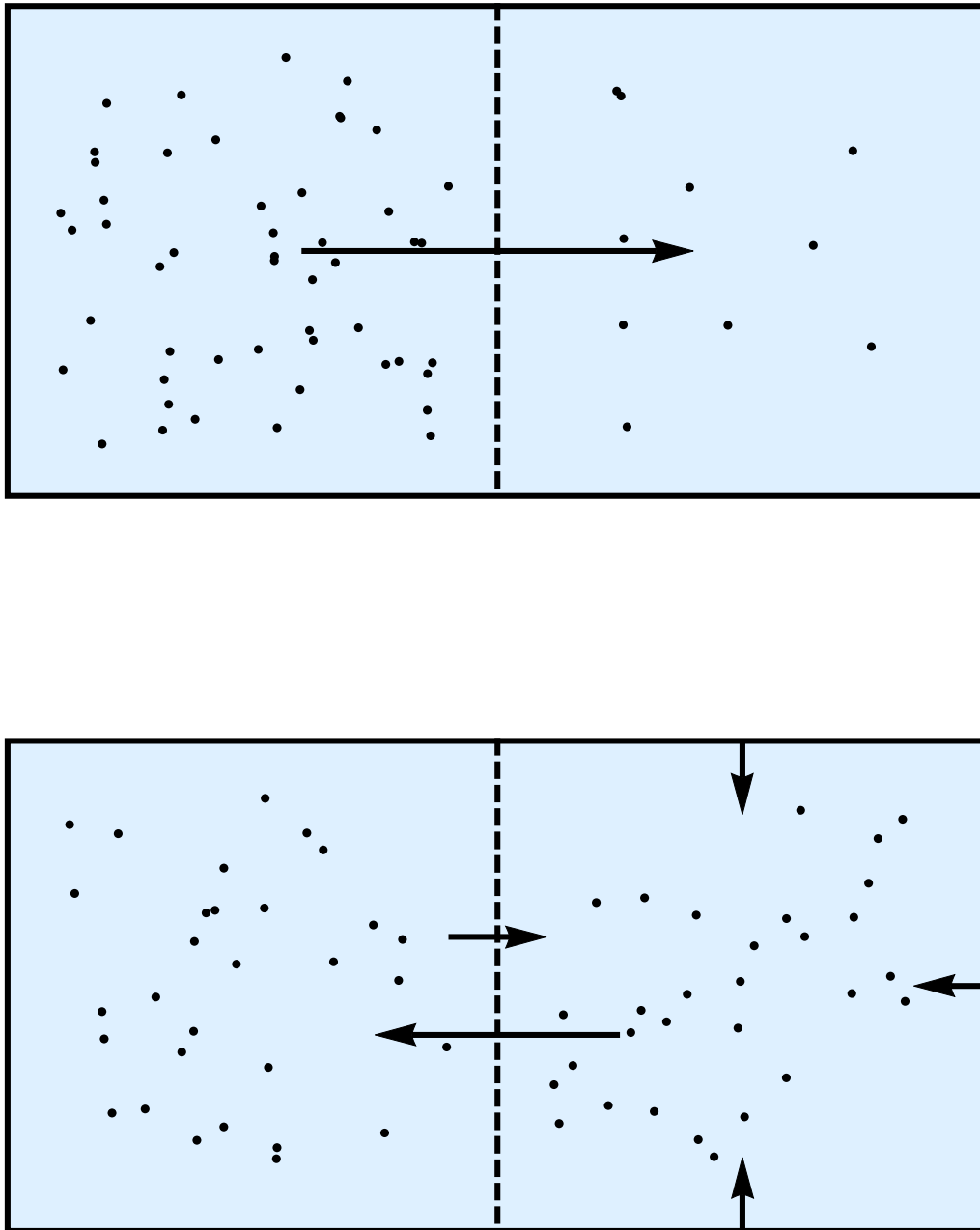


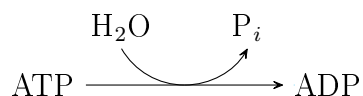
Figure 2.1: Thermodynamic reversible processes. In the top Figure there is a net flow of particles from the left chamber to the right through a semi-permeable membrane. Eventually the net movement of particles across the membrane reaches zero as the environment reaches equilibrium. In the bottom Figure, by increasing the pressure in the right chamber the particles are forced to flow from right to left, reversing the spontaneous flow of particles as shown in the top Figure. However, there is also a flow of particles from left to right as the concentration gradient increases. Eventually the system will reach a steady state which is similar to the top Figure.

be arranged, of which only a certain configuration will yield a viable working protein [4]. Even if the protein in question was subject to a series of random mutations in the form of structural changes, if one mutation takes place approximately every 10^{-8} s, then $\approx 10^{122}$ s would be necessary to "manufacture" this desired protein. The earth itself is only 10^{17} s old, this scenario becomes increasingly improbable. Given the energy requirements for a such a system, these biological systems, or living systems, cannot be equilibrium structures. Instead, these are non-equilibrium structures that operate away (sometimes far away) from equilibrium under the laws of irreversible thermodynamics in a constant state of entropy production. In concordance with the conservation of energy, with the continuous uptake of energy from the environment, the biological system can remain ordered, while the entropy of the system plus the environment increases.

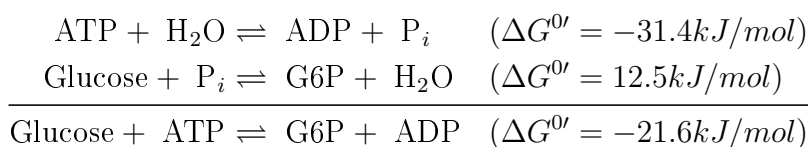
At (and near) thermodynamic equilibrium, the laws of nature can be well explained using linear mathematical relations (linear equations), but these relations fall apart when we move away from thermodynamic equilibrium [4]. Non-equilibrium is naturally associated with gradients such as temperature gradients, potential differences, osmotic gradients etc. and as these gradients become increasingly larger there is a deviation between what is experimentally observed and classical linear thermodynamics. An example that is often used is that of a fluid between two plates that are kept at different temperatures [3]. This causes a temperature gradient which causes the liquid to move from the hot plate to the cold plate through convection and the system eventually reaches a steady state. But the system does not reach an equilibrium as the plates remain at a constant temperature so there is a constant supply of energy to the system. Under the scope of linear thermodynamics the system reaches an homogeneous state of minimum entropy production known as a steady state which is different from an equilibrium state. However, if the temperature difference between the two plates is increased, experimentally we observe what seems to be chaotic behaviour as convection currents start to swirl and cycle around within the system. But what is actually being observed is the microscopic organisation of the liquid into cycles of heating and cooling, a type of steady state that is not predictable using linear thermodynamics. Linearised thermodynamics hides these instances of chaos and singularities. Much like the chaotic convection currents of the liquid, a biological system is seemingly chaotic, but is actually very well organised. Biological systems have to be treated as being in this non-linear thermodynamic range where they act as dissipative structures which maintain order through a constant exchange of energy and/or matter with the outside world. These systems dissipate entropy and retain order within themselves.

The amount of energy needed for, or released by a chemical reaction, can be determined by calculating the difference between the Gibbs free energy of the substrate and product at a constant temperature and pressure, $\Delta G^{0'}$. Generally a living system ingests matter with a higher Gibbs energy than the

matter it excretes into its environment ($\Delta G^{0'} < 0$). The Gibbs energy contains both the enthalpy and entropy of a structure. The energy difference between the matter ingested and excreted is needed to keep the biological system ordered (decrease entropy) and is also dissipated into the environment through heat. The way that a living system uses this energy to maintain order within itself is by means of coupled reactions which transports the energy to where it is required. There are two kinds of chemical processes that occur within a living cell: exergonic (spontaneous, energetically favoured, $\Delta G^{0'} < 0$) and endergonic (non-spontaneous, energetically unfavourable, $\Delta G^{0'} > 0$) reactions. Exergonic reactions dissipate energy and result in an increase in entropy while endergonic reactions result in a decrease in entropy. In biological systems exergonic reactions are coupled to endergonic reactions and used to 'drive forward' the endergonic reaction. Biologically the most important coupling reaction is the hydrolysis of ATP:



At biochemical standard conditions the hydrolysis of ATP produces approximately 34.1 kJ/mol ($\Delta G^{0'} = -34.1$ kJ/mol) and is the driving force of many biological reactions. For example, the first reaction of glycolysis involves the incorporation of an inorganic phosphate (orthophosphate) to a glucose molecule to produce glucose 6-phosphate (G6P). This reaction has a large activation energy and is not energetically favoured to proceed in the forward direction ($\Delta G^{0'} = 12.5$ kJ/mol). Instead the exergonic reaction of ATP hydrolysis is coupled to the phosphorylation of glucose in order to drive the reaction forward.



With ATP hydrolysis coupled to the phosphorylation of glucose the net forward reaction becomes energetically favourable ($\Delta G^{0'} < 0$). If ATP hydrolysis were to happen without coupling, the energy would just be dissipated as heat. In the cell these coupled reactions occur in the presence of enzymes and in this case, hexokinase (HK) facilitates the conversion of glucose to G6P. The enzymes bring the various substrates within close proximity of each other, stabilise the reaction intermediates and thereby lower the activation energy of the reaction. Consecutive enzyme catalysed reactions modify chemicals through what is known as a metabolic pathway. Metabolic pathways share common metabolites with each other which couples the metabolic pathways

together. Pathways are further separated and compartmentalised by cellular membranes as certain metabolic processes occur within certain organelles of the same cell which are then coupled by the flow of metabolites through these membranes. Individual cells are then coupled by the same process of metabolite flow through cellular membranes.

At their core these biological systems are a mixture of linear and non-linear chemical reactions coupled through various flows. The flow of particles arises from the movement of molecules over membranes by either passive diffusion, active diffusion, active transport or group translocation, which causes concentration gradients. The existence of a constant gradient is characteristic of a system which is not at equilibrium but instead exists at a steady state. The non-linearity of biological systems allows for the existence of some interesting phenomena as it moves further away from equilibrium, one of which is bifurcations. A bifurcation is when a system undergoes a change in some parameter(s) (the bifurcation parameter(s)) and transitions from one state to a qualitatively different state e.g. from a steady state to an oscillatory one [5]. To exhibit stable oscillatory behaviour the system requires some sort of regulatory structure where the products of a particular reaction affects reactions up/downstream regulating the rates of the reactions. Positive feedback loops, such as autocatalysis, enhance previous reactions which increases the flux through the reaction pathway which could then in turn be regulated by a negative feedback loop which downregulates prior reactions and decreases the flux of the reactions. Positive and negative feedforward loops are also possible but instead of affecting reactions upstream, they regulate reactions further downstream. Once the bifurcation parameter reaches a critical point, the system enters a bifurcation. There are many types of bifurcations, but for this study we will consider the Hopf bifurcation which describes the evolution of a system into or out of a limit cycle. A limit cycle is a stable oscillatory state that, when visualised in a 2-dimensional phase diagram, forms a closed trajectory (Fig. 2.2).

2.3 Oscillations in nature

There are many examples of oscillations in nature e.g. circadian cycle, predator-prey populations, the cell cycle. These cycles extend to the cellular and molecular levels. At the cellular level oscillations are plentiful and occur in various systems of enzyme catalysed reactions, protein synthesis, membrane potential, secretory cells, neural oscillators, muscle oscillators and cell movement, growth and development [6]. Table 2.1 shows examples of the various oscillations found at the cellular level. These cellular oscillations can be organised into two types: 1) membrane oscillators and 2) cytoplasmic oscillators. Membrane oscillations occur in the form of rhythmic changes in permeability and/or potential of the membrane and are usually linked to cytoplasmic oscillations which involve

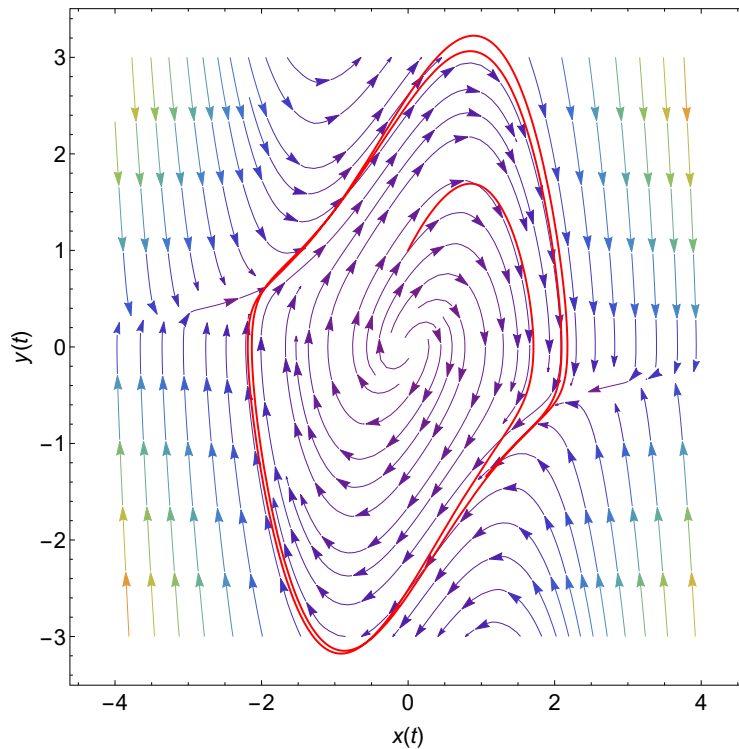


Figure 2.2: Example of a phase diagram which shows the trajectory for any combination of $x(t)$ and $y(t)$. The red line traces the trajectory of a point over time as it evolves into the limit cycle. Figure 2.3 shows the same point, $x(t)$ plotted over time

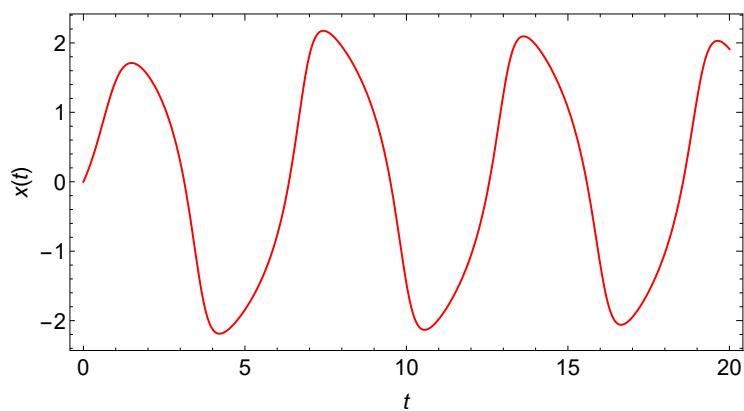
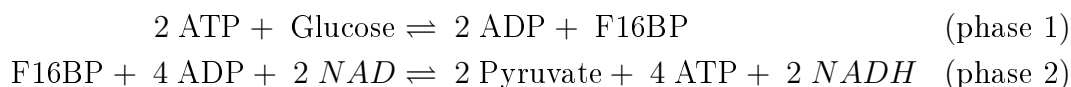


Figure 2.3: This plot shows the same limit cycle from Figure 2.2, but $x(t)$ is now plotted over time. The oscillations in this graph correspond to the red line in Figure 2.2

metabolic processes. For example, oscillations in the membrane potential of the heart cells of guinea pigs was linked to fluctuations in cytosolic NADH concentrations, which is a product of glucose catabolism [7]. These fluctuations in membrane potential could be altered by changes in the amount of glucose available to the cells. The life cycle of *Dictyostelium discoideum* (slime mould) is also very interesting in terms of oscillations and combines both membrane and cytoplasmic oscillations. *D. discoideum* forms fruiting bodies at a certain point in its life cycle where up to about 100,000 cells aggregate together to release spores, after which they return to their normal lives. The amoeba use cAMP to communicate between cells and the release of cAMP causes the cells to aggregate as the separate cells move chemotactically toward the cAMP [8]. Within the cells, adenylate cyclase forms cAMP from ATP which is then transported to the cell membrane and secreted by the cell. The cAMP binds to receptors on the cell membrane which in turn promote the synthesis of adenylate cyclase. This positive feedback loop causes more cAMP to be produced and secreted. As the cells aggregate to form a fruiting body the cAMP travels radially outwards from a central point in waves through the aggregated mass. The autocatalytic nature of the cAMP production is regulated by a reduced receptor sensitivity to cAMP over time and also the degradation of cAMP by phosphodiesterase.

2.4 Glycolytic oscillations

The most well known oscillating system at the cellular level is the glycolytic oscillator. The metabolic pathway of glycolysis (Figure 2.4) breaks down glucose to pyruvate and produces free energy in the form of ATP during this process. Glycolysis can be broken into two phases: 1) a free energy investing phase or 6-carbon phase and 2) a free energy formation phase or 3-carbon phase. In the free energy investment phase, 2 ATPs are consumed to form fructose 1,6-bisphosphate (F16BP), a molecule with a higher free energy than the glucose molecule at the start. In the second phase, one F16BP is converted to 2 pyruvates and 4 ATPs, yielding a net production of 2 ATP. Downstream of glycolysis on a branching pathway, NADH is consumed with pyruvate to form compounds such as ethanol or lactate which maintains the redox balance.



The energy investing phase (phase 1) of glycolysis involves the enzyme phosphofructokinase (PFK) and other ATP utilising enzymes. PFK has an increased activity under low ATP conditions, so the consumption of ATP causes the rate of the pathway to increase which in turn increases the formation of

Table 2.1: A short table of some oscillating phenomena at the cellular level [6].

Type of oscillations	Example	Period time
Enzyme catalysed oscillators	Oscillations in the concentrations of the glycolytic intermediates of <i>Saccharomyces cerevisiae</i> whole cells or extracts	30 s - 10 min
Protein synthesis oscillations	Periodic synthesis of beta-galactosidase by <i>E. coli</i>	50 min
Membrane potential oscillations	Periodic hyperpolarisation of mammalian macrophages	1 s
neural oscillators	Oscillatory release of neurotransmitter at neuromuscular junctions of frogs	2 - 14 s
	Periodic neural firing to flight motor of <i>c. vomitoria</i> (Blowfly)	0,1 s
muscle oscillators	Oscillations in intracellular levels of cAMP in ventricular muscle of frogs	1 s
Oscillations of cell movement,	Periodic synthesis of cAMP by <i>D. discoideum</i>	10 min
	Periodic movement of <i>D. discoideum</i>	5 - 10 min
	Periodic spore release by <i>Penicillium diversum</i>	24 h
Miscellaneous	Periodic flashing of fireflies	0,5 - 1 s

F16BP. This is counter-intuitive and unusual as most of the reactions in glycolysis are more 'homoeostatic' where a decrease in substrate causes a decrease in the reaction rate. The F16BP and ADP from phase 1 is fed into the second phase of glycolysis which produces ATP and in turn inhibits the first phase of glycolysis, decreasing the rate of production of F16BP and reducing the rate of ATP production from phase 2. When the rate of ATP consumption is greater than ATP production, phase 1 is then 'reactivated' and the cycle repeats itself. It is apparent that fundamentally this oscillatory behaviour arises from alternating between the two phases of glycolysis. Unlike conventional linear reactions where compound A is converted to product B and so on, the non-linearity of the reactions within glycolysis, such as the PFK reaction, allow for feedback and feed-forward loops which contribute to the oscillatory behaviour.

When a bifurcation parameter, such as glucose influx in cell free extracts, reaches a critical point, the concentrations of the metabolites in glycolysis begin to oscillate in concentration (Figure 2.5). This phenomenon is most well studied within the yeast *Saccharomyces sp.* although, glycolytic oscillations have been shown to occur in various cell types including muscle cells and

pancreatic cells [9]. The oscillations are made up of alternating phases of increased and decreased rates through the glycolysis. During periods of high glycolytic flux the cell will experience an increase in NADH concentration and decreased levels of NAD. The rate of glucose influx is one of these bifurcation parameters which was previously described in §2.2 and has been noted to have a relatively large control on the frequency of the oscillations [10]. When the glucose influx rate is plotted as the bifurcation parameter there exists two supercritical Hopf bifurcations which lie either side of a limit cycle [11]. Only a small range of influx rates will allow for glycolytic oscillations to occur as any rate below or above the first and second bifurcation point does not meet the kinetic requirements for oscillations. This is however not seen in whole cells as the influx rate is biologically limited by import proteins.

2.4.1 Whole cells

For whole cells, the rate of glucose transport into the cell is determined by the capacity of the hexose transporter proteins in the cell membrane and the saturation of these transporter proteins places the glucose influx rate between the two supercritical Hopf bifurcations and in the range of a limit cycle. While glucose elicits the strongest response for oscillations, oscillations also occur using other carbon sources such as fructose and mannose [13]. Yeast cells in solution have been shown to couple their glycolytic activity through external acetaldehyde [14], a product of pyruvate metabolism. Acetaldehyde is membrane permeable and when added to media induces phase shifts in an already oscillating culture. The acetaldehyde in the media was also shown to oscillate along with the glycolytic oscillations however there has to be a balance between the rate at which acetaldehyde is excreted and absorbed, and also the rate at which it disappears from the environment. Cyanide is widely used in yeast whole cell oscillation experiments to trap extracellular acetaldehyde. Acetaldehyde influences glycolysis by affecting alcohol dehydrogenase (ADH) which converts ethanol and NAD to acetaldehyde and NADH. This directly influences the NADH/NAD ratio which affects the upstream reaction of glyceraldehyde 3-phosphate dehydrogenase (GAPDH) and this influences subsequent ATP production by phosphoglycerate kinase (PGK). An experiment where two batches of suspended yeast cells, which were oscillating 180° out of phase, were added together demonstrated that initially the macroscopic oscillations disappeared, but returned after a given amount of time demonstrating the cellular coupling [15]. Single yeast cells have been found to continue to oscillate even once the macroscopic oscillations have disappeared, further demonstrating that the macroscopic oscillations are a consequence of the cells ability to couple their metabolisms. Glycolytic oscillations in whole yeast cells in a continuous stirred tank reactor could be sustained for up to 14 hours with a frequency of approximately 1 minute when they were supplied with a constant concentration of glucose and cyanide [16].

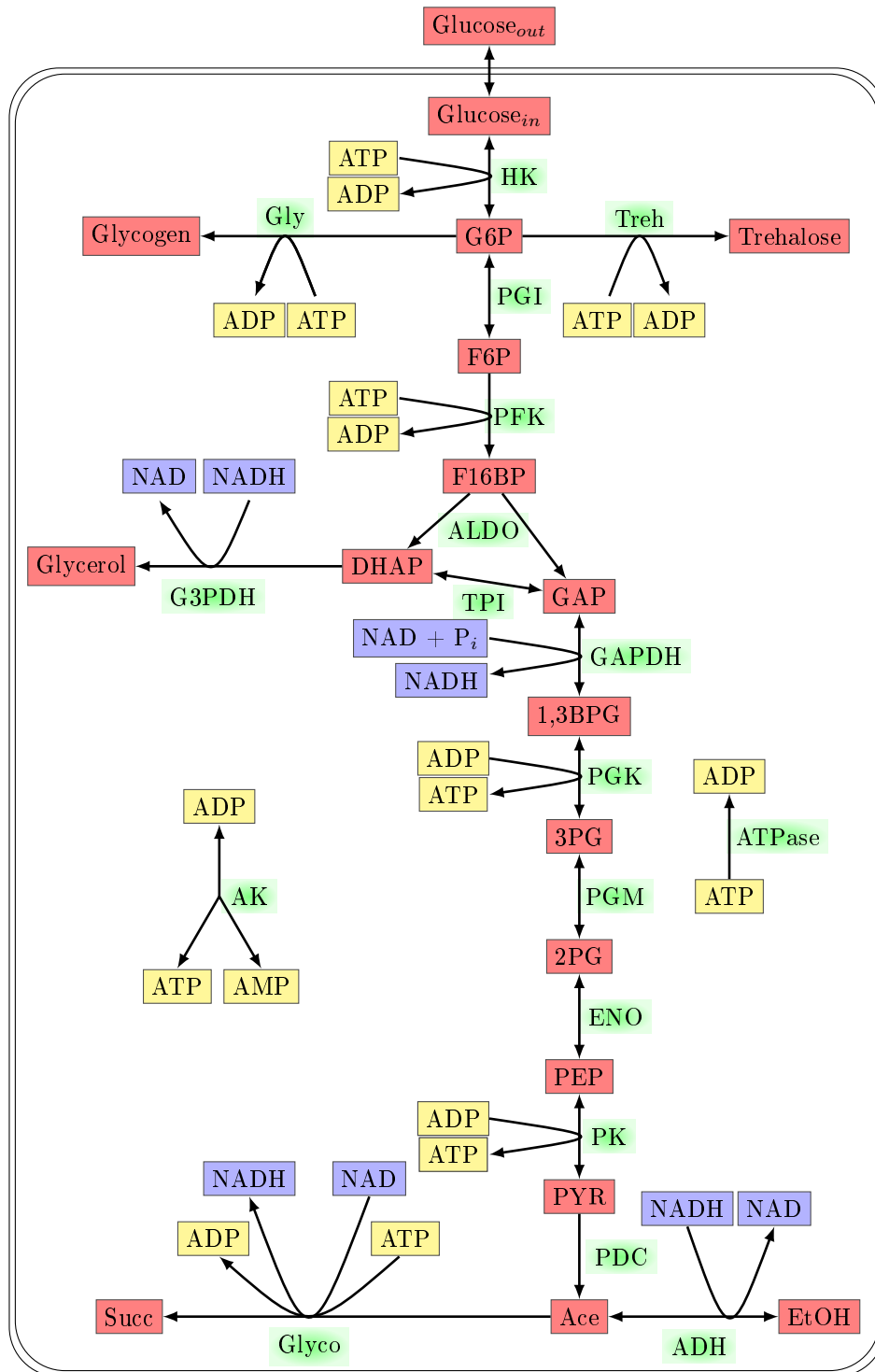


Figure 2.4: The glycolytic pathway of yeast adapted from the dupreez6 model [11; 12]. This pathway shows additional branches of glycogen, trehalose and glycerol synthesis as well as pyruvate metabolism to ethanol (EtOH) and succinic acid (Succ). For more information see §2.5.2

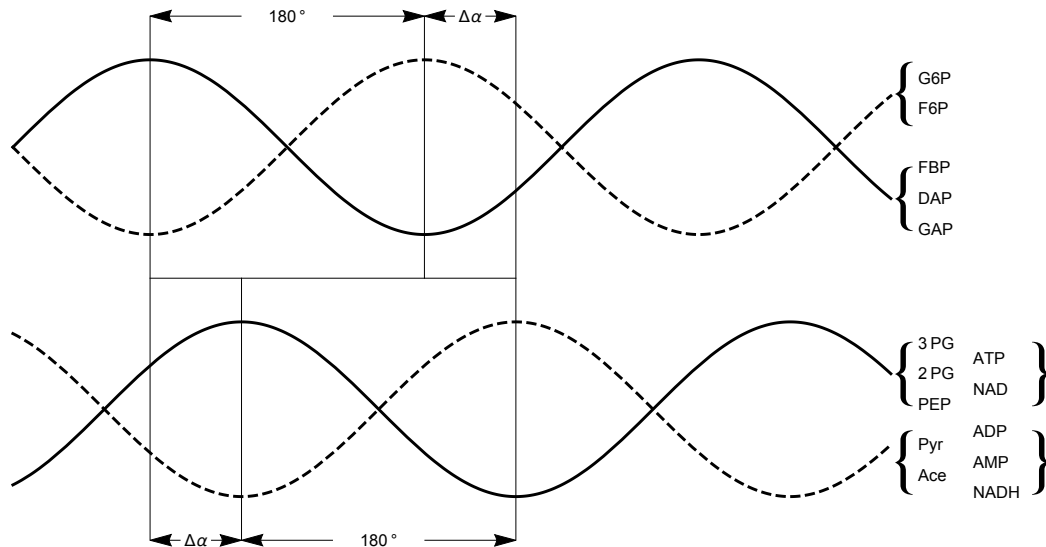


Figure 2.5: Phase relationships between between the glycolytic intermediates during glycolytic oscillations [1]. The respective concentrations of the intermediates have been normalised so that their relationships with each other is easy to see.

Speculation on the evolutionary importance of the ability of single celled organisms to couple together is still ongoing. The cyclic nature of glycolysis acts as a metabolic 'clock' and couples various other metabolic processes together. This may be of importance in the coupling of adenosine phosphate ratios (ATP/ADP) to the periodic secretion of insulin by β -pancreatic cells. Insulin is secreted from the beta-pancreatic cells in a pulsatile manner and the blood levels of insulin oscillate with a similar frequency to that of glycolytic oscillations [9]. It is thought that the oscillations in ATP concentration caused by glycolytic oscillations in the beta-pancreatic cells inhibit ATP-dependant K^+ ion channels which causes hyper-polarisation of the cell membrane [17]. A subsequent influx of Ca^{2+} ions causes vesicles within the cell to move to the membrane and release insulin. The glycolytic oscillations cause oscillations in the polarisation of the cell membrane which is correlated to insulin secretion. Mathematical models of pulsatile insulin secretion have been successful in their use of glycolytic oscillations as the mechanism for controlling for the ATP concentration [18; 19].

2.4.2 Cell extracts

In 1964, Chance *et al.* reported on the occurrence of glycolytic oscillations in yeast cell-free extracts [20]. Just like whole cell oscillations, a constant supply of glucose causes the glycolytic metabolites to fluctuate periodically. The glycolytic oscillations in cell free extracts are predominantly relaxation type

oscillations which are characteristic of short quick changes in a variable followed by a slow change of the same variable in the opposite direction over time [21]. They do however, also exhibit sinusoidal wave patterns as well chaotic behaviour [13]. The frequency of glycolytic oscillations in cell free extracts are dependent on the influx rate of glucose to the system, with a higher rate of glucose influx leading to an increase in the frequency of the oscillations [1]. The frequency of the oscillations was also shown to be temperature dependent. By increasing or decreasing the temperature, the frequency of the oscillations increased and decreased respectively with long period oscillations observed at 0°C [20]. This is intuitive as the oscillations are a characteristic of the pathway which is a collection of the individual enzymatic reactions which are by nature temperature sensitive [22]. An increase in temperature would cause an increase in the activities of most of the enzymes which would cause an increase in the overall frequency of the oscillations. As mentioned in §2.3, a limit cycle exists between two supercritical Hopf bifurcations when glucose influx is plotted as the bifurcation parameter. Unlike in whole cells where the metabolite influx is regulated by transport proteins, there is no such system in cell free extracts to regulate the influx of metabolites such as glucose. The simple addition of glucose to the extract puts the glucose influx parameter well above the aforementioned bifurcation points and does not induce an oscillatory state. Instead glucose must be injected into the system in a controlled manner by the use of trehalose or maltose which can be broken down enzymatically to produce glucose. The enzymatic rate at which these molecules are metabolised to glucose becomes the 'glucose injection rate' or 'glucose influx rate'. It has been reported that the injection of various carbon sources such as fructose, mannose, fructose 6-phosphate as well as glucose 6-phosphate, but not fructose 1,6-bisphosphate, induces an oscillatory state which highlights the importance of phosphofructokinase (PFK) as glycolytic oscillations can only be stimulated using metabolites upstream of PFK [23].

Although Sel'kov shows these oscillations can occur stoichiometrically through feedback and feed-forward loops within the pathway [24], Goldbeter proposes that the origin of these oscillations is the kinetic regulation of PFK for which he uses a Monod-Wyman-Changeux type of mechanism [2]. These solutions are both distinct, but are similar in that they both use PFK as an essential part of their solutions. The non-linearity of PFK, as discussed in §2.2 is an essential element in the oscillatory system. PFK converts fructose 6-phosphate (F6P) to fructose 1,6-bisphosphate (F16BP) with the transfer of a phosphate from ATP. The PFK reaction forms part of the first phase of glycolysis where ATP is consumed and ADP is produced, however, PFK is inhibited by its substrate ATP. So a reduction in the ATP/ADP ratio causes an increase in the rate of the PFK reaction. At a low ATP/ADP ratio the flux through PFK will be large and F16BP will accumulate causing the flux through the second phase of glycolysis to increase and subsequently ATP is produced at a faster rate. The opposite is true for the reverse situation where the ATP/ADP

ratio is high and PFK is inhibited, and a large amount of fructose 6-phosphate accumulates as F16BP is consumed in lower glycolysis. As a result of this 'on' and 'off' switching of PFK the glycolytic metabolites upstream of PFK tend to oscillate at a 180° phase shift to the metabolites downstream of PFK. This is demonstrated in Figure 2.6 by plotting the phase relationships of adjacent glycolytic intermediates [1]. Note that Figure 2.6 shows GAPDH and PGK as part of a reaction couple. GAPDH and PGK are often assumed to be coupled together as the PGK reaction is thought to pull the GAPDH reaction forward by maintaining a low concentration of 1,3BPG [25]. Although the PGK enzyme is energetically favoured to produce 3-phosphoglycerate (3PG) in the forward direction, it is a reversible enzyme reaction that forms part of gluconeogenesis, the formation of glucose from pyruvate. This is different to the reversibility of an enzyme such as PFK which, while it is theoretically reversible, it is near impossible to reach the chemical conditions for the reverse reaction to occur. GAPDH catalyses the conversion of glyceraldehyde 3-phosphate (GAP) to glycerate 1,3-bisphosphate (1,3BPG) by incorporating an inorganic phosphate and the reduction of NAD to NADH. The crossover plot (Figure 2.6) reveals that there are phase shifts between the substrates and products of not only PFK, but also around the glyceraldehyde 3-phosphate dehydrogenase (GAPDH) and phosphoglycerate kinase (PGK) couple and pyruvate kinase (PK), all of which are reactions that include ATP as either a product or substrate. There is a variable phase shift $\Delta\alpha$ at the enzyme couple GAPDH-PGK which is determined by the experimental conditions of the system, and PK introduces a 180° phase shift between phosphoenolpyruvate (PEP) and pyruvate. This $\Delta\alpha$ phase shift is a result of not only the energy level of the system (ATP/ADP), but also the oxidation state (NAD/NADH). PK displays a much larger influence on the phase shift than GAPDH-PGK and this is most likely because PK, like PFK, is allosterically activated by F16BP and like most kinases is sensitive to the ATP/ADP ratio. This makes PK inherently linked to PFK as its activated by its products, F16BP and ADP and inhibited by its substrate ATP, so the activity of PFK not only affects every kinase due to its involvement with ATP, but also further activates PK because of F16BP and ADP. The three control points in Figure 2.6, as highlighted by Hess and Boiteux, show a clear responsibility of the ATP system to propagate the wave of the oscillations down the chain of glycolysis. NADH/NAD also play a role in communication down the chain of glycolysis as acetaldehyde is able to induce phase shifts in the oscillations in whole cells which is likely due to the GAPDH-PGK enzymes as described in §2.3. With regards to the cofactors of glycolysis, ATP and NAD oscillate with a phase shift of 180° with respect to ADP, AMP and NADH [13].

The Harden-Young effect has been observed in yeast cell free extracts when fermenting carbon sources such as glucose, and is characterised by an accumulation of F16BP [26]. This is because of an insufficient ATPase activity and limiting free inorganic phosphate levels. For every molecule of hexose

fermented there must be two inorganic phosphate molecules consumed. This occurs at the enzyme GAPDH where NAD is reduced to NADH as GAP is converted to 1,3BPG. ATPase is often coupled to membrane transporter proteins such as proton pumps and is responsible for hydrolysing ATP to ADP and an inorganic phosphate. ATPase uses the energy from ATP hydrolysis to then export protons from the cytosol hence keeping the internal pH constant. However, as ATPase is primarily membrane bound, the levels of ATPase are usually low in cell free extracts. Under inorganic phosphate limiting situations the flux through the bottom half of glycolysis is slowed down, unless ATPase is able to provide sufficient amounts of inorganic phosphates from the hydrolysis of ATP. The Harden-Young effect is primarily a result of inorganic phosphates being the limiting reagent for GAPDH and due to low ATPase levels in cell free extracts, alcoholic fermentation gets stuck upstream of GAP and metabolites such as F16BP and hexose phosphates start to accumulate. A similar phenotype is found in whole cells where there is an accumulation of F16BP and other phosphorylated hexoses and pentoses, however this is instead due to a mutation that gives the cell a decreased trehalase 6-phosphate synthase activity (Δtps mutation), the *tps1* phenotype [27]. It was found that the *tps1* phenotype shows a very fast decrease in inorganic phosphate with the addition of glucose as well as acidification of the cytosol. It is unclear how, but the *tps1* phenotype has a decreased ATPase activity as well which explains why there is both an insufficient level of inorganic phosphates as well as an acidification of the cytosol. The Δtps mutation leads to a high glucose influx rate without a concomitant increase in ATPase activity and this imbalance of the enzymes gives rise to the *tps1* phenotype. Much like the Harden-Young effect, glycolysis gets stuck upstream of GAP and there is a large accumulation of F16BP.

2.4.2.1 Inducing glycolytic oscillations

A necessary component of glycolytic oscillations is the rate at which glucose is supplied to the system. With the glucose influx as the bifurcation parameter a limit cycle exists between two supercritical Hopf bifurcations for a narrow range of glucose influx rates for cell free extracts. In whole cells there is a separation between the external environment and the internal environment of the cell by a cellular membrane and the hexose influx rate is controlled by the hexose transporter proteins on the membrane. Hence, even at saturating levels of glucose in solution, the influx rate does not pass the second bifurcation point due to the natural capacity of the transporter proteins. For cell extracts there is no cell membrane and no transporter proteins to regulate the hexose influx rate. Any metabolite added to the solution is immediately a part of the cellular contents, so all the glucose that is supplied to the extract is almost immediately consumed by hexokinase, the first enzyme of glycolysis. Oscillations are not observed if the glucose influx is too fast. The glucose influx rate is to the right of the second supercritical Hopf bifurcation, and the systems

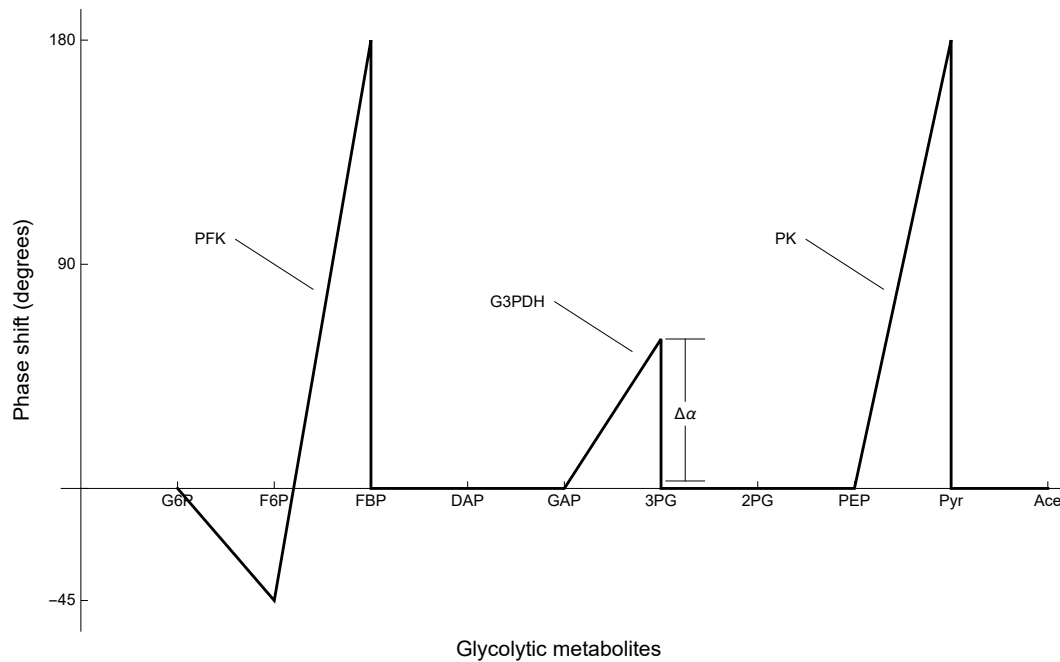


Figure 2.6: Crossover plot of the glycolytic intermediates phase relationship between adjacent intermediates [1].

finds a steady state or may exhibit the *tps1* phenotype. What is required is a mechanism to supply hexose to the cell extract in a controlled manner at a rate fast enough to allow for glycolytic oscillations to occur. A way to circumvent the direct addition of hexose such as glucose, is to add a molecule such as trehalose which can be broken down to glucose when added to the extract. Trehalose is comprised of two glucose molecules joined by an $\alpha(1\rightarrow1)$ bond which can be broken down by the enzyme trehalase which is expressed by most *Saccharomyces sp.*. The rate at which trehalase breaks down trehalose to glucose then determines the glucose influx rate. This rate can be reduced by mechanically injecting trehalose at a rate slower than it is broken down or the influx of glucose can be increased by adding extracellular trehalase to the extract, the latter being easier to accomplish than the former. There is another approach which works on the same principle but uses glycogen instead of trehalase [28]. Glycogen is a glucose polysaccharide with chains of about 8-12 glucose molecules joined by $\alpha(1\rightarrow4)$ bonds with intermittent branching chains joined by $\alpha(1\rightarrow6)$ bonds. Before a glucose monomer from glycogen can enter glycolysis, *Saccharomyces sp.* breaks down glycogen in a two step process using two enzymes, namely phosphorylase-b (Phos-b) and phosphoglucomutase (PGMu). Phos-b cleaves a glucose monomer from glycogen and forms glucose 1-phosphate (G1P) using free inorganic phosphate. G1P is then converted to G6P by the PGMu enzyme, at which point it can enter glycolysis. However, Phos-b is only able to cleave the $\alpha(1\rightarrow4)$ bonds in glycogen and not the $\alpha(1\rightarrow6)$ branching bonds, so in order to break glycogen down completely,

a debranching enzyme is essential. When there are about 4 glucose residues left on a specific branch, the glucose debranching enzyme (GDE) transfers 3 of the 4 glucose residues to another branch at which point the $\alpha(1\rightarrow6)$ bond can be reached and broken [25]. In yeast this transfer of glucose residues and cleaving of the $\alpha(1\rightarrow6)$ are both done by GDEs which has both oligo($\alpha1,4\rightarrow\alpha1,4$) glucotransferase and $\alpha(1\rightarrow6)$ glucosidase activity [29]. While trehalase is the most common way to elicit oscillations in a yeast cell free extract, glycogen has been used [28]. Theoretically it should be possible to induce oscillations using any form of compound that can be broken down at the correct rate to a hexose or hexose-phosphate, without harmful byproducts, that can be metabolised by glycolysis.

2.4.3 Phosphofructokinase as an oscillophore

Glycolytic oscillations are a product of the entire glycolytic pathway and the interactions between the enzymes within the pathway. In this study the term oscillophore does not imply control over the oscillatory characteristics such as frequency and amplitude as these controls are shared among the various reactions of glycolysis [11]. Instead the notion of an oscillophore implies a central reaction or set of reactions that leads to the emergence of oscillations [30]. Sel'kov and Goldbeter showed that a simplified model of PFK was able to demonstrate self-oscillations [24; 2]. PFK has thus been identified as integral component in the emergence of glycolytic oscillations and can be considered the oscillophore for glycolytic oscillations. A good display for the necessity of PFK for glycolytic oscillations is that only metabolites upstream of PFK are able to induce glycolytic oscillations indicating that if PFK is bypassed, oscillations do not occur [13]. This shows that PFK plays a central role in initiating and maintaining glycolytic oscillations. The reason for PFK's central role in the propagation of glycolytic oscillations is due to the autocatalytic nature of the enzyme's regulation [2]. Positive feedback loops lead to instability, which is required for a system to display oscillations, but negative feedback is also needed for stable limit cycle oscillations.

The reaction that PFK catalyses is shown in Figure 2.7 and is essentially a non-reversible reaction. PFK is inhibited by its substrate ATP. Indirectly, PFK is activated by its product ADP, which when converted to AMP by adenylate kinase (AK), allosterically activates PFK, thus PFK is activated or 'switched on' at low ATP/ADP ratios and is inhibited or 'switched off' at high ATP/ADP ratios. The initial stage of glycolysis involves the investment of ATP into the glycolytic intermediates and so there is a net decrease in ATP and a decrease in the ATP/ADP ratio. With a decrease in ATP the activity of PFK accelerates and the carbon flux through lower glycolysis increases. Lower glycolysis involves enzymes such as phosphoglycerate kinase (PGK) and pyruvate kinase (PK) which produce ATP and increase the ATP/ADP ratio. This increase in ATP by lower glycolysis inhibits the activity of PFK and so the

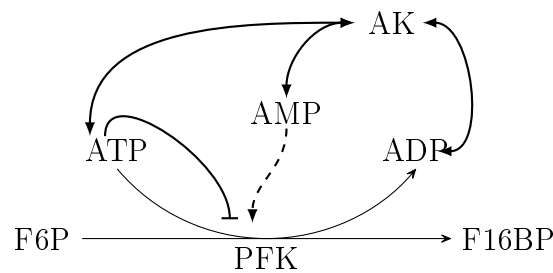


Figure 2.7: The reaction mechanism of PFK, with AK, demonstrating PFKs regulatory mechanism. The dashed arrows ($--\rightarrow$) show allosteric activation and the flat arrow ($-$) shows allosteric inhibition.

flux through glycolysis decreases. This 'on' and 'off' of PFK or alternatively, 'start and stop' mechanism is what causes the oscillations to occur.

To be exact, the activation of PFK at low ATP/ADP ratios is partially due to the decrease in ATP and partially due to the increase of AMP that is a result of ADP production. The enzyme adenylate kinase (AK) is responsible for the interconversion of $2\text{ADP} \rightleftharpoons \text{ATP} + \text{ADP}$. Because AK is always considered to be operating at equilibrium, an increase in ADP leads to a direct increase in AMP and it's by this mechanism that the production of ADP indirectly activates PFK. AMP allosterically activates PFK and ATP allosterically inhibits PFK, but the extent to which this allosteric control is distributed is still unclear.

PFK is a 4 subunit enzyme which displays cooperativity. There are currently two proposed models for cooperativity: 1) the Koshland-Némethy-Filmer (KNF) model and 2) the Monod-Wyman-Changeux (MWC) model, both of which are phenomenological models. The two models rely on the same principles that the enzyme's subunits are identical and exist in one of two states, one being a more active or 'relaxed' state (R-state) with a higher ligand affinity and the second being the less active or 'tense' state (T-state) with a lower ligand affinity, and that the binding of the allosteric ligand induces a conformational change from the T-state to R-state or vice versa. The models differ only in the extent of the conformational change imposed by the ligand. In the KNF model the binding of a ligand induces a conformational change in the ligand bound subunit but also in subunits adjacent to the ligand bound subunit. The KNF model has been used to successfully model the way in which haemoglobin acts when one of the four subunits of haemoglobin binds to oxygen, the affinity for oxygen on the adjacent subunits increases. The MWC model on the other hand suggests that instead only the ligand bound subunit undergoes the conformational change and all adjacent subunits remain in either the T- or R-state. This is the model that is proposed for PFK and

has been successful in modelling glycolytic oscillations. As AMP binds to the allosteric site on PFK, the bound subunit undergoes a conformational change from the T-state to the R-state and the activity of PFK increases. However when ATP binds to PFK the subunit remains in the T-state and cannot be activated. So the state of the tetrameric PFK structure in solution is a blend of these T- and R-state subunits and hence the state of PFK's overall activity at any given point in time is dependent on the relative concentrations of AMP and ATP. It is however still unclear whether any specific allosteric activator or inhibitor has a larger control on the PFK enzyme.

2.4.4 Adenylate kinase and its role in glycolytic oscillations

Adenylate kinase (AK) is an enzyme responsible for the interconversion of ATP, ADP and AMP ($2\text{ADP} \rightleftharpoons \text{ATP} + \text{AMP}$) [31]. AK has fast kinetics and is assumed to be operating close to equilibrium under cellular conditions, so the adenosine phosphates are expected to be close to a ratio of $K_{eq}[\text{ADP}]^2 : [\text{ATP}][\text{AMP}]$. The fast kinetics of AK and conserved moiety allows one to calculate the concentrations of all three adenosine phosphates at any time even if the concentration of only one of the adenosine phosphates is known. AK plays an essential role in regulating PFK activity by linking the initial increase in ADP in upper glycolysis to an increase in AMP and ATP. As PFK consumes ATP, it produces ADP as a product, which due to the fast kinetics of AK, 2 ADPs are immediately converted to ATP and AMP. This production of AMP from ADP is what ultimately interacts allosterically with PFK and causes the activation of the enzyme. This is a crucial positive feedback loop which is required for the occurrence of glycolytic oscillations.

Adenylate kinase is inhibited by the molecule P1,P5-di(adenosine-5') pentaphosphate (Ap5A) which has the structure of two ADP molecules linked via an extra phosphate group so it mimics the product-substrate transitional state. Ap5A is assumed to act as a competitive inhibitor in the direction of $\text{ATP} + \text{AMP} \rightarrow 2\text{ADP}$ and as an uncompetitive inhibitor in the direction of $2\text{ADP} \rightarrow \text{ATP} + \text{AMP}$, the exact reason for the different types of inhibition of the two reactions is largely unknown [32].

The nature of adenylate kinase prevents distinguishing between the extent to which PFK relies on either AMP activation or ATP inhibition for proper functioning in terms of glycolytic oscillations. Because of the dynamics of AK being close to equilibrium, a perturbation in either of the adenosine phosphates is almost immediately dissipated as the equilibrium ratio is restored and it becomes difficult to examine the individual effects of the adenosine phosphates on glycolytic oscillations.

2.5 Systems biology

Systems biology can be described as an interdisciplinary approach to studying complex biological systems such as cells. We can describe the individual components of a cell using mathematics and create subsequent models which combine these individual components in a mathematical framework of a model. These models can be used to study these interacting components, and the mechanism by which they lead to systemic behaviour.

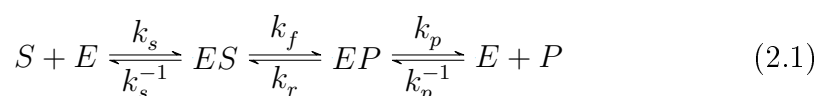
Metabolism has been a big focus for mathematical models in systems biology. Glycolysis is a well studied metabolic pathway and many mathematical models of glycolysis have been constructed over time. The cellular environment is very compact and most metabolic processes occur in what we assume to be a mostly homogeneous, single compartment with relatively high particle numbers, which allows for the rates of the process to be modelled using ordinary differential equations (ODEs) instead of stochastic differential equations. There are two major approaches to modelling metabolic pathways: 1) the top-down approach and 2) the bottom-up approach. In a nutshell the top-down approach (phenomenological) starts with the whole picture and tries to break it down into smaller operating parts. The bottom-up (mechanistic) approach involves identifying the working components of the system and piecing these together to make the whole picture. In terms of metabolic modelling, each individual enzyme is kinetically characterised in terms of its substrates and products and allosteric effectors. Put together, this results in a model comprised of the ODEs for all the individual metabolites.

In this study we use the bottom-up approach. The bottom-up approach allows us to investigate each enzyme individually. We can derive individual rate equations for each enzyme and fit these equations to experimental data for the isolated enzyme. The individual equations, after fitting, are then put together to create a metabolic pathway. This creates a model where each equation has been individually fitted to its own data set. This is powerful as each equation is based on discrete biochemical data. The model as a whole is not necessarily fitted to data and so model simulations are predictions, and e.g. oscillations are emergent properties. The downside to this approach is that it can create very large models with many parameters and to accurately determine the rate equations and parameters of each enzyme in the model is extensive work. However, when correctly done, mechanistic models are tools which allow us to analyse individual reactions in terms of the whole pathway as well as how individual parameters will affect the network. One outcome of such an approach is drug target identification. The next section describes briefly the process of deriving a rate equation for an enzyme.

2.5.1 Deriving rate equations of enzymes

In this study we use the bottom-up approach, and as mentioned in the previous section, the rate equations of each enzyme in the metabolic pathway forms the building blocks of the model and is required for the formation of the model's ODEs. There are many ways to derive rate equations of enzymes, but most are built on the method of King and Altman [33]. The method presented below can be followed for a variety of enzymes that have any number of substrates and products or inhibitors.

When discussing the derivation of enzymatic rate equations it is easiest to start with an example. Most enzyme catalysed reactions are reversible, so we'll consider a single substrate and product reversible reaction (eq. 2.1):



In this reaction, the enzyme E binds its substrate S to form the enzyme-substrate complex ES . The enzyme then converts S to its product P at the rate k_f . P is then released from the enzyme-product complex EP to the environment. All k_n 's are rate constants.

Using the law of mass conservation, for a closed system where the total enzyme concentration remains constant.

$$[E]_T = [E] + [ES] + [EP] \quad (2.2)$$

$$\frac{d[E]_T}{dt} = \frac{d[E]}{dt} + \frac{d[ES]}{dt} + \frac{d[EP]}{dt} = 0 \quad (2.3)$$

A steady state the rate of change of each enzyme-substrate complex is zero:

$$\frac{d[E]}{dt} = \frac{d[ES]}{dt} = \frac{d[EP]}{dt} = 0 \quad (2.4)$$

If we divide eq. 2.2 by the total enzyme concentration, $[E]_T$ we get an expression for the fractions of the various enzyme states in the system

$$Y_e + Y_{es} + Y_{ep} = 1 \quad (2.5)$$

Naturally we can express each enzyme-substrate complex as a fraction of the total enzyme concentration.

$$[E]_0 = Y_e[E]_T \quad [ES] = Y_{es}[E]_T \quad [EP] = Y_{ep}[E]_T \quad (2.6)$$

In the King-Altman method for the derivation of kinetic equations of enzymes, individual rate constants are used for each step in the enzymatic process. A simpler approach is to assume equilibrium binding of substrates and

products and to use the dissociation constants of the enzyme-substrate complexes, which in themselves contain the individual rate constants. From eq. 2.1 shown above, at equilibrium

$$K_s = \frac{[E][S]}{[ES]} = \frac{k_s^{-1}}{k_s} \quad (2.7)$$

where K_s is the dissociation constant of the substrate S . Now, if we consider the net rate of the reaction to be the rate of the forward reaction minus the rate of the reverse reaction we obtain

$$v = k_f[ES] - k_r[EP] \quad (2.8)$$

Using the relations shown in eqs. 2.6, eq. 2.8 becomes

$$v = k_f Y_{es}[E]_T - k_r Y_{ep}[E]_T \quad (2.9)$$

For the case that the entire enzyme concentration is in the form ES , $[E]_T = [ES]$, the forward rate is at a maximum. This applies to the reverse rate as well.

$$v_{maxf} = k_f[E]_T \quad v_{maxr} = k_r[E]_T \quad (2.10)$$

By including the relation for the maximum of the forward and reverse reactions, eq. 2.10 the following arises

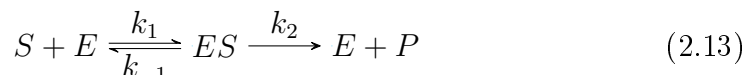
$$v = \frac{v_{maxf}[ES] - v_{maxr}[EP]}{[E]_T} \quad (2.11)$$

Lastly, by substituting in eq. 2.2 for the total enzyme concentration, as well as by expressing the enzyme-substrate complexes in terms of their respective dissociation constants eq. 2.7 we obtain

$$v = \frac{v_{maxf} \frac{[S]}{K_s} - v_{maxr} \frac{[P]}{K_p}}{1 + \frac{[S]}{K_s} + \frac{[P]}{K_p}} \quad (2.12)$$

Eq. 2.12 is the general form of the reversible Michaelis-Menten equation. Both the substrate and the product play a role in the regulation of the rate of the reaction. The numerator determines the direction the reaction will proceed and the denominator gives insight into how the enzyme is regulated. The magnitude of the enzyme's response to a substrate is determined by its respective dissociation constant. If $[S] \gg K_s$ then $\frac{[S]}{K_s} \gg 1$ and $[S]$ will have a weaker effect on the overall rate, but if $K_s \gg [S]$ then $\frac{[S]}{K_s} \ll 1$ and $[S]$ will have a stronger effect on the overall rate.

It is important to note that the constants K_s and K_p are not the same as the Michaelis-Menten constant K_m as the Michaelis-Menten equation describes the kinetics of a strictly irreversible enzymatic reaction (eq. 2.13).



Generally, the Michaelis-Menten constant K_m has the following description

$$K_m = \frac{k_{-1} + k_2}{k_1} \quad (2.14)$$

which is not the same as a dissociation constant. Only when the rate constant $k_2 \ll k_{-1}$ will K_m be comparable to the dissociation constant. Therefore the dissociation constants do not have the same properties as K_m 's do. In this study we use the assumption of equilibrium for the derivation of rate equations, and although the equations are identical, the strict meaning of the K 's differ.

2.5.2 The dupreez6 mathematical model of glycolytic oscillations in yeast cell free extracts

For this study we used a model of yeast glycolysis in cell free extracts, dupreez6 model, previously developed in our lab [12; 34], and can be found on the JWS Online model database (<http://jjj.biochem.sun.ac.za/models/dupreez6/>), also developed in our lab [35]. This model was constructed from a previously existing model (Teusink model [36]) through a series of optimisation steps to obtain an oscillating cell extract model. The overall network of the dupreez6 model is shown in Figure 2.4. Although the model is of a cell extract the $glucose_{in}$ and $glucose_{out}$ terms are still present as there is a steady influx of glucose to the system from a source such as trehalose. The various enzymes, metabolites and branches are labelled accordingly: hexokinase (HK), glucose 6-phosphate (G6P), phosphoglucose isomerase (PGI), fructose 6-phosphate (F6P), phosphofructokinase (PFK), fructose 1,6-bisphosphate (F16BP), aldolase (ALDO), dihydroxyacetone phosphate (DHAP), glyceraldehyde 3-phosphate (GAP), triosephosphate isomerase (TPI), glyceraldehyde 3-phosphate dehydrogenase (GAPDH), 1,3-bisphosphoglycerate (1,3BPG), phosphoglycerate kinase (PGK), 3-phosphoglycerate (3PG), phosphoglycerate mutase (PGM), 2-phosphoglycerate (2PG), enolase (ENO), phosphoenolpyruvate (PEP), pyruvate kinase (PK), pyruvate (PYR), pyruvate decarboxylase (PDC), acetaldehyde (Ace), alcohol dehydrogenase (ADH), ethanol (EtOH), succinic acid (Succ), adenylate kinase (AK), glyceraldehyde 3-phosphate dehydrogenase (G3PDH), glycogen branch (Glyco) and trehalose branch (Treh).

The model makes various assumptions such as a constant inorganic phosphate concentration, a constant glucose influx rate and constant removal of end products such as trehalose, glycogen, succinic acid and ethanol. Additionally,

the metabolites GAP and DHAP are grouped together as triosephosphates in the model and there is no term for TPI. TPI is assumed to be at equilibrium, therefore aldolase reaction increases the pool of triosphosphates which are then converted to either glycerol or by G3PDH and GAPDH respectively.

The dupreez6 model lacks a detailed kinetic description of adenylate kinase and the rate of AK is modelled using equilibrium kinetics. For the sake of this study, a more detailed description of AK, including the effect of inhibition by Ap5A, was necessary.

2.5.3 Epilogue

Glycolysis, under certain conditions, displays oscillations. These chemical oscillations are a form of order in what seems like chaotic behaviour and so behaves as a dissipative structure under these oscillatory conditions. These dissipative structures are not uncommon in nature and are a requirement for life. The non-linearity of the PFK reaction allows glycolysis to enter an oscillatory state by means of autocatalysis. PFK causes both positive and negative feedback loops which are necessary for limit cycle oscillations. This was demonstrated stoichiometrically by Sel'kov, and kinetically by Goldbeter where a model based on the PFK reaction was able to show oscillations [24; 2]. PFK is dependent on AMP and ATP for its transitioning between the R and T states. This places an importance on AK which is responsible for the interconversion of the adenosine phosphates and is the sole source of AMP for glycolysis. AK has not yet been studied with regards to its role in glycolytic oscillations. The next chapters attempt to further investigate the effect AK has on glycolytic oscillations both experimentally and using mathematical modelling. This may elucidate the individual contributions of AMP and ATP toward the oscillations.

Having introduced all the relevant topics necessary for this study, I will now present (Chapter 3) the various methods used to obtain the results (Chapter 4) to investigate the effect of adenylate kinase on glycolytic oscillations and to elucidate the contributions of ATP and AMP toward these oscillations.

Chapter 3

Methods

3.1 Introduction

This chapter presents the methods used during the course of this project. The methods have been split into sections according to where in the experimental process they were utilised. First is the methods used in the experimental induction of the glycolytic oscillations which includes culturing the yeast cell and ends with visualising the glycolytic oscillations as well as the inhibition of adenylate kinase during these oscillations. Secondly the various assays used to determine enzymatic activities and protein concentrations are discussed. Lastly, there is a section describing the software used in the mathematical modelling section of the project. All enzymes and cofactors were supplied by Sigma Aldrich.

3.2 Experimental induction of glycolytic oscillations and the inhibition of adenylate kinase

Culturing and harvesting *Saccharomyces cerevisiae* *Saccharomyces cerevisiae* was grown in suspension in media that consisted of 10 g/L glucose, 6.7 g/L yeast nitrogen base and 100 mM potassium phthalate at pH 5. The cultures were incubated at 30°C on a shaker until diauxic shift (glucose depletion). The cells are harvested at the point of diauxic shift as this is the point where the cells were predicted to have a cellular make-up most likely to exhibit oscillations [23]. The point of diauxic shift was monitored using glucose test strips. The cells were harvested via centrifugation for 10 minutes at 5000xg and the supernatant discarded. The harvested cells were subsequently washed by re-suspending the cells in 100 mM phosphate buffer at pH 6.8, followed by centrifugation and discarding supernatant. The cells were washed twice to get rid of any remnants of metabolites from the growth media that might still be

in the external environment of the cell. The pelleted cells were re-suspended in approximately 20 ml of 100 mM phosphate buffer. The re-suspended cells were then starved for 2 hours by incubating the cells at 30°C on a shaker. The cells were starved to allow the cells to utilise any remaining glycolytic intermediates and energy stores. The cells are starved so that the primary source of energy for the cells will be provided by the substrate given to the cells when glycolytic oscillations are induced. After starvation, the cells were pelleted again via centrifugation as mentioned previously. Any pellets that were not used directly after harvesting were stored at -20°C.

Cell lysis The washed and starved yeast cells were lysed using acid washed glass beads. The glass beads were added at a 1:1 ratio of gram wet weight pellet to glass beads. 100 µl of 100 mM phosphate buffer (pH 6.5) was also added for each 1g wet weight cells that were being lysed. Approximately 6 to 10 cycles of 10 minutes vortexing and 5 minutes cooling on ice was needed to fully lyse all the pelleted cells. The glass beads and cell debris were pelleted by centrifugation (15 minutes at 5000xg) and the supernatant was collected. The raw cell extract was then transferred to a 1 mL Eppendorf microcentrifuge tube. The raw cell extract underwent two steps of centrifugation at 20817xg for 25 min which further removed any remaining cell debris. Cell extracts could be stored at - 80°C in aliquots of 200 µl.

Induction and measurement of glycolytic oscillations Firstly 45 µL of cell extract was placed into a 96 well F-bottom black Greiner microtiter plate. 5 µL of 1 M trehalose was then added to the cell extract at which point the microtiter plate was inserted into the TECAN Spark 10M fluorimeter and the NADH fluorescence of the cell extract was recorded using an excitation wavelength of 345 nm and reading the emission wavelength at 460 nm. The fluorescence was recorded over several hours and the samples were kept at 30 °C during the experiment. In some cases the addition of exogenous trehalase resulted in better oscillations. In the case where trehalase was added, the volume of trehalase added was compensated by reducing the volume of cell extract added to the well by an amount equal to the volume of trehalase added so that the total volume of the sample remains at 50 µL.

Inhibiting Adenylate kinase After glycolytic oscillations were induced, adenylate kinase was inhibited using the inhibitor Ap5A. To prevent excessive perturbation of the sample volume size, only 2 µL of Ap5A was added to each sample. The final concentration of the inhibitor in the wells ranged from 0 to 1000 µM.

3.3 Protein and Enzymatic Assays

Protein determination The protein content of the cell extract was determined using the Linearisation of Bradford method according to the paper by Ernst et al. [37]. 10 μL of standard bovine serum albumin and sample was added to 190 μl of Bradford reagent and was left to incubate for a minimum of 10 minutes before spectrophotometrically reading absorbance at both 450nm and 590nm using a SPECTROstar^{Nano} from BMG LABTECH.

Enzymatic assays Enzymatic activities were determined using NAD(P)/NAD(P)H coupled assays. All reactions were monitored at 340nm wavelength and at 30 °C. All assays were performed in 100 mM potassium phosphate buffer (pH 6.5) and contained 10 mM MgCl_2 .

ATPase activity was determined by coupling the reduction of ATP (2 mM) to ADP by ATPase to the enzyme couple pyruvate kinase (PK, 5U) and lactate dehydrogenase (LDH, 5U). PK facilitates the conversion of ADP and phosphoenolpyruvate (10 mM) to ATP and pyruvate. LDH then converts NADH (0.4 mM) and pyruvate to NAD^+ and lactate.

Trehalase activity was determined by coupling the production of glucose from trehalose by trehalase to the enzyme couple hexokinase (HK, 5U) and glucose 6-phosphodehydrogenase (G6PDH, 5U). HK converts ATP (2 mM) and glucose to ADP and glucose 6-phosphate. G6PDH then utilises glucose 6-phosphate in the reduction of NADP^+ (2 mM) to NADPH.

The adenylate kinase characterisation assays were coupled to HK and G6PDH for ADP as substrate (forward reaction) and to PK and LDH for ATP and AMP as substrates (reverse reaction). For both the forward and reverse reactions the substrates were varied from 0 to 5 mM. For ADP as the substrate, the assay contained glucose, HK (5U), G6PDH (5U), NADP (0.4 mM) and varying concentrations of ADP. For ATP as the substrate, the assay contained phosphoenolpyruvate, PK (5U), LDH (5U), NADH (0.4 mM), AMP (2 mM) and varying concentrations of ATP. For AMP as the substrate, the assay contained phosphoenolpyruvate, PK (5U), LDH (5U), NADH (0.4 mM), ATP (2 mM) and varying concentrations of AMP.

To parametrise the inhibitor Ap5A in the rate equation of adenylate kinase an inhibitor titration was performed on AK. Varying concentrations of Ap5A were added (0 –1000 μM) to the coupled adenylate kinase assay where ADP was used as the substrate. The assay contained glucose (20 mM), HK (5U), G6PDH (5U), NADP (0.4 mM), ADP (2 mM) and varying concentrations of Ap5A. As previously described these assays were also performed in 100 mM phosphate buffer (pH 6.5) with 10 mM MgCl_2 .

3.4 Mathematical modelling

All mathematical modelling was performed on Wolfram Mathematica[®] Version 11.

Adenylate kinase rate equation The adenylate kinase rate equation was derived using a method similar to that of King and Altman. The equations were fitted to the experimental data and the parameters estimated using the Mathematica[®] functions `NonlinearModelFit` with the method `NMinimize`.

From the derived rate equations a best equation was selected using the corrected Akaike information criterion.

Glycolytic model analysis The `dupreez6` model of glycolytic oscillations in cell extracts was utilised and can be found on the online model database JWSOnline [35]. The `dupreez6` model was extended with the parametrized adenylate kinase equation to create the `vanwyk1` model. The protein concentration was also adjusted to reflect the experimental parameters.

Chapter 4

Results

4.1 Introduction

This chapter presents the results of the various experiments and model simulations that were necessary for this study. This chapter starts with the derivation of a kinetic mechanism for adenylate kinase. We make use of the `dupreez6` model of glycolysis which shows oscillatory behaviour and can be found on JWS Online. Because the `dupreez6` model of glycolytic oscillation does not include a detailed adenylate kinase mechanism and has no term for the inhibition of adenylate kinase, this needed to be included into the model. Firstly, in order to characterise adenylate kinase, a few kinetic mechanisms by which the enzyme may operate had to be hypothesized. 4 kinetic mechanisms are presented here with their fitted parameters. Of these four mechanisms, one was selected according to the Akaike's information criterion (AIC) to be included into the `dupreez6` model. AIC selects the best model by weighting the sum of squared differences of the fits of the different models against the number of fitted parameters of each model [38]. The next section deals with the experimental induction and recording of glycolytic oscillation as well as experimentally inhibiting adenylate kinase during these oscillations. A brief paragraph on all the problems faced in sight of achieving an oscillatory cell free extract is also included. The last section focuses on the model predictions for the inhibition of adenylate kinase during glycolytic oscillations, and compares the `dupreez6` model, with and without the new adenylate kinase mechanism, to the data collected in the second section.

4.2 Adenylate kinase kinetics

Adenylate kinase reversibly converts two molecules of ADP to ATP and AMP, therefore all the enzyme kinetic mechanisms should be Bi-Bi. The distinguishing factors between the mechanisms presented here lie in the binding order of the substrates and products to the enzyme. To my knowledge the

enzyme is only able to bind two substrates at a time for both the forward and reverse reactions and has no allosteric binding sites. We also introduce here an inhibitory term i which is the concentration of the inhibitor Ap5A. Because of the size of Ap5A which mimics the ADP-ADP or AMP-ATP complex, only one inhibitor molecule can bind the enzyme at a time and it can only bind to the free enzyme. This section presents 4 kinetic mechanisms of adenylate kinase. Each kinetic mechanism is presented firstly by its respective binding schema followed by the rate equation derived from that binding schema and lastly the equation is fitted to a data set. After all the kinetic models have been presented they are compared using AIC.

The first kinetic model will have its derivation shown in full. Because each derivation of the subsequent kinetic models is essentially the same, only their final rate equations will be shown. For the remaining three derivations please see Appendix A.

The various rate equations that were derived for the 4 mechanisms were tested with an experimental dataset. To parametrize the adenylate kinase reaction, NADH-coupled assays were used. In these NADH-coupled assays, auxiliary enzymes are incorporated to link the monitored enzyme (AK) to NAD(P)/NAD(P)H oxidation/reduction. In this study, the ADP production by AK (reverse reaction) was linked to NADH oxidation via pyruvate kinase (PK) and lactate dehydrogenase (LDH) (Figure 4.1). Phosphoenolpyruvate (PEP), NADH, PK and LDH are added in excess to ensure that the rate limiting step is the rate at which ADP is supplied by AK. For the forward AK reaction where ATP is produced, the ATP production is coupled to NADP reduction via hexokinase (HK) and glucose 6-phosphate dehydrogenase (G6PDH) (Figure 4.2). Glucose, NADP, HK and G6PDH were added in excess to ensure that the rate limiting step is the rate at which ATP is supplied by AK.

For the forward reaction (ADP converted to ATP and AMP), ADP was varied and the rate of NADH production was recorded for each ADP con-

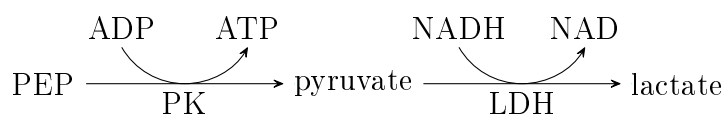


Figure 4.1: PK-LDH assay couple. ADP production by AK is linked to NADH oxidation using the enzymes PK and LADH.

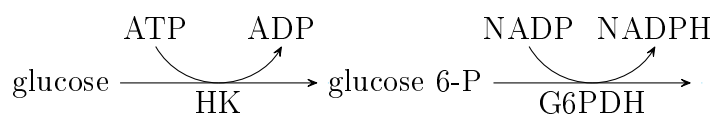


Figure 4.2: HK-G6PDH assay couple. ATP production from AK is linked to NADP reduction using the enzymes HK and G6PDH.

centration. The assay could be initiated by adding the cell extract which contained the adenylate kinase enzyme last. For the reverse reaction (ATP and AMP converted to ADP), the production of ADP was coupled to NADH disappearance. Either ATP had to be kept constant while AMP was varied or AMP had to be kept constant while ATP was varied. Unlike the forward reaction where the assay cocktail remained very stable (NADH remained constant until the reaction was initiated), for the assay where ATP was varied and AMP was kept constant, when the coupling enzymes PK and LDH were added to the assay cocktail the NADH concentration started to spontaneously decrease. This was strange as it did not occur in the situation where AMP was varied and ATP was kept constant. To overcome this problem, the cell extract was mixed with LDH and PK and the assay was initiated with this solution. The rate of spontaneous NADH disappearance was then subtracted from the rates of the other samples. The reason for the spontaneous disappearance of NADH is still unknown, but the only factor that is different from the other experiments is that the concentration of AMP that remains relatively high and constant. Because different cell extracts have varying protein concentrations and the enzyme expression and yields are not constant, each set of data was normalised to its maximum rate so the data of separate experiments could be pooled together, therefore the rates are displayed as V/V_{max} .

4.2.1 Random order Bi-Bi mechanism

The first kinetic mechanism is a random ordered Bi-Bi mechanism. A random binding order results in the following schema below (Figure 4.3). There are two binding sites on the enzyme, both of which have equal affinity for the various substrates. Any substrate or product can bind the enzyme unless the enzyme is already bound to two substrates or products except for the inhibitor which can only bind to free enzyme. Any combination of the substrates and products is possible. For all the binding schemas that follow, T = ATP, D = ADP, M = AMP and i = inhibitor (Ap5A).

Following the steps as described in §2.5.1, we firstly write down the mass conservation equation. We can assume that the two binding sites have equal affinity for the substrates so $E_{D_1} = E_{D_2} = E_D$. Similarly, $E_{TM} = E_{MT}$. The random order binding schema, Figure 4.3 then leads to the following mass conservation equation:

$$E_{Tot} = E + 2E_D + 2E_{DT} + 2E_{DM} + E_{DD} + 2E_{MT} + 2E_M + 2E_T + E_{TT} + E_{MM} + E_i \quad (4.1)$$

The next step is to list the various dissociation constants of the substrates in terms of all the enzyme-substrate species (eqs. 4.2-4.10).

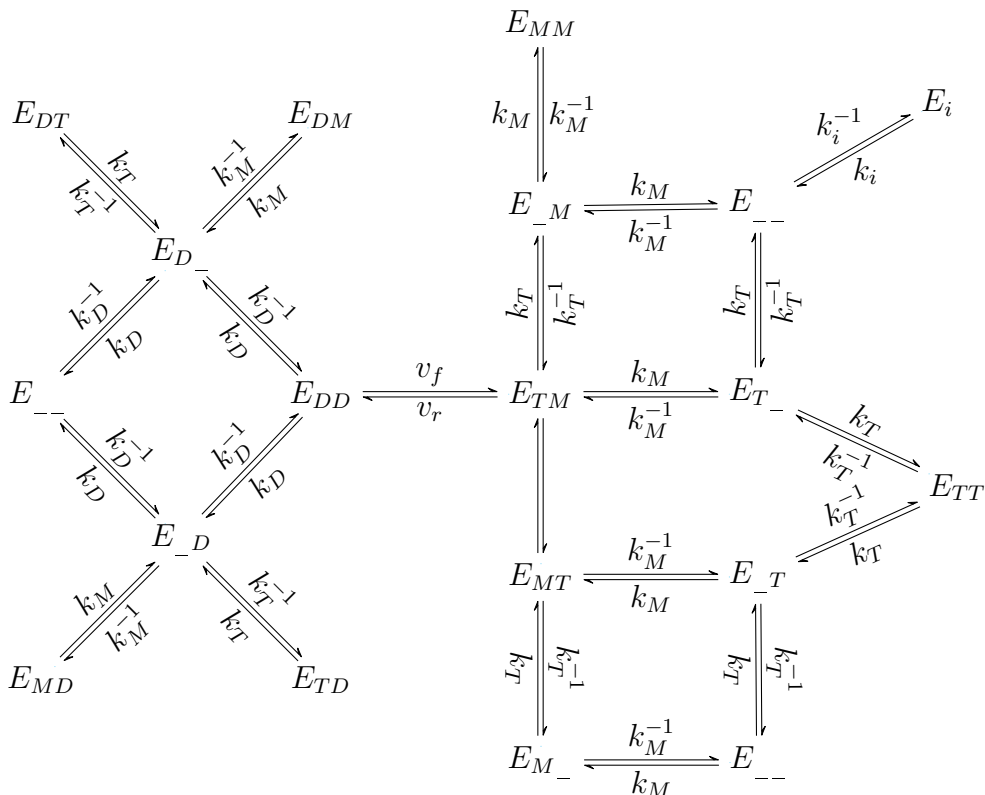


Figure 4.3: Random order Bi-Bi binding schema for adenylate kinase. E denotes the enzyme adenylate kinase and the subscript denotes the substrate bound to the enzyme (ATP: T, ADP: D, AMP: M, Ap5A: i). The position of the subscript shows which catalytic site the substrate is bound to. The dissociation constants k_T , k_D , k_M , k_i are the dissociation constants of enzyme bound ATP, ADP, AMP and Ap5A respectively.

$$E_D = \frac{E \text{ adp}}{K_D} \quad (4.2)$$

$$E_{DT} = \frac{E \text{ adp atp}}{K_D K_T} \quad (4.3)$$

$$E_{DM} = \frac{E \text{ adp amp}}{K_D K_M} \quad (4.4)$$

$$E_{DD} = \frac{E \text{ adp}^2}{K_D^2} \quad (4.5)$$

$$E_{MT} = \frac{E \text{ amp atp}}{K_M K_T} \quad (4.6)$$

$$E_M = \frac{E \text{ amp}}{K_M} \quad (4.7)$$

$$E_T = \frac{E \text{ atp}}{K_T} \quad (4.8)$$

$$E_{TT} = \frac{E \text{ atp}^2}{K_T^2} \quad (4.9)$$

$$E_{MM} = \frac{E \text{ amp}^2}{K_D^2} \quad (4.10)$$

The rate of a reaction at any time is equal to the difference between the forward and reverse reaction rates which can be written as follows:

$$vAK_{rand} = v_f [E_{DD}] - v_r [E_{MT}] \quad (4.11)$$

By converting the enzyme-substrate complexes E_{DD} and E_{MT} to their respective fractional saturation ratios we get:

$$Y_{DD} = \frac{[E_{DD}]}{[E_{Tot}]} \quad Y_{MT} = \frac{[E_{MT}]}{[E_{Tot}]} \quad (4.12)$$

By including eq. 4.12 in 4.11 :

$$vAK_{rand} = v_f [E_{Tot}] Y_{DD} - v_r [E_{Tot}] Y_{MT} \quad (4.13)$$

We can assume that if all the enzyme species are in the form E_{DD} , the forward rate reaches a maximum. So, if $E_{DD} \rightarrow E_{Tot}$, $v_f \rightarrow V_f$. The same is true for the reverse reaction, therefore:

$$v_f [E_{Tot}] = V_f \quad v_r [E_{Tot}] = V_r \quad (4.14)$$

Substituting eq. 4.14 in 4.13, we get:

$$vAK_{rand} = V_f Y_{DD} - V_r Y_{MT} \quad (4.15)$$

With the use of the fractional saturations (eq. 4.12) we get a denominator term E_{Tot} :

$$vAK_{rand} = \frac{V_f E_{DD} - V_r E_{MT}}{E_{Tot}} \quad (4.16)$$

Lastly, by using the conservation of mass eq.4.1 and the dissociation constant eqs. 4.2-4.10 we get the final rate equation for the random binding schema in Figure 4.3:

$$vAK_{rand} = \frac{V_f \frac{adp^2}{K_D^2} - V_r \frac{amp \ atp}{K_M K_T}}{\left(1 + \frac{amp}{K_M} + \frac{adp}{K_D} + \frac{atp}{K_T}\right)^2 + \frac{i}{K_i}} \quad (4.17)$$

We can also show the rate equation 4.17 in terms of its equilibrium constant (K_{eq}) and mass action ratio ($\Gamma = \frac{amp \ atp}{adp^2}$) by introducing the Haldane relation (eq. 4.18):

$$K_{eq} = \frac{V_f K_M K_T}{V_r K_D^2} \quad (4.18)$$

Using eq. 4.18 and the mass action ratio in 4.17 we get:

$$vAK_{rand} = \frac{V_f \frac{adp^2}{K_D^2} \left(1 - \frac{\Gamma}{K_{eq}}\right)}{\left(1 + \frac{amp}{K_M} + \frac{adp}{K_D} + \frac{atp}{K_T}\right)^2 + \frac{i}{K_i}} \quad (4.19)$$

Eq. 4.19 demonstrates in its denominator how the enzyme is regulated when it is assumed to follow a random binding order. Because any substrate can bind as long as there is at least one free catalytic site, each metabolite can act as a competitive inhibitor. For instance, if ADP binds to an AK-ATP complex, the AK-ATP-ADP complex is unable to catalyse any reaction.

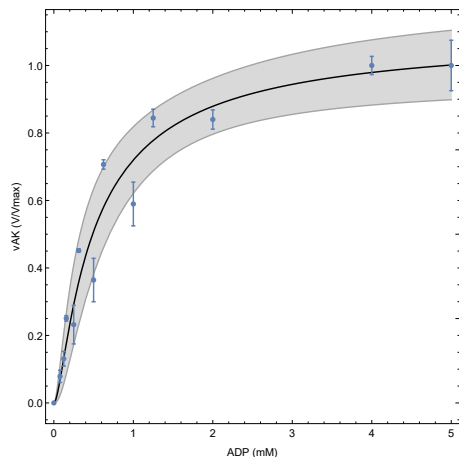
Fitting rate equation 4.19 to data yields the Figures 4.3 (a), (b), (c) and (d). The fit describes inhibition of AMP at high concentrations, but not for ADP or ATP. The fit results in an almost linear relationship between the rate of the reaction and ATP concentration. The sum of squared differences when fitting eq. 4.19 to the data is 1.896 and the adjusted R^2 value is 0.9479 (shown below in Table. (4.2)). The fitted parameters are displayed in Table 4.1.

4.2.2 Iso-random Bi-Bi mechanism

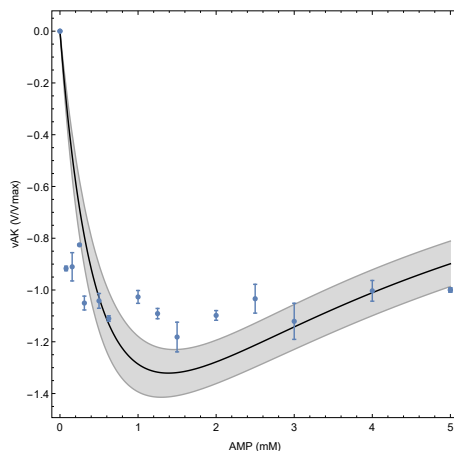
This mechanism was developed by Sheng *et al.* [39] and describes the enzyme as being in either of two conformation states (isoforms), each binding different substrates. Isoform 1E can bind only to ADP while isoform 2E can bind both ATP and AMP (Figure 4.5). The inhibitor (Ap5A) is also only able to bind to isoform 2E . The assumptions of this mechanism are based on the observations that adenylate kinase is found in different conformational states at equilibrium. There are two conformational changes that adenylate kinase undergoes in this mechanism: (1) during the conversion of product to substrate and (2) the ability of the unbound enzyme to exist in either of the two conformational states and to convert freely between them.

The major assumptions of this mechanism is that isoform 1E is specific for only ADP and isoform 2E , which is specific for AMP and ATP, has an AMP binding site which is more specific than the ATP binding site. Hence AMP can bind to the ATP binding site and act as a competitive inhibitor for the 2E isoform. The equilibrium constant K_E is introduced to describe the ratio of the two isoforms 1E and 2E . At equilibrium $K_E = \frac{k_1}{k_{-1}} = \frac{^1E}{^2E}$. This approach differs from that in the study of Sheng *et al.*, but the overall mechanism scheme is the same.

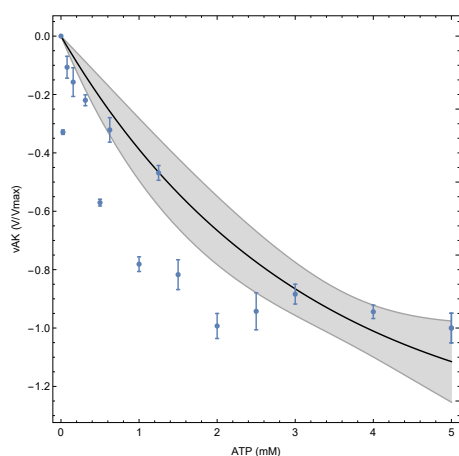
The iso-random binding scheme results in the following rate equation:



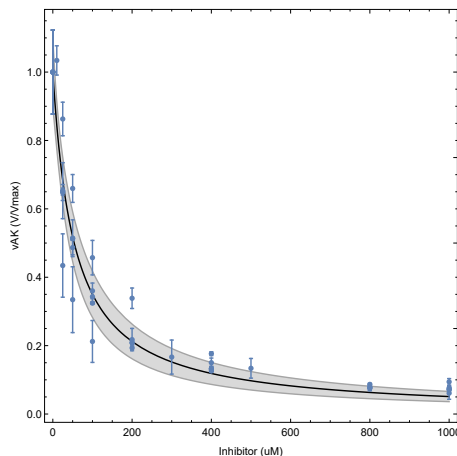
(a) Adenylate kinase rate against the concentration of the substrate ADP



(b) Adenylate kinase rate against the concentration of the substrate AMP



(c) Adenylate kinase rate against concentration of the substrate ATP



(d) Adenylate kinase rate against the concentration of the inhibitor Ap5A

Figure 4.4: Random order bi-bi mechanism fitted rate equation 4.19 (black curve) to the data for adenylate kinase rate (v/V_{max}) against its substrates ADP (a), AMP (b), ATP, (c) and the inhibitor Ap5A (d). Error bars show the standard error. The shaded areas indicate the 95% confidence interval.

$$vAK_{iso} = \frac{V_f \frac{adp^2}{K_D^2} \left(1 - \frac{\Gamma}{K_{eq}}\right)}{1 + \frac{1}{K_E} + \frac{adp}{K_D} \left(2 + \frac{adp}{K_D}\right) + \frac{amp}{K_E K_M} \left(2 + \frac{amp}{K_M} + \frac{atp}{K_T}\right) + \frac{atp}{K_T K_E} + \frac{i}{K_i K_E}} \quad (4.20)$$

After fitting equation 4.20 to the data the resulting graphs (Figure 4.6 (a), (b), (c) and (d)) seem fairly similar to those in Figure 4.8. The only notable difference is a slight widening of the confidence intervals at the higher

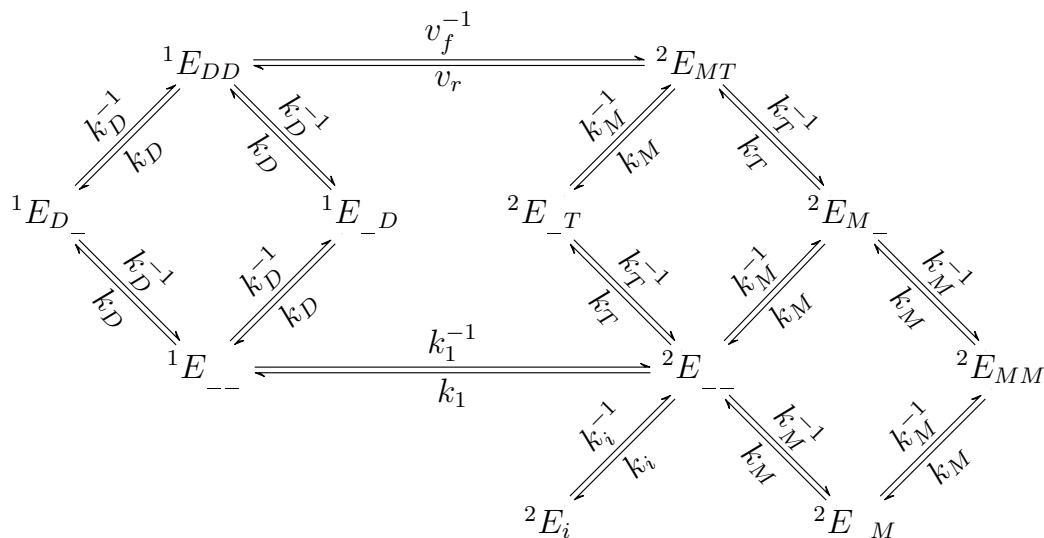
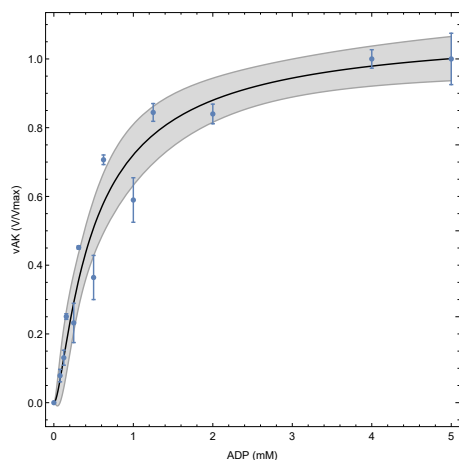


Figure 4.5: Iso-random ordered Bi-Bi binding schema for adenylate kinase. 1E and 2E indicate the two isoforms of AK. The subscript denotes the substrate bound to the enzyme (ATP: T, ADP: D, AMP: M, Ap5A: i). The position of the subscript shows which catalytic site the substrate is bound to. The dissociation constants k_T , k_D , k_M , k_i are the dissociation constants of enzyme bound ATP, ADP, AMP and Ap5A respectively.

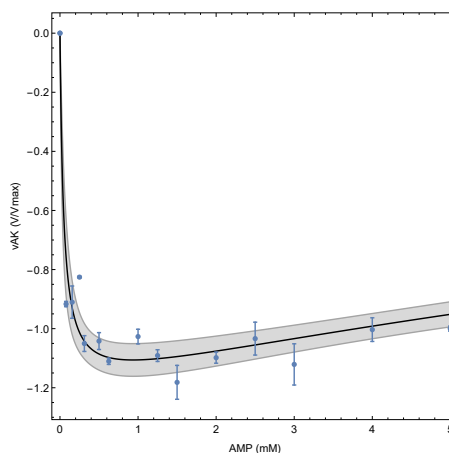
concentrations in Figure 4.8 (b) and (c). The fitted parameters are displayed in Table 4.1. The sum of squared differences when fitting the iso random bi bi mechanism to the data is 0.6764 and has an adjusted R^2 of 0.9812 (Table 4.2) which is evident of a better fit than eq. 4.19 ($SS=1.896$, $R^2=0.9479$), however this mechanism does introduce another parameter.

4.2.3 Spatio-temporal Bi-Bi mechanism

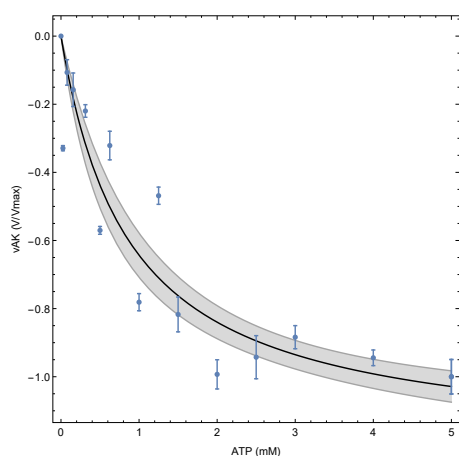
Using the iso-random binding scheme as a starting point, let's assume that the enzyme retains its specificity for the various substrates, but there is a negligible rate of interconversion between the two isoforms, eliminating the need for a K_E term. Next, we shall assume there is a spatial constraint in the active site of the enzyme. If we consider the reaction taking place, there is a transfer of a single phosphate from one adenosine phosphate molecule to the next. In order to facilitate the transfer of the phosphate we can assume that the enzyme must bind both adenosine phosphate molecules with their phosphates in close proximity to one another [40]. The reactive enzyme-substrate complexes AK-ADP-ADP and AK-ATP-AMP all have a total of 4 phosphate groups, so we can assume there is no room for a fifth phosphate group. This assumption then only allows enzyme-substrate complexes to occur as long as the total phosphates of the substrates does not exceed 4. As an example, if AK is bound to ADP, the AK-ADP complex can only further bind an AMP or



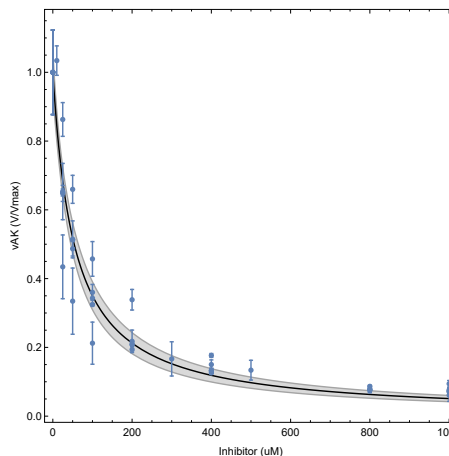
(a) Adenylate kinase rate against the concentration of the substrate ADP



(b) Adenylate kinase rate against the concentration of the substrate AMP



(c) Adenylate kinase rate against the concentration of the substrate ATP



(d) Adenylate kinase rate against the concentration of the inhibitor Ap5A

Figure 4.6: Iso random bi-bi mechanism fitted rate equation 4.20 (black curve) to the data for all adenylate kinase substrates ADP (a), AMP (b), ATP, (c) and the inhibitor Ap5A (d). Error bars show the standard error. The shaded areas indicate the 95% confidence interval.

ADP, and cannot bind ATP. This argument would appear to break down when considering the AK inhibitor Ap5A, as the inhibitor has 5 phosphates in its centre. There is, however, a conformational difference between the phosphates of Ap5A and the AK bound adenosine phosphates as there is a 'bend' in the phosphates of Ap5A, which is not present in the phosphates of the adenosine phosphates, allowing it to fit in the active site [40].

The mechanism is based on the amount of space available at a given time and so is called the spatio-temporal mechanism for this study. For the schema below (Figure 4.7) the following enzyme-substrate complexes are possible: AK-AMP-AMP, AK-AMP-ADP, AK-AMP-ATP and AK-ADP-ADP as well as all

single-substrate bound enzyme complexes.

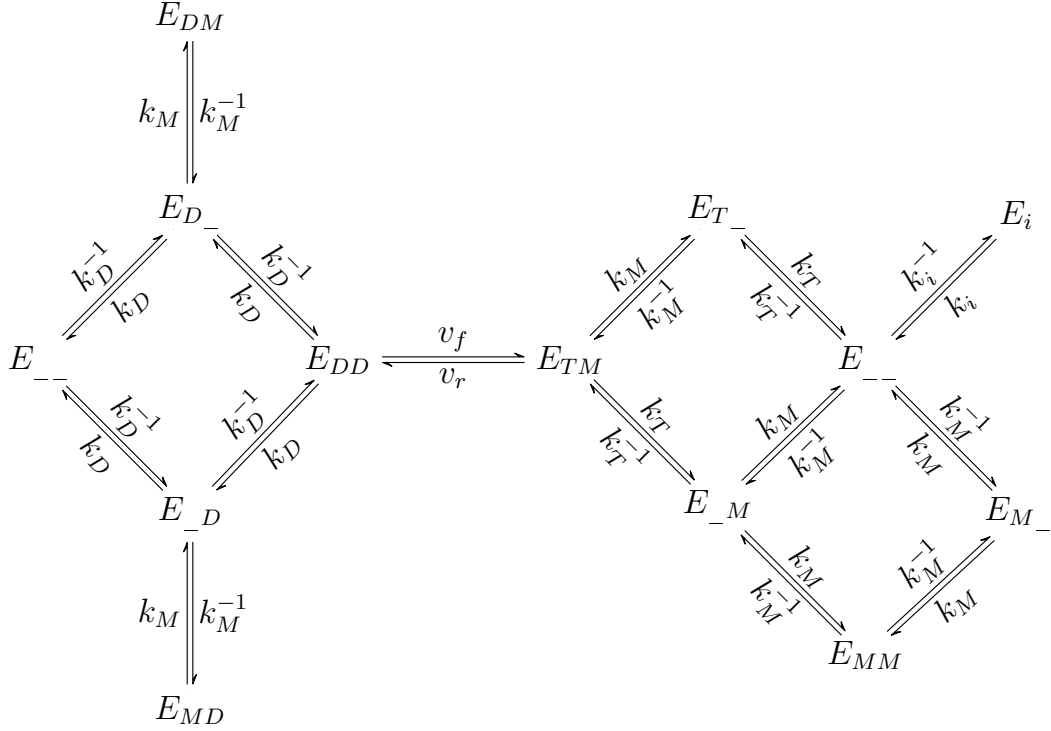
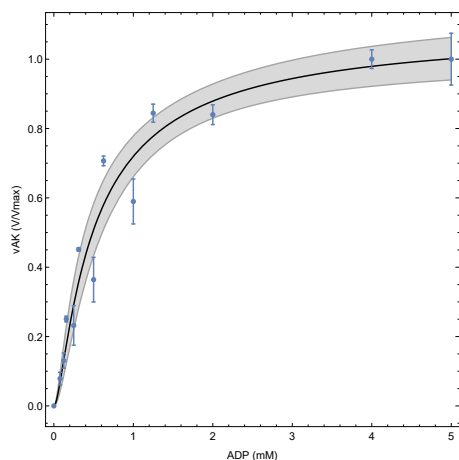


Figure 4.7: Spatio-temporal ordered Bi-Bi binding schema for adenylate kinase. E denotes the enzyme adenylate kinase and the subscript denotes the substrate bound to the enzyme (ATP: T, ADP: D, AMP: M, Ap5A: i). The position of the subscript shows which catalytic site the substrate is bound to. The dissociation constants k_T , k_D , k_M , k_i are the dissociation constants of enzyme bound ATP, ADP, AMP and Ap5A respectively.

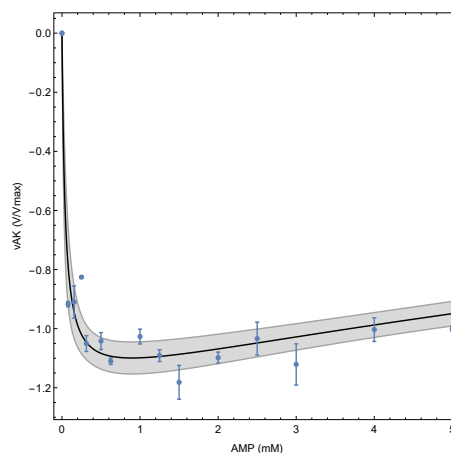
The spatio-temporal binding mechanism (Figure 4.7) results in the following rate equation (eq. 4.21):

$$vAK_{spatio} = \frac{V_f \frac{adp^2}{K_D^2} \left(1 - \frac{\Gamma}{K_{eq}}\right)}{1 + \frac{adp}{K_D} \left(2 + \frac{adp}{K_D} + 2\frac{amp}{K_M}\right) + \frac{amp}{K_M} \left(2 + \frac{amp}{K_M} + \frac{atp}{K_T}\right) + \frac{atp}{K_T} + \frac{i}{K_i}} \quad (4.21)$$

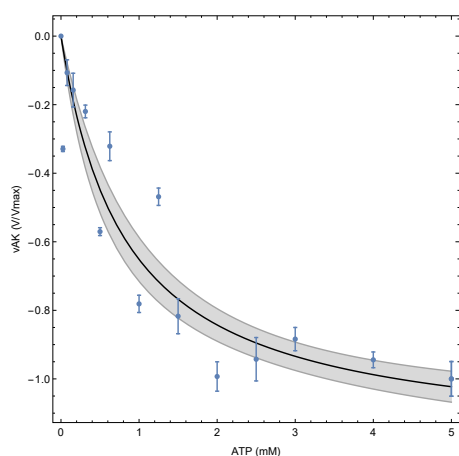
After fitting eq. 4.21 to the experimental data set, Figure 4.8 (a), (b), (c) and (d) was obtained. These fits immediately appear better than the completely random mechanism (eq. 4.19). The sum of squared differences when fitting eq. 4.21 to the data was of 0.6741 and an adjusted R^2 value of 0.9815 (see table 4.2). The fitted parameters are displayed in Table 4.1.



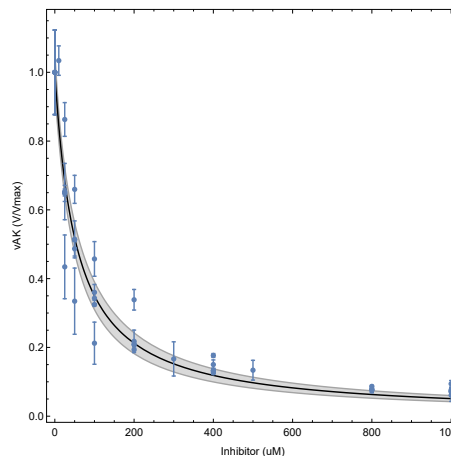
(a) Adenylate kinase rate against the concentration of the substrate ADP



(b) Adenylate kinase rate against the concentration of the substrate AMP



(c) Adenylate kinase rate against the concentration of the substrate ATP



(d) Adenylate kinase rate against the concentration of the inhibitor Ap5A

Figure 4.8: Spatio-temporal mechanism fitted rate equation 4.21 (black curve) to the data for all adenylate kinase substrates ADP (a), AMP (b), ATP, (c) and the inhibitor Ap5A (d). Error bars show the standard error. The shaded areas indicate the 95% confidence interval.

4.2.4 Combination of the Iso-random and spatio-temporal Bi-Bi adenylate kinase mechanisms

Considering that both the iso random bi bi mechanism of Sheng *et al.* [39] and the spatio-temporal mechanism had similar evaluations for their respective sum of squares and adjusted R^2 values, it is of interest to explore what a combination of the two mechanisms might yield. Using the concept that the isoforms from Figure 4.5 bind separate substrates, 1E binds only ADP and 2E binds ATP, AMP and the inhibitor, we shall extend this concept to include

the ability of AMP to bind to the ADP binding sites of 1E because of its small size in comparison to the other adenosine phosphates. The resulting binding schema is presented as Figure 4.9.

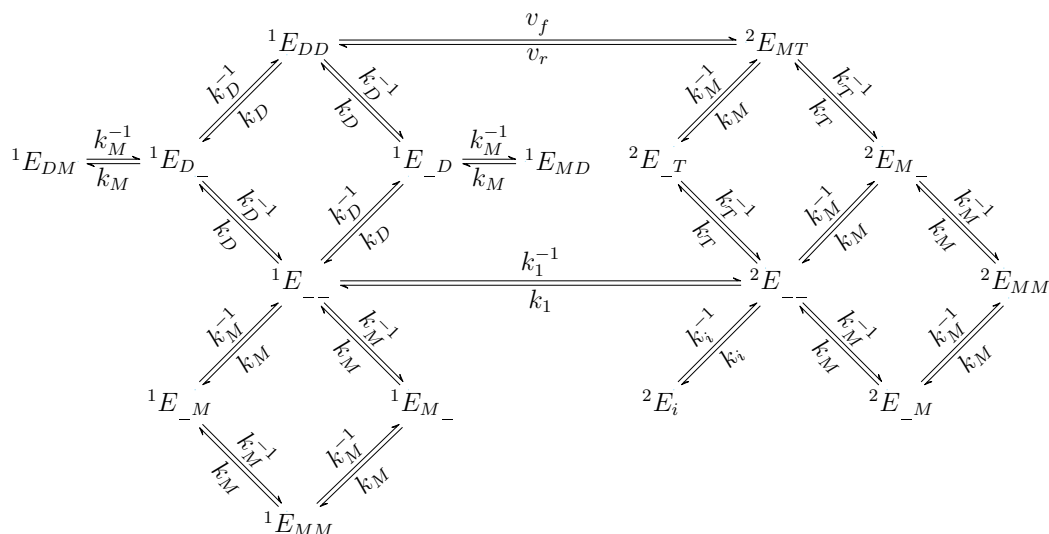


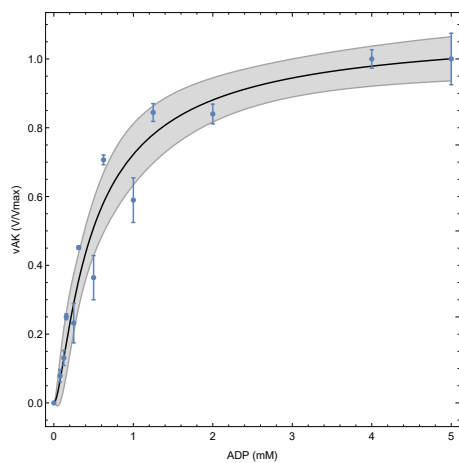
Figure 4.9: Combination mechanism. 1E and 2E indicate the two isoforms of AK. The subscript denotes the substrate bound to the enzyme (ATP: T, ADP: D, AMP: M, Ap5A: i). The position of the subscript shows which catalytic site the substrate is bound to. The dissociation constants k_T , k_D , k_M , k_i are the dissociation constants of enzyme bound ATP, ADP, AMP and Ap5A respectively.

Figure 4.9 results in the following rate equation (eq. 4.22):

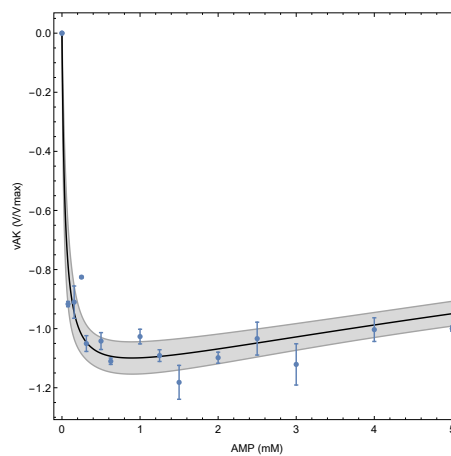
$$vAK_{comb} = \frac{V_f \frac{adp^2}{K_D^2} \left(1 - \frac{\Gamma}{K_{eq}}\right)}{1 + \frac{1}{K_E} + \frac{adp}{K_D} \left(2 + \frac{adp}{K_D} + 2 \frac{amp}{K_M}\right) + \frac{amp}{K_M K_E} \left(2 + \frac{atp}{K_T} + \frac{amp}{K_M}\right) + \frac{amp}{K_M} \left(2 + \frac{amp}{K_M}\right) + \frac{1}{K_E} \left(\frac{atp}{K_T} + \frac{i}{K_i}\right)} \quad (4.22)$$

After fitting equation 4.22 to the experimental data set we get Figures 4.10 (a)-(c). The fitted equation yields a sum of squared differenced value of 0.6751 and an adjusted R^2 value of 0.9812 (Tab. 4.2). The fitted parameters are displayed in Table 4.1.

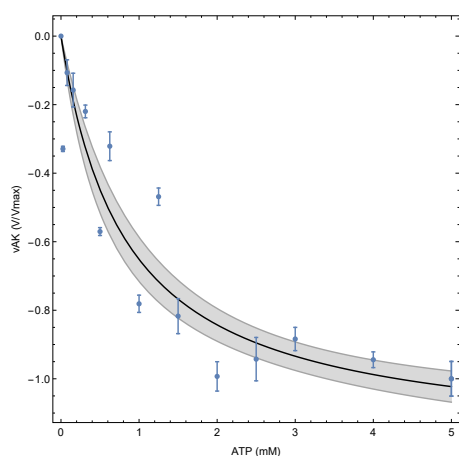
Of the 4 mechanisms constructed and fitted, the completely random mechanism (Figure 4.3) performed the worst. The remaining 3 mechanisms which were all based on the published mechanism by Sheng *et al.* (Figures 4.5-4.9)



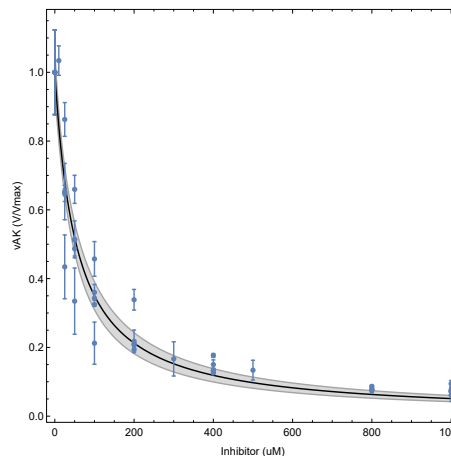
(a) Adenylate kinase rate against the concentration of the substrate ADP



(b) Adenylate kinase rate against the concentration of the substrate AMP



(c) Adenylate kinase rate against the concentration of the substrate ATP



(d) Adenylate kinase rate against the concentration of the inhibitor Ap5A

Figure 4.10: Combination mechanism fitted rate equation 4.22 (black curve) to the data for all adenylate kinase substrates ADP (a), AMP (b), ATP, (c) and the inhibitor Ap5A (d). Error bars show the standard error. The shaded areas indicate the 95% confidence interval.

were quite close in terms of their sum of square and R^2 values. Using the Akaike Information Criterion, the spatio-temporal mechanism (Figure 4.7) was chosen as the optimal fitting mechanism [39]. This does not however, mean that the spatio-temporal mechanism is the correct kinetic mechanism for AK, but for the purpose of this thesis, it was the best candidate and according to AIC produced the best fit to the data. The results from this section, §4.2 are used again in section 4.4.2 when the mathematical model of glycolytic oscillations is analysed. The following section, §4.3, focuses on the experimental induction and analysis of the glycolytic oscillations in cell free extracts.

Table 4.1: Table of fitted parameters K_M, K_D, K_T, K_E and K_i for each AK rate equation.

Eqn.	Model Predictions				
	K_T (mM)	K_D (mM)	K_M (mM)	K_E	K_i (μ M)
4.19 vAK_{rand}	14.9×10^{-6}	0.235	5.17×10^{-6}	-	0.108
4.20 vAK_{iso}	0.01	0.231	0.0460	12.7	0.008.60
4.21 vAK_{spatio}	0.00842	0.235	0.0410	-	0.108
4.22 vAK_{comb}	0.00124	0.226	0.0410	5.80	0.0174

Table 4.2: Table of the sum of squares (SS) of each adenylate kinase rate equation as well as the adjusted R^2 values, corrected AIC (AIC_c), the differences in AIC with regards to the best candidate (Δ_i) and the Akaike weights (ω_i)

Eqn.	SS	R^2	AIC_c	Δ_i	ω_i
4.19 vAK_{rand}	1.896	0.9479	-72.358	91.0039	$\ll 0.005$
4.20 vAK_{iso}	0.6764	0.9812	-160.563	2.79961	0.1628
4.21 vAK_{spatio}	0.6741	0.9815	-163.362	0	0.6599
4.22 vAK_{comb}	0.6751	0.9812	-160.734	2.62856	0.1177

4.3 Experimental induction and analysis of glycolytic oscillations in yeast cell free extracts

Glycolytic oscillations are dependent on the influx of glucose to the system. Stable limit cycle glycolytic oscillations lie between two supercritical Hopf bifurcations which are located at the minimum and maximum glucose influx rates that allow for oscillations to occur. Yeast whole cells have membrane proteins which transport glucose into the system and these transporters limit the rate at which glucose can enter the cell. For cells which have been treated appropriately i.e. harvested at glucose diauxic shift followed by a 2 hour starvation period, the glucose influx rate lies between the two Hopf bifurcations and limit cycle glycolytic oscillations are observed. However, in cell free extracts the membrane and its proteins have been removed. Any glucose added to the extract is quickly utilised by hexokinase and glycolytic oscillations are not observed as the influx rate is too large (i.e. not limited by glucose transport capacity) and the glucose influx rate lies to the right of the second Hopf bifurcation. So instead a glucose injection technique is used. This section describes how the glycolytic oscillations were induced using both trehalose and glycogen as well as discusses some of the difficulties in these techniques. This is followed by the experimental inhibition of adenylate kinase during these oscillations.

4.3.1 Inducing and controlling glycolytic oscillations

Much like whole cells, for a yeast cell extract to be able to oscillate it must be harvested at the right moment. The optimal conditions arise at around the point of diauxic shift where the cells run out of glucose. This is easily determined using urine test strips that can detect the presence of glucose. Once at diauxic shift the cells are washed and starved for up to 2 hours so as to remove as many metabolites from the cell as possible. It is from these cells which have the correct phenotypic make-up that the cell lysate is made. This procedure to prepare the cells for glycolytic oscillations is important for whole cells to display oscillations and this is true for the cell free extracts as well. When the cell were harvested too late after the diauxic shift or not washed properly, oscillations were not inducible. One of the most important criteria for a yeast extract to oscillate is that it must have a relatively high protein concentration, this can range from around 10 - 20 mg/ml. This makes lysis of the cells tricky as only a small amount of buffer can be added, and therefore the sample heats up easily during lysis, and the cells must be kept cool during lysis to reduce the amount of enzymatic degradation. A protease inhibitor can be added to the cell extract such as PMSF, although we found that oscillations occurred in the samples that did not contain PMSF, so a protease inhibitor was not used. The cells were lysed using both sonication and glass beads. We thought that sonication may be a more gentle technique to lyse the cells and reduce enzyme damage from collisions with glass beads and the sample could be kept in ice during the sonication process, however the sonication technique yielded consistently lower protein concentrations than glass beads. A glass bead lysis was therefore used. To induce oscillations, glucose must be supplied to the extract at a constant rate. To control the influx of glucose to the system a secondary glucose source can be utilised (a source which releases glucose molecules at a steady rate from within the extract). There are two easily accessible candidates for this method, (1) glycogen and (2) trehalose, both of which are broken down by yeast to glucose.

The most common oscillations that occurred, only lasted for about 2-3 cycles, after which we could not induce longer periods of oscillations. Even with the re-addition of trehalose the extract would oscillate with the same amount of cycles, and this was not a case of running out of glucose as there was still trehalose left in the extract after the oscillatory cycles. It was thought that maybe the phosphates became limiting as the cells were only diluted by a very small amount with 100mM phosphate buffer before lysing (100 μ L buffer per 1 g cells wet weight). We attempted to use a 1M phosphate buffer when lysing the cells, but there was no apparent difference in oscillations.

The most important realisation was that with the addition of trehalase to the cell extract oscillations occurred almost every time, as long as the extract was prepared properly. This may mean that the most common problem with the extracts was that the expression of trehalase was too low to observe oscil-

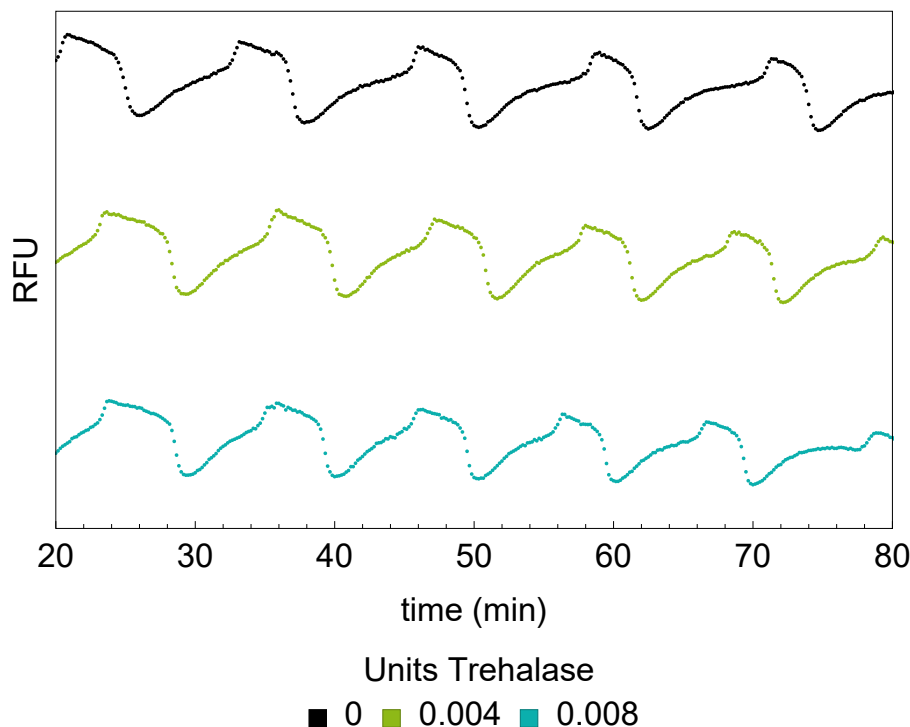


Figure 4.11: Experimentally induced oscillations using trehalose as a carbon source and adding varying amounts of trehalase enzyme. The oscillations were observed using NADH fluorescence over time.

lations. Figure 4.11 nicely demonstrates how these oscillations are visualised and also shows the effect of adding trehalase to a cell extract, even though this cell extract was able to oscillate without the addition of exogenous trehalase. By increasing the amount of trehalase added to the extract we essentially increase the rate at which glucose enters the glycolytic system and so an increase in trehalase causes an increase in frequency. Approximately 8 mU of trehalase were added for each experiment yielding glycolytic oscillations with an average period time of around 10 minutes.

Glycogen was also used to induce glycolytic oscillations, but this was not more reliable (more often it was less reliable) than the trehalose method. We did not attempt to add exogenous phosphorylase-b to the extract to try and regulate the glucose influx, however this may be a valid method to increase the glucose influx when using glycogen, as phosphorylase-b was measured to have a lower activity than phosphoglucomutase in the cell extract. Phosphoglucomutase is necessary to convert the glucose 1-P produced by phosphorylase-b to glucose 6-P, at which point it can enter glycolysis. Figure 4.12 shows glycolytic oscillations induced using glycogen as a carbon source.

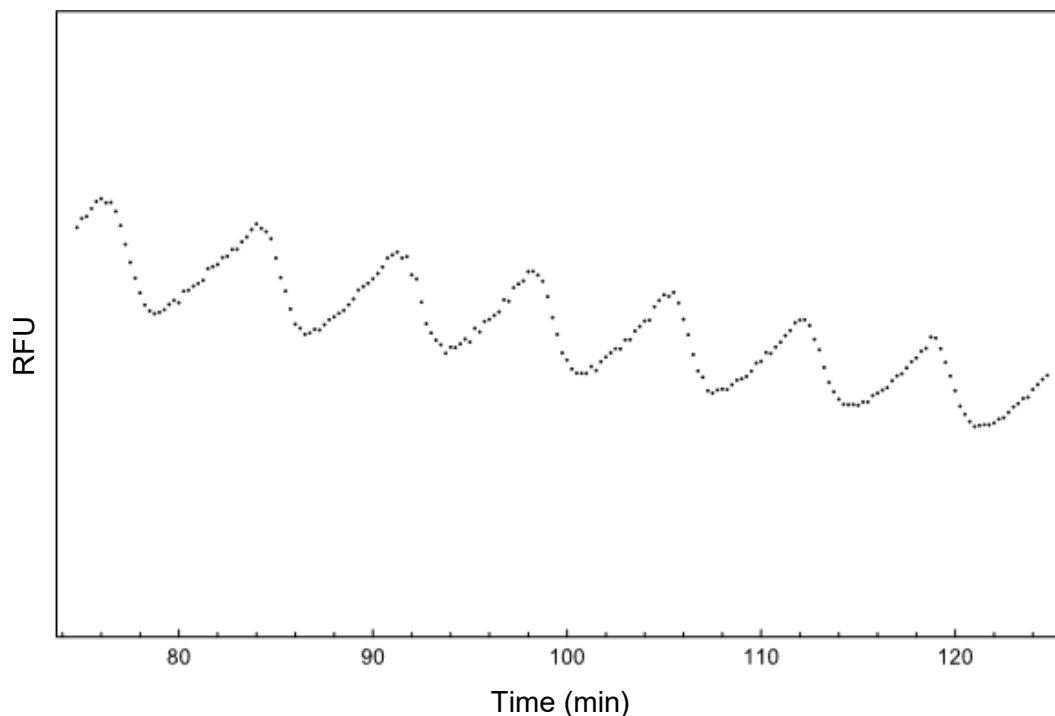


Figure 4.12: Experimentally induced oscillations using glycogen as a carbon source. The oscillations were observed using NADH fluorescence over time.

4.3.2 Inhibiting adenylate kinase during glycolytic oscillations

After glycolytic oscillations were induced using trehalose as the carbon source, varying amounts of adenylate kinase inhibitor (Ap5A) were added to the cell extract and the NADH fluorescence was recorded over time. Figure 4.13 shows an example of such an inhibitor (Ap5A) titration. When adding the inhibitor to the cell extract only 1 μ L of a concentrated inhibitor solution was added so that the final concentrations in the extract were the concentrations displayed in Figure 4.13. Only 1 μ L of buffer was added to the control (0 μ M Ap5A) so the volume increase amongst the extracts remained constant. We plot the oscillations so that they are in the same phase at $t = 0$, however, the addition of the inhibitor causes a phase shift in the oscillations with higher concentrations causing a larger phase shift. In comparison to the control (0 μ M Ap5A) the frequency of the oscillations decreases with increasing inhibitor concentrations. There is also a very slight decrease in amplitude. Hence, as the activity of adenylate kinase decreases, so does the frequency. There also appears to be a limit to which adenylate kinase can be inhibited before oscillations cease.

To compare the effect of the inhibitor on various cell extracts which have slightly varying frequencies in the absence of inhibitor, after addition of the

inhibitor, the change in period with respect to the control can be converted to fractional change in period. This fractional change in period can then be plotted with the adenylate kinase activity or fractional adenylate kinase activity using the rate equation 4.21 developed in §4.2.3. This results in Figure 4.14 when the percentage increase in period time of the oscillations is plotted against the percentage adenylate kinase activity.

From Fig. 4.14 it is now clear that a decrease in adenylate kinase activity results in an increase in period time. While the magnitude of the effect that inhibiting adenylate kinase has on the oscillations differs amongst extracts, the proportional change in period time in relation to the control is more consistent. Because various cell extracts have varying protein concentrations, the overall inhibition of Ap5A in one cell extract will not necessarily be the same as with another cell extract prepared separately. As mentioned previously there seems to be a threshold of adenylate kinase activity with which oscillations will occur. The threshold (according to fig 4.14) lies loosely somewhere below 20% adenylate kinase activity. This is also where the standard error of the data starts to increase dramatically.

With the data presented so far it is possible to calculate the control of AK on the frequency of the oscillations. The control is determined by calculating the control coefficient,

$$C_j^i = \frac{\partial \ln i}{\partial \ln j} \quad (4.23)$$

which represents the % change in i caused by a 1% change in j . By plotting both the % AK activity and % frequency against the inhibitor concentration we can calculate the control coefficient, $C_{AK}^{frequency}$, by finding the ratio of the two slopes at 100% AK activity (Figure. 4.15).

$$C_{AK}^{frequency} = \frac{d \%frequency}{d \%AK} = \frac{d \%frequency}{d[inhibitor]} \times \frac{[inhibitor]}{d \%AK} \quad (4.24)$$

The gradients at 100% AK activity were determined using the fitted eqn. 4.21 for the AK vs inhibitor data, and a generic fitted hyperbola equation for the frequency vs inhibitor data. The control for the AK on the frequency was calculated to be 0.072.

4.4 Model predictions of the effect of adenylate kinase on glycolytic oscillations

4.4.1 Analysing the dupreez6 model

The dupreez6 model of glycolytic oscillations employs the adenylate kinase reaction as an equilibrium reaction (eq. 4.25) and has no term describing the

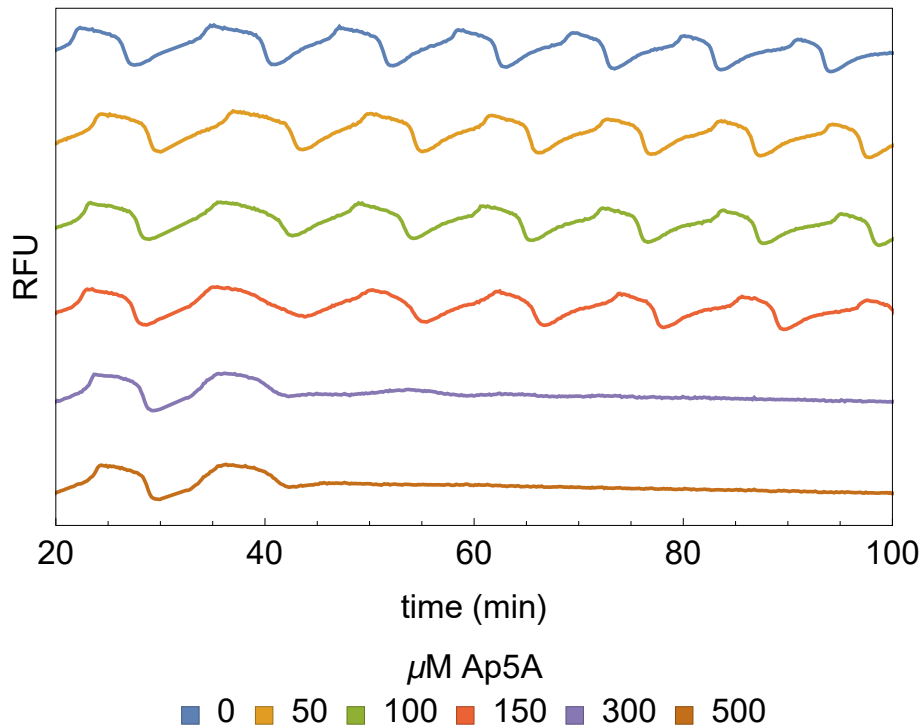


Figure 4.13: Effect of adenylate kinase inhibitor (Ap5A) titration on glycolytic oscillations. Glycolytic activity was measured using fluorescence and recorded as relative fluorescent units (RFU). The inhibitor was added at approximately 40 min to an already oscillating cells extract.

effect of the inhibitor Ap5A.

$$vAK_{dupreez6} = AK_{opt} \text{biomassFac} \left([adp]^2 - \frac{[amp][atp]}{K_{eq}AK} \right) \quad (4.25)$$

Where AK_{opt} represents a rate constant, biomassFac the scaling of the protein concentration and $K_{eq}AK$ is the equilibrium constant of adenylate kinase. Because this eq. 4.25 has no inhibition term, to simulate the effect of an adenylate kinase inhibitor in the dupreez6 model as published, we can simply multiply the rate constant by the fractional activity of enzyme due to inhibition. The fractional activity for a specific inhibitor concentration can be calculated using rate equation 4.21. Note that the concentration of ATP, ADP and AMP are fixed at their uninhibited state values.

$$F_i = \frac{vAK_{spatio, [i] = [Ap5A]}}{vAK_{spatio, [i] = 0}} \quad (4.26)$$

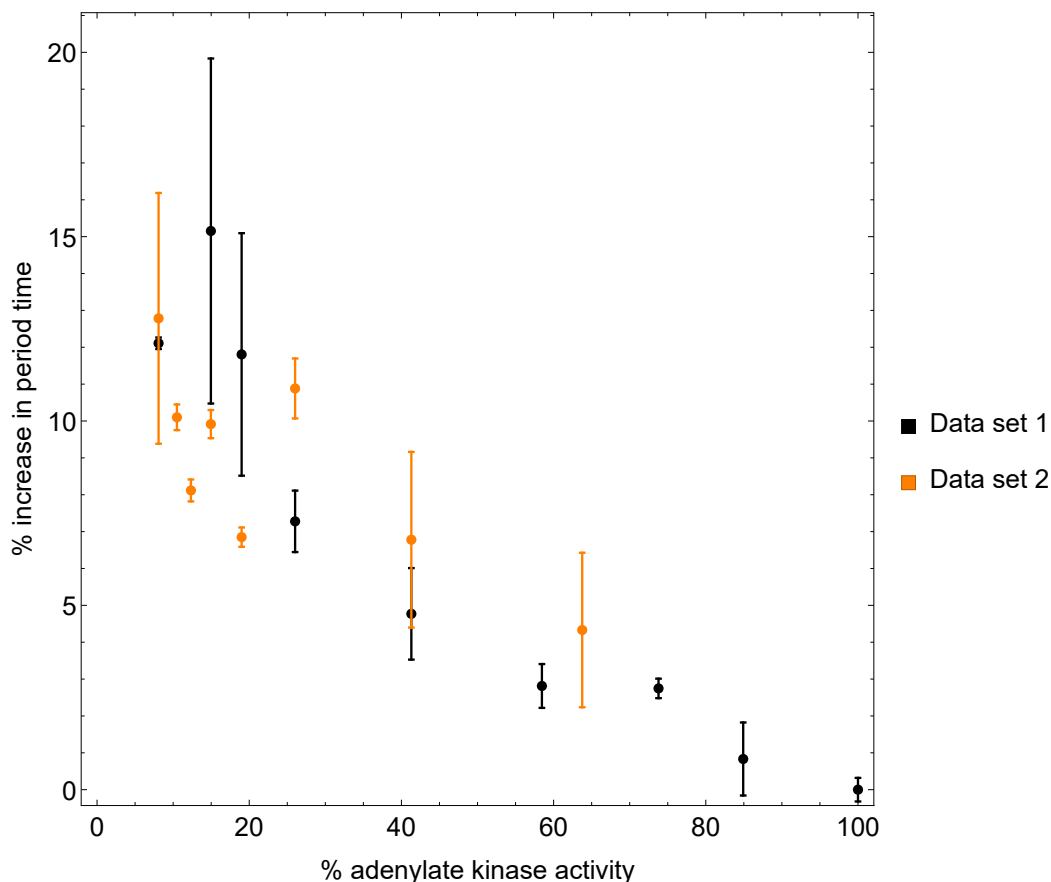


Figure 4.14: Data showing the fractional increase in period time in relation to the fractional adenylate kinase activity

F_i is the fractional activity of adenylate kinase at a specific Ap5A concentration. F_i becomes 1 if there is no inhibitor and tends to zero as Ap5A gets very large ($[i] \gg 1000 \mu\text{M}$). Experimentally the inhibition of adenylate kinase by Ap5A never reaches 100% (AK activity = 0), but we can reduce the adenylate kinase activity to zero using the mathematical model. With equation 4.26 the model description for adenylate kinase then becomes:

$$vAK_{model} = F_i vAK_{dupreez6} \quad (4.27)$$

Except for the inclusion of the fractional activity to the adenylate kinase rate equation, all other equations and variables in the model were kept the same as when published. By varying the fractional activity from 0 to 1 and recording the period time of the simulated oscillations, Figure 4.16 (red curve) is the result. When the graph shows 100% AK activity, it indicates the wild type (WT) or control, when there is no inhibitor present. The enzyme is free to operate at its full capacity. The 100% AK activity was experimentally measured to be approximately 3030 U/mg protein. The trend for the model is similar to the trend in the data and as the activity of adenylate kinase

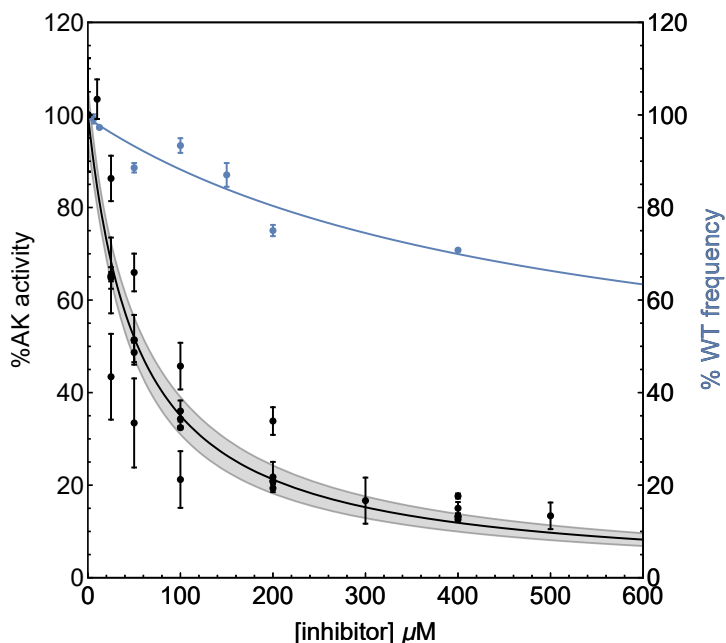


Figure 4.15: %AK activity plotted alongside the %frequency, both against the inhibitor concentration ([Ap5A]). The ratio of the slopes at 100% AK activity is indicative of the control coefficient of AK on the frequency. Full data sets can be found in Figure 4.8 (d) and Figure 4.14.

decreases, the fractional increase in period time increases as well. The increase in period is small when adenylate kinase activity is relatively high (above 50%), but the change becomes larger when adenylate kinase activity is low.

The dotted blue curves in Figure 4.16 are model simulations of the same inhibitor titration, but with the model parameters for the adenylate kinase activity and protein concentration as determined experimentally. The glucose influx rate was then also altered so that the period of the modelled simulations matched the experiments. The two dotted blue curves represent the upper and lower bound of these simulations which have had their parameters altered to be closer to the experimental conditions.

Overall, the `dupreez6` model follows the same trend as the data. As the activity of adenylate kinase decreases there is a notable increase in the period of the oscillations. There still appears to be a threshold of adenylate kinase activity for which these oscillations will exist, at approximately 10% AK activity according to the simulations.

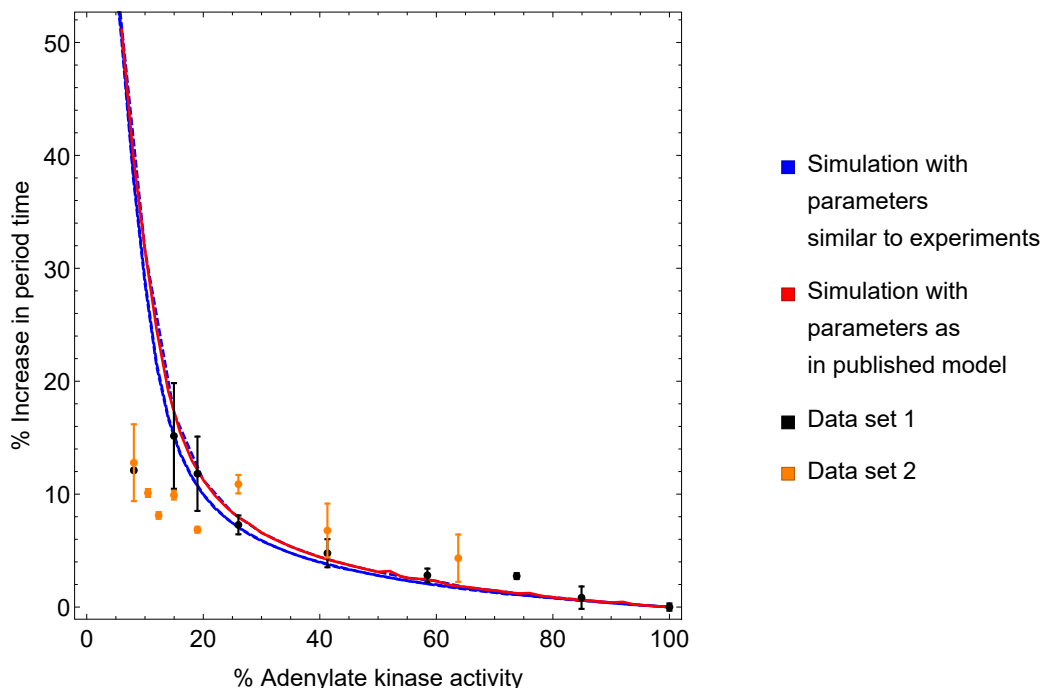


Figure 4.16: Model simulations of the dupreez6 model (solid and dashed curves) showing the fractional increase in period time in relation to the fractional adenylate kinase activity plotted with the experimental data (black and orange dots). Experimentally, 100% AK is indicative of the control where no inhibitor was added and the enzyme functions as the wild type.

4.4.2 Including a mechanistic description of adenylate kinase into the dupreez6 model

From the adenylate kinase mechanisms produced in §4.2 the spatio-temporal model (eq. 4.21) had the best AIC_C score (Table 4.2). Therefore the spatio-temporal mechanism (eq. 4.21) was chosen to be included in place of the AK equilibrium reaction (eq. 4.25) in the dupreez6 model. The V_{max} for AK (100% AK activity) was recorded to be approximately 3030 $\mu\text{mol}/\text{min}/\text{mg}$ protein and this was reflected in the model. The subsequent model with eq. 4.21 is further referred to as the vanwyk1 model for the sake of clarity. It was then possible to include the inhibitor Ap5A in the overall model simulations using the vanwyk1 model. However, the inhibitor concentration was not used in the model simulations to reduce the activity of AK. Instead, when inhibiting AK in the vanwyk1 model, AK was multiplied by the same fractional activity as in the dupreez6 model simulations.

The trend of the simulation is very similar to the data (Figure 4.17). Keeping in mind that the curve is not fitted to the data, but instead predicts the

data. The dotted blue curves in Figure 4.17, much like Figure 4.16 represent the upper and lower limits of the simulations where the adenylate kinase rate, protein concentration and the glucose influx parameters were altered to be similar to those that were experimentally recorded. The glucose influx rate was altered so that the frequency of the oscillations simulated by the model for the non inhibited rate was the same as the frequencies experimentally observed. We are uncertain about the actual glucose influx rates, however we did estimate the influx rate by assaying trehalase activity. This estimation was at least 2 fold lower than the rate necessary for the frequency to be identical in the model and experiment for the non-inhibited state. It is possible that glycogen stores in the yeast may provide an alternate glycolytic substrate. The dotted blue curves follow the same trend as the red curve and the data, although the apparent threshold of adenylate kinase activity for the oscillations lies more to the right.

From Figure 4.17 we can determine the control of adenylate kinase on the period time of the oscillations. As shown previously, the control coefficient can be obtained by calculating the gradient of the model at 100% AK activity, as shown on the inset in Figure 4.17, the control coefficient is $C_{AK}^{period\ time} = -0.027$. The control of AK on the period time is negative because a decrease in AK activity causes an increase in period time and vice versa. This is comparable to the control of AK on the frequency (0.072). According to the control coefficients calculated, a 1% decrease in adenylate kinase activity results in a 0.027% increase in period time and a 0.072% decrease in frequency. In principle, the magnitude of these two control coefficients should be the same since frequency = 1/period, however, because the one was calculated using a fit to data and the other using a model prediction, the magnitudes are slightly different.

This brings us to the end of the results section for this thesis. Chapter 5, discusses these results in relation to the model analysis and the current literature and present some conclusion.

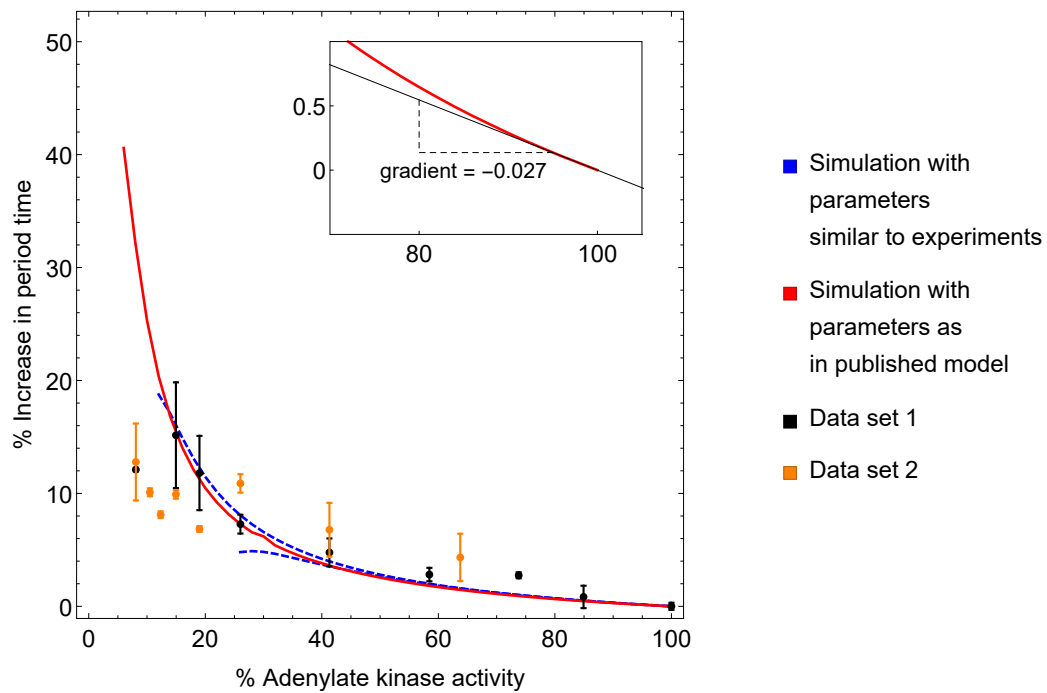


Figure 4.17: Model simulations of the vanwyk1 model (solid and dashed curves) showing the fractional increase in period time in relation to the fractional adenylate kinase activity plotted with the experimental data (black and orange dots). Experimentally, 100% AK is indicative of the control where no inhibitor was added and the enzyme functions as the wild type.

Chapter 5

General Discussion and Conclusion

This chapter discusses the results of this study and places them in context with what has already been published. Firstly I will discuss the adenylate kinase kinetics results. This is followed by a discussion on the experimental oscillations and model predictions and an attempt to give a mechanistic interpretations of these results using model analysis. I will end with the conclusions of the thesis revisit the research questions posed in the introduction. Finally I will make some suggestions for future research.

5.1 Adenylate kinase kinetics

To decouple ATP and AMP in the model analysis of the glycolytic oscillations, a detailed description of adenylate kinase was needed to be included in the model. However, it was not within the scope of this study to derive what could be considered to be the correct mechanism of AK. We needed a simple, but sufficiently accurate kinetic description of AK which fitted the experimental data. For the data analyses that follow, it is important that the kinetic mechanism used for the analysis behaves as the data would.

In §4.2 various kinetic mechanisms were derived for AK and fitted to a set of experimental data. The predictions for each of the four kinetic equations are shown in Figures 4.4, 4.6, 4.8 and 4.10 and the estimated parameters are shown in table 4.1. The completely random mechanism (eq. 4.19) shows what looks like a good fit for ADP and inhibitor vs rate curves (Figure 4.4 (a) and (d) respectively). However, the curve of ATP vs rate shows an almost linear relationship which is contrary to the data (Figure 4.4 (c)). There is also an incorrect estimation on the behaviour of AMP vs rate. The rate is quite sensitive to the AMP concentration, more than the data indicate (Figure 4.4 (b)), which may be related to an underestimation of the K_M (AMP dissociation constant). This underestimation of the K_M ultimately affects the ATP vs substrate curve, and the fits of K_M and K_T are not totally independent. For the rest of the AK mechanisms (eqs 4.20, 4.21 and 4.22) the rate vs substrate

curves match the data more closely, especially the AMP and ATP substrate curves. Judging by eye, it may be clear that the completely random binding order would not be sufficient to describe the AK kinetics, and this is proven true as the completely random binding order mechanism showed the highest sum of squared differences after fitting (SS) at ≈ 2.21 (table 4.2). Also, the AIC analysis predicted the completely random mechanism to have the lowest probability ($\ll 0.005$) of being the most likely mechanism to correctly describe the data (Table 4.2).

The iso-random, spatio-temporal and combination mechanisms showed better fits than the random mechanism, but compared to one another had very similar SS values of ≈ 0.67 and adjusted R^2 values of ≈ 0.98 (table 4.2). The predicted K_D (ADP dissociation constant) values of these three mechanisms is very close at ≈ 0.23 mM which is comparable to the study of Russel *et al.* which predicts a K_m (Michaelis constant) for ADP at 0.27 mM [41]. However, another study from Sheng *et al.* predicts a K_m value for ADP 10-fold lower at 0.027 mM [39]. It should be noted that we assume that the dissociation constants are comparable to the Michaelis constants which have been published in the literature. The predictions for the AMP dissociation constant for the iso-random, spatio-temporal and combination mechanisms were also quite close at approximately 0.032, 0.041 and 0.041 mM respectively. This is again comparable to the K_m of AMP recorded by Russel *et al.* (0.058 mM) but is not similar to that which was predicted in the study of Sheng *et al.* (0.12 mM) [41; 39]. AMP was the only substrate which showed some inhibitory behaviour at higher concentrations in the experiments. The smaller predictions for the K_M (AMP dissociation constant) value of AK makes inhibition by AMP more probable, especially in cases where AMP is able to bind to already bound enzyme-substrate complexes. The predicted values for K_T for all the mechanisms, except the iso-random mechanism (14.9×10^{-6} , 0.00842, 0.00124 mM (Table 4.2)) are all at least approximately 10-fold lower than the those in the study of either Russel *et al.* or Sheng *et al.* (0.054 and 0.06 mM respectively). For the predicted K_i values we get similar values when comparing the completely random mechanism with the spatio-temporal mechanism. This is most likely because K_i is independent of any other parameters in these equations unlike the iso-random and combination mechanisms which both feature the K_E variable which is always multiplied to K_i . The study by Sheng *et al.* predicts the K_m of Ap5A to be 0.002 μ M which is not comparable to either of the predicted K_i values predicted in this study. However, it is mentioned in a study by Cohn *et al.* [42] the dissociation constant for Ap5A is 0.2 μ M which is more comparable to the values predicted in the completely random and spatio-temporal mechanisms.

As the sum of squares and R^2 values for the iso-random, spatio-temporal and combination mechanisms were all so close, in order to identify the best kinetic mechanism we applied AIC which gives a hierarchy for the derived mechanisms in terms of their probabilities of being the best mechanism (Ta-

ble 4.2). Of the four mechanisms, the spatio-temporal mechanism showed the highest probability for being the best mechanism (0.655). According to the AIC, the added complexity of an additional variable for the conformational isomerization of AK is not necessary in this case. The spatio-temporal mechanism is not presented as the true mechanism of AK, but rather a working mechanism that can reliably describe the behaviour of yeast AK under these conditions. The Spatio-temporal mechanism replaces the equilibrium equation in the dupreez6 model and the new model is referred to as the vanwyk1 model.

5.2 Experimental oscillations and model analysis

Upon addition of the inhibitor Ap5A to an already oscillating extract, the oscillations show first a slight phase shift followed by an increase in period time (Figure 4.13). This first phase shift is due to a slight dilution of the extract when adding the inhibitor to the experiment as the same behaviour is observed in the control where only buffer was added to the oscillating extract. In each experiment 2 μL of inhibitor (or buffer for control) was added to 50 μL of oscillating extract resulting in a dilution factor of $\frac{25}{26}$ times. The oscillations are sensitive to the protein concentration and a disturbance in this parameter causes a slight phase shift with a proportional change in frequency. Compared to the control there is a clear trend that an increase in AK inhibitor causes an increase in oscillation period time.

More interestingly, if we convert the inhibitor concentrations to the % AK activity we can then show the control that AK has over the period time of the oscillations. From Figure 4.14 we can already see that AK has a negative control on the period time of the oscillations which translate to a positive control on the frequency. As the AK activity increases we can see a subsequent decrease in period time ($C_{AK}^t < 0$) or an increase in frequency ($C_{AK}^{Hz} > 0$). The control coefficients, $C_{AK}^{period\ time\ increase}$ and $C_{AK}^{frequency}$ were calculated to be -0.027 and 0.0721 respectively. Experimentally there appears to be a threshold of AK activity that allows for the oscillations to occur. If the inhibitor concentration becomes too high, the oscillations cease and this is shown in both Figure 4.13 and 4.14.

Model simulations of the effect of AK activity on the period time show a similar trend to the data presented in Figure 4.14. Starting with the dupreez6 model (Figure 4.16) we see a small gradient at higher AK activities indicating a relatively low control on the period of the oscillations, but the absolute gradient starts to increase as the AK activity decreases indicating a higher control over the period time of the oscillations at lower AK activities. This is true for the simulation which has no altered parameters as well as for the simulations where parameters were altered to be consistent with the experiment.

The vanwyk1 model simulation in Figure 4.17 shows a slightly different result than the du Preez model in Figure 4.16. The vanwyk1 model seems to follow the data slightly closer than the simulation of dupreez6 but ultimately shows the same trend of having a low control on the period time of the oscillations at high AK activities and this control increases as the AK activity decreases.

On the basis that the model (vanwyk1) follows the trend of the data closely when inhibiting adenylate kinase we assumed that the model is correct. The model can then be used to analyse the individual contributions of ATP and AMP to the glycolytic oscillations, mainly in their influence on PFK activity. Two types of simulations were made during the analysis of the effect of AMP and ATP on the oscillations: 1) a wild type (WT) simulations where all the enzyme activities were kept at 100% and 2) a inhibited simulation where adenylate kinase activity was reduced to 5.8% which is close to bifurcation but still shows limit cycle oscillations. It should be noted that all of these investigations are done under the assumption that PFK operates as suggested by Goldbeter, in an allosteric fashion by existing in one of two states, T- or R-state [2]. This differs from the stoichiometric model by Sel'kov which relies on the stoichiometry of the reactions involved in glycolysis [24]. We do note that in the allosteric model the only source of the oscillations is the allosteric nature of PFK as given by Goldbeter, unlike the stoichiometric mode of Sel'kov. However, given the biological evidence for such an allosteric mechanism in nature, it seems the best candidate for such a study.

In the WT model simulation, the ATP-AMP phase difference is approximately -164° (Figure 5.1). This is -26° off from the expected -180° phase difference between ATP and AMP as shown by Hess and Boiteux in their illustration of the oscillations of all the glycolytic intermediates [1]. We might have expected ATP and AMP to oscillate close to 180° out of phase as this would contribute nicely to the allosteric regulation of PFK, allowing PFK to be allosterically activated and inhibited for equal amounts of time. Instead, a -164° phase difference causes PFK to be allosterically inhibited for slightly longer periods of time than it is activated, as is shown by the asymmetry in the the $R/(T+R)$ ratio in Figure 5.1. The troughs of the $R/(T+R)$ ratio in the WT simulation are far wider than its peaks. The model simulations do show that the ATP oscillation peaks still do coincide largely with the AMP oscillation troughs and vice versa as the peaks and troughs of both metabolites are relatively broad. Because the production of AMP is influenced by both ATP and ADP, which are present in both upper and lower glycolysis, this deviation from the 180° phase difference, as illustrated by Hess and Boiteux [1], may be expected. Altogether, as we show later, the phase difference between ATP and AMP may not be too important, so long as the peaks and troughs of ATP are loosely aligned with the troughs and peaks of AMP respectively.

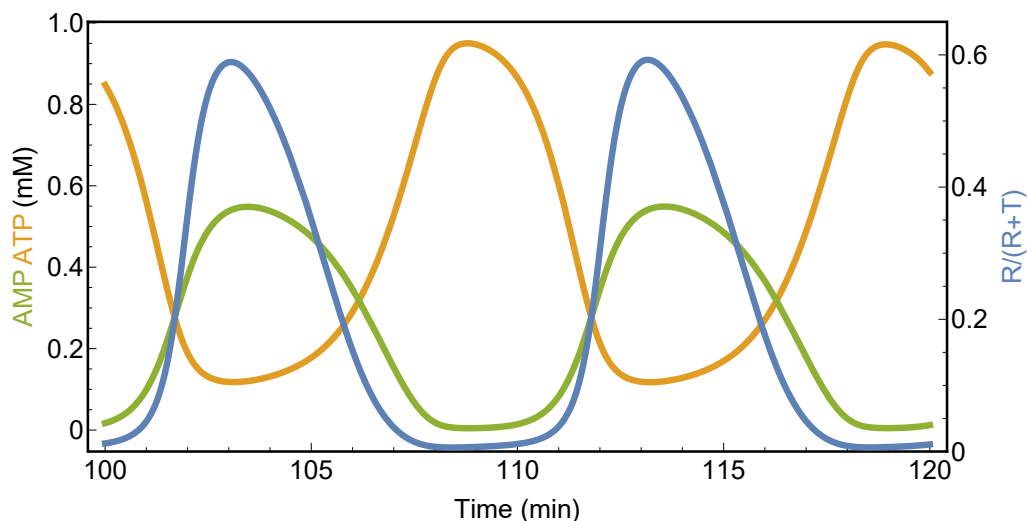


Figure 5.1: Wild type model simulation of vanwyk1 model tracing the ATP (orange) and AMP concentrations (green) over time. A corresponding PFK $R/(T+R)$ ratio (blue) is plotted along side the ATP and AMP traces.

For the inhibited model simulations where AK activity is reduced to 5.8%, the phase difference between AMP and ATP shifts from -164° to -130° (Figure 5.2). The shape of the oscillations of both ATP and AMP changes to more symmetrical peaks and troughs compared to the relatively wide and asymmetrical peaks and troughs from the WT simulations. The more sinusoidal appearance of these oscillations is likely due to the oscillations being close to Hopf bifurcation as oscillations near a bifurcation tend to be more sinusoidal. If a -180° phase difference between ATP and AMP would indicate PFK being activated and inhibited for equal amounts of time, and in the WT model the ATP-AMP phase difference of -164° showed PFK being activated for shorter periods of time than it was inhibited, we would expect that, for a 130° phase difference, PFK would be activated for an even shorter time than it is inhibited and this is shown in the $R/(T+R)$ fraction in Figure 5.2. We also see that the peaks of ATP hardly overlap the troughs of AMP and vice versa. There is also a noticeable decrease in amplitude of both the ATP and AMP oscillations when AK is reduced to 5.8%.

The main differences between the WT simulation (Figure 5.1) and the inhibited simulation (Figure 5.2) is the change in ATP-AMP phase difference as well as the change in ATP and AMP oscillation amplitude. There are obviously also differences in the $R/(T+R)$ fraction between the two simulations, but these ratios are determined from the ATP and AMP oscillations. The T- and R- states of PFK are highly dependent on the ATP and AMP concentrations

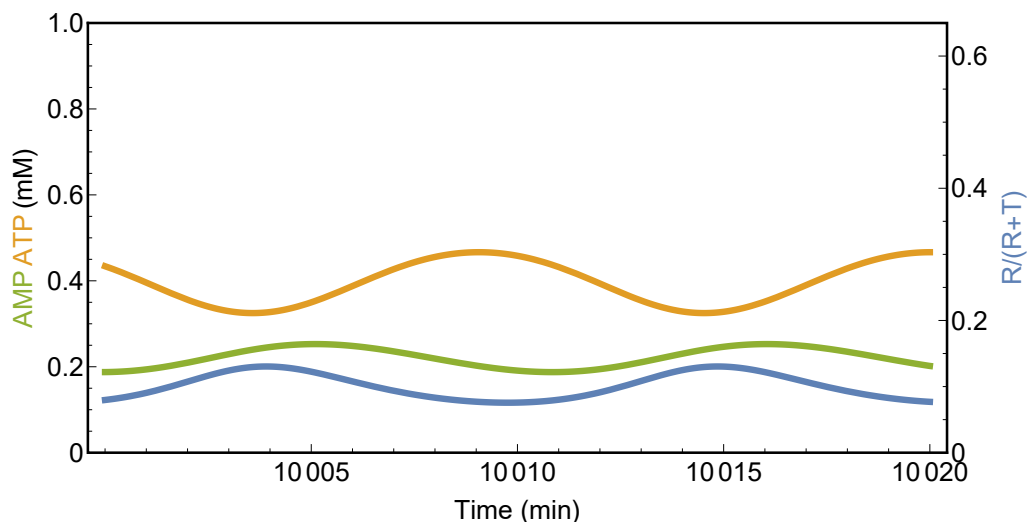


Figure 5.2: Inhibited model simulation of vanwyk1 model tracing the ATP (orange) and AMP concentrations (green) over time. A corresponding PFK R/(T+R) ratio (blue) is plotted along side the ATP and AMP traces.

in the environment. The T/R state ratio can be calculated using the following relation:

$$L_{eq} = L_0 \left(\frac{1 + \frac{C_i PFK ATP [ATP]}{K_i PFK ATP}}{1 + \frac{[ATP]}{K_i PFK ATP}} \right)^2 \left(\frac{1 + \frac{C PFK AMP [AMP]}{K PFK AMP}}{1 + \frac{[AMP]}{K PFK AMP}} \right)^2 \left(\frac{1 + \frac{C PFK F26BP [F26BP]}{K PFK F26BP} + \frac{C PFK F16BP [F16P]}{K PFK F16BP}}{1 + \frac{[F26BP]}{K PFK F26BP} + \frac{[F16P]}{K PFK F16BP}} \right)^2 \quad (5.1)$$

where L_{eq} gives us the T/R state ratio. However, it is more constructive to interpret this T/R state ratio instead as the fraction of the PFK enzyme which is in the R state (more active state), giving a means of visualising the extent of PFK activation. The fraction of PFK in the R state can be calculated using the following equation:

$$\frac{R}{T+R} = \frac{1}{1+L_{eq}} \quad (5.2)$$

Plotting this R/(T+R) fraction over time gives an indication of the extent to which PFK switches between the T and R states. Using the metabolite time

course simulations of the WT model we can see how PFK switches between the T and R states over time (Figure 5.1). We can also see from Figure 5.1 that the AMP and ATP peaks correspond to when PFK is primarily in the R and T states respectively.

As mentioned previously, we can separate the two potential causes (decreased ATP and AMP oscillation amplitude and the decreased phase difference between ATP and AMP) for the change in T and R state switching from the WT model simulation to the inhibited model simulation (Figure 5.3). To simulate the effect of a decreased phase difference between ATP and AMP on the $R/(T+R)$ fraction, the WT model was simulated and the AMP time course was replaced by a forcing function, mimicking the WT AMP but was shifted in time ($t_0 \rightarrow t_0 + x$) so that the ATP-AMP phase difference was the same as that of the inhibited model simulation where AK activity was close to bifurcation ($\phi_{ATP} - \phi_{AMP} \approx -130^\circ$). This ensures that the amplitudes of the metabolites stay the same as in the WT model and that the only change is that of the phase shift in the AMP oscillations which remain unaffected by the system. All other metabolite time courses were kept the same as when simulated by the WT model. Figure 5.3 (orange line) shows the effect of a -130° ATP-AMP phase difference on the $R/(T+R)$ ratio when all oscillation amplitudes are kept the same as in the WT model simulations. Compared to the -164° phase difference in the WT model simulation (Figure 5.3 blue line), we see a slight decrease in the amplitude of the $R/(T+R)$ ratio along with a slight phase shift. When the phase shift is combined with low oscillations amplitudes (Figure 5.3 green line), the $R/(T+R)$ ratio amplitude falls even lower. The change in phase difference between ATP and AMP has a slight influence on the extent to which PFK switches between its T and R states, but the combination of the phase shift with the reduced amplitudes causes a much larger decrease in the amplitude of the $R/(T+R)$ ratio. The reduced amplitudes of the metabolites must then have a larger effect on the T to R state switching than the phase shifts which are a result of lower AK activities.

To simulate the change in amplitude of the ATP and AMP oscillations, the oscillations were multiplied by 0.5 to reduce the amplitude by 50% in attempt to analyse the effect of amplitude on the T and R switching. In the inhibited model simulation the amplitude of AMP and ATP drop to less than half of the WT model simulation (Figure 5.2). Figure 5.4 shows simulations of the WT model with a 50% reduction in amplitude for either only ATP, only AMP or both ATP and AMP. Figure 5.4 shows the effect of a reduced ATP and AMP amplitude on the T and R switching of PFK. Calculating the $R/(T+R)$ ratio for the WT simulation, but reducing the AMP amplitude to half of its WT amplitude, there is a relatively large decrease in the amplitude of the $R/(T+R)$ ratio (Figure 5.4 orange line) when compared to the WT simulation (Figure 5.4 blue line). Alternately, when reducing the ATP amplitude to half of its WT amplitude we reduce the inhibitory effect of ATP on PFK and there is an increase in the $R/(T+R)$ ratio amplitude (Figure 5.4 green line). When

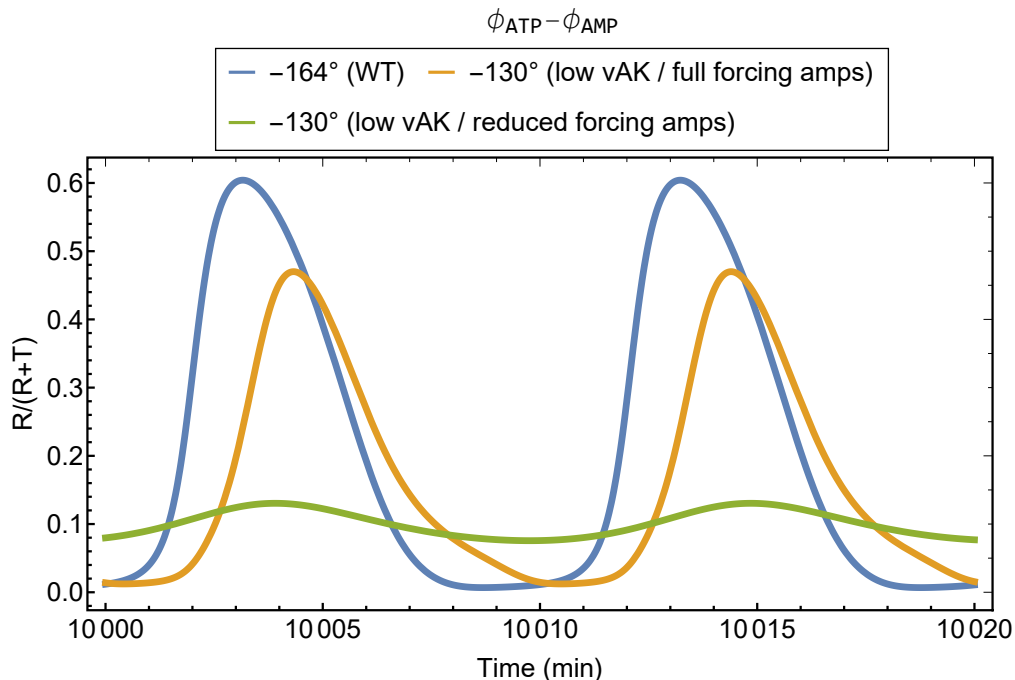


Figure 5.3: The $R/(T+R)$ ratios of PFK over time plotted according to the corresponding phase differences between ATP and AMP ($\phi_{\text{ATP}} - \phi_{\text{AMP}}$). The WT simulation is shown in blue and the inhibited simulation is shown in green. The orange shows the effect of an AMP phase shift but with the amplitude the same as in the WT model simulation

reducing the AMP amplitude by 50% we decrease the extent to which AMP can activate PFK and so the fraction of PFK in the R state is diminished. Interestingly, when the amplitudes of both ATP and AMP are reduced to 50% (Figure 5.4 red line), there is an increase in the $R/(T+R)$ ratio amplitude. This result was unexpected as the ratio of ATP to AMP was essentially unchanged. We also see that for the simulations in Figure 5.4, they all reach the same minimum irrespective of the changes made to the amplitudes of either ATP or AMP and this is because the ATP-AMP phase difference remains constant. This shows that the AMP to ATP ratio is indeed responsible for the extent of the PFK activation, but at the low AMP concentrations and high ATP concentrations, ATP inhibition is strong enough to fully inhibit PFK.

From what we've seen so far, ATP could be responsible for the shape and frequency of the $R/(T+R)$ ratio oscillations, but AMP has a larger influence on the amplitude of these $R/(T+R)$ oscillations. As shown in Figure 5.3 and 5.4. When the amplitude of the AMP oscillations is kept the same as in the WT simulation, the amplitude of the $R/(T+R)$ ratio stays relatively high (Figure 5.3), but when the AMP amplitude is reduced, the amplitude of the $R/(T+R)$ ratio decreases, sometimes to the state of near non-existence (Figure 5.3 and 5.4).

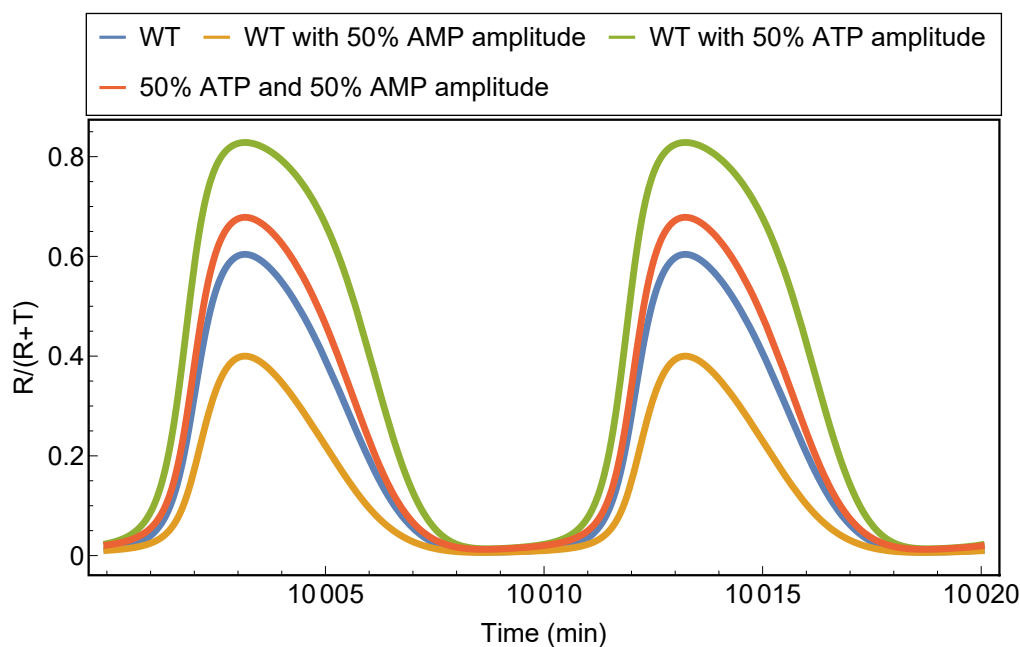


Figure 5.4: The effect of ATP and AMP amplitude on the T and R state switching of PFK.

We have explored how the reduction of adenylate kinase activity affects the AMP and ATP oscillations which in turn affects the T and R state switching of PFK ($R/(T+R)$). Next we investigate how the diminished T to R state switching, as simulated in the inhibited model simulation, affects the oscillations in the model as a whole. To do this the WT model was simulated, but the T and R state switching was altered to that of the inhibited model. L_{eq} was implemented as a forcing function. PFK was, in a sense, blind to the ATP and AMP within the WT model itself and saw only the ATP and AMP traces of the inhibited model. Figure 5.5 shows the effect on the oscillations of AMP for the WT model with WT T and R state switching, and for the inhibited T and R state switching. Figure 5.6 shows the same but for the ATP oscillations. In both simulations, when PFK was forced to act as though adenylate kinase was inhibited, the oscillations were reduced in amplitude and frequency.

We've shown that a change in AK activity changes the oscillations in both ATP and AMP which affects the T and R states of PFK. Figure 5.5 and 5.6 shows how the change in T to R state switching affects the oscillations as a whole. When the WT T and R switching in the model is replaced with the attenuated T and R switching which is obtained by inhibiting AK to 5.8%, the oscillations of the metabolites decrease in amplitude and frequency. In these simulations all metabolites and enzyme activities were as in the WT model simulation, but the PFK rate was replaced by the inhibited PFK rate where AK was inhibited to 5.8% activity. This results in PFK switching not

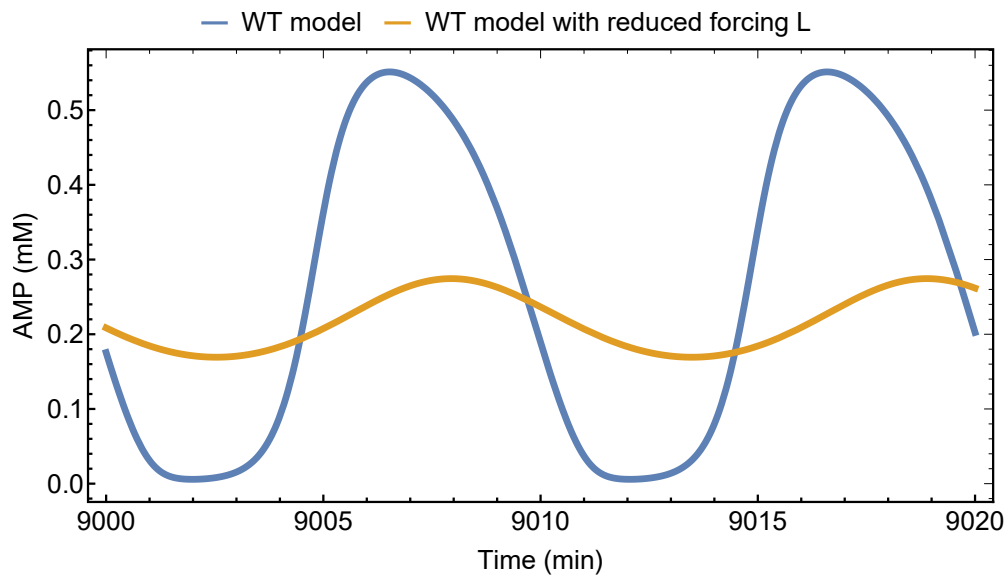


Figure 5.5: AMP oscillations simulated by the vanwyk1 model with WT T to R switching over time (blue) and with the inhibited T to R switching (orange)

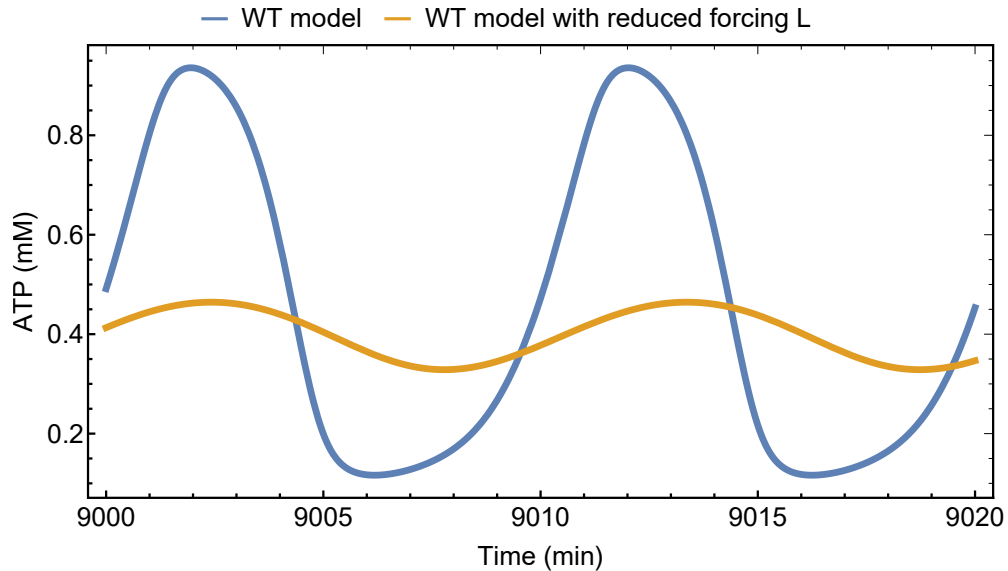


Figure 5.6: ATP oscillations simulated by the vanwyk1 model with WT T to R switching over time (blue) and with the inhibited T to R switching (orange)

being affected by the metabolite signals from the WT model simulation, but all substrates and products still respond to model variables. PFK acts as if it were a part of the inhibited model simulation. We can then deduce that the change in amplitude and frequency of the oscillations can be caused directly from a change in the T/R switching of PFK which is induced by relative changes AMP and ATP phase and amplitude by adenylate kinase.

5.3 Conclusion

With the inclusion of a detailed rate equation of adenylate kinase, the model of glycolytic oscillations follows the data closely when we inhibit adenylate kinase. Because of this we assume that the model is correct. We have shown that experimentally and through model simulations that adenylate kinase is essential for glycolytic oscillations. We calculate the control of AK on the period time of the oscillations to be $C_{AK}^{period\ time} = -0.027$. When adenylate kinase is sufficiently inhibited, glycolytic oscillations cease. Subsequently, with a decrease in adenylate kinase activity there is a decrease in frequency of the oscillations and this is shown both experimentally and in the models, *dupreez6* and *vanwyk1*. How a decrease adenylate kinase causes this decrease in oscillation amplitude and frequency is explored in the *vanwyk1* model.

With the assumption that the model is correct, we subsequently analysed the model, and a decrease in adenylate kinase activity results in a decrease in the oscillation frequency and amplitude of ATP and AMP, as well as decreasing the phase difference between the two metabolites. The decrease in amplitude of ATP and AMP has a larger effect on the state of PFK than the change in phase difference. The T and R state switching seems to follow the shape of the ATP oscillations with the peaks and troughs of ATP and the R/(T+R) ratio coinciding for both the WT and inhibited simulations. But the extent to which PFK switches between the T and R states seems to be dependant on the amplitude of the AMP oscillations. With a large AMP amplitude, the R/(T+R) ratio amplitude is large and when the AMP amplitude is small, the R/(T+R) ratio amplitude is small (Figure 5.3 and 5.4). Lastly, the change in T and R state switching causes the glycolytic oscillation frequency to change. When the T and R state switching of PFK is changed in the model, leaving all other parameters and enzyme activities as in the WT simulation, the oscillation frequency decreases.

5.3.1 Epilogue

For this thesis we set out to determine not only the effect of adenylate kinase on glycolytic oscillations as a whole, but to piece apart the individual contribution of ATP and AMP toward these glycolytic oscillations. The decrease

in adenylate kinase activity causes a decrease in oscillation frequency. This is because a decrease in AK causes a decreased amplitude in the ATP and AMP oscillations as well as a decrease in phase difference between the two metabolites. There also seems to be more of a dependence on the oscillation amplitude of the metabolites than on the phase shift. This change in ATP and AMP oscillations causes an alteration in the function of PFK with reduced T and R state switching. A reduction in T and R state switching causes the decrease in glycolytic oscillations frequency. In terms of separating AMP from ATP in these oscillations, the $R/(T+R)$ ratio follows the same shape of as the ATP oscillations irrespective of the phase difference between ATP and AMP. It is still unclear whether ATP inhibition or AMP activation is dominant, however, when both ATP and AMP amplitudes were reduced to 50% AMP activation seems to dominate. Future work could entail analysing the oscillations of ATP and AMP experimentally by use of HPLC in cell extracts both in the presence of the AK inhibitor and without.

Appendices

Appendix A

A.1 Adenylate kinase rate equation derivations

The following sections show the derivation of the adenylate kinase mechanisms not shown in the main body of the thesis, namely the iso random bi-bi mechanisms, spatio-temporal mechanism and the combination mechanism.

A.1.1 Iso random bi-bi mechanism

We write the mass conservation equation. We can assume the two binding sites have equal affinity for the substrates so ${}^1E_{D-} = {}^1E_{-D} = {}^1E_D$. Similarly, $E_{TM} = E_{MT}$. The iso-random bi-bi binding schema, Figure 4.5, leads to the following mass conservation equation:

$$E_{Tot} = {}^1E + {}^2E + 2{}^1E_D + {}^1E_{DD} + {}^2E_{MT} + {}^2E_T + 2{}^2E_M + {}^2E_{MM} + {}^2E_i \quad (\text{A.1})$$

The next step is to list the various dissociation constants of the substrates in terms of all the enzyme-substrate species (eqs. A.2-A.11).

$${}^1E = K_E {}^2E \quad (\text{A.2})$$

$${}^2E = \frac{{}^1E}{K_E} \quad (\text{A.3})$$

$${}^1E_D = \frac{{}^1E \text{ adp}}{K_D} \quad (\text{A.4})$$

$${}^1E_{DD} = \frac{{}^1E \text{ adp}^2}{K_D^2} \quad (\text{A.5})$$

$${}^2E_{MT} = \frac{{}^2E \text{ amp atp}}{K_M K_T} = \frac{{}^1E \text{ amp atp}}{K_E K_M K_T} \quad (\text{A.6})$$

$${}^2E_T = \frac{{}^1E \text{ atp}}{K_E K_T} \quad (\text{A.7})$$

$${}^2E_M = \frac{{}^1E \text{ amp}}{K_E K_M} \quad (\text{A.8})$$

$${}^2E_{MM} = \frac{{}^1E \text{ amp}^2}{K_E K_M^2} \quad (\text{A.9})$$

$${}^2E_i = \frac{{}^1E i}{K_E K_i} \quad (\text{A.10})$$

$$(\text{A.11})$$

The rate of the reaction can be written as the following:

$$vAK_{iso} = v_f [{}^1E_{DD}] - v_r [{}^2E_{MT}] \quad (\text{A.12})$$

By converting the enzyme-substrate complexes ${}^1E_{DD}$ and ${}^2E_{MT}$ to their respective fractional saturation ratios we get:

$$Y_{DD} = \frac{[{}^1E_{DD}]}{[E_{Tot}]} \quad Y_{MT} = \frac{[{}^2E_{MT}]}{[E_{Tot}]} \quad (\text{A.13})$$

By including eq. 4.12 in A.12 :

$$vAK_{iso} = v_f [E_{Tot}] Y_{DD} - v_r [E_{Tot}] Y_{MT} \quad (\text{A.14})$$

If $E_{DD} \rightarrow E_{Tot}$, $v_f \rightarrow V_f$. The same is true for the reverse reaction, therefore:

$$v_f [E_{Tot}] = V_f \quad v_r [E_{Tot}] = V_r \quad (\text{A.15})$$

Substituting eq. A.15 in A.14, we get:

$$vAK_{iso} = V_f Y_{DD} - V_r Y_{MT} \quad (\text{A.16})$$

With the use of the fractional saturations (eq. A.13) we get a denominator term E_{Tot} :

$$vAK_{iso} = \frac{V_f {}^1E_{DD} - V_r {}^2E_{MT}}{E_{Tot}} \quad (A.17)$$

By using the conservation of mass eq.A.1 and the dissociation constant eqs. A.2-A.11 we get:

$$vAK_{iso} = \frac{V_f \frac{{}^1E \text{ adp}^2}{K_D^2} - V_r \frac{{}^1E \text{ amp atp}}{K_E K_M K_T}}{{}^1E + \frac{{}^1E}{K_E} + \frac{{}^1E \text{ adp}}{K_D} + \frac{{}^1E \text{ amp atp}}{K_E K_M K_T} + \frac{{}^1E \text{ atp}}{K_E K_T} + \frac{{}^1E \text{ amp}}{K_E K_M} + \frac{{}^1E \text{ amp}^2}{K_E K_M^2} + \frac{{}^1E i}{K_E K_i}} \quad (A.18)$$

Simplifying equation A.18 give us the final rate equation for the iso random bi-bi binding schema in Figure 4.5:

$$vAK_{iso} = \frac{V_f \frac{\text{adp}^2}{K_D^2} - V_r \frac{\text{amp atp}}{K_E K_M K_T}}{1 + \frac{1}{K_E} + \frac{\text{adp}}{K_D} + \frac{\text{amp atp}}{K_E K_M K_T} + \frac{\text{atp}}{K_E K_T} + \frac{\text{amp}}{K_E K_M} + \frac{\text{amp}^2}{K_M^2} + \frac{i}{K_E K_i}} \quad (A.19)$$

A.1.2 Spatio-temporal mechanism

The conservation of mass equation for the spatio-temporal mechanism is as follows:

$$E_{Tot} = E + 2E_D + 2E_{DM} + E_{DD} + E_{TM} + E_T + 2E_M + E_{MM} + E_i \quad (A.20)$$

The next step is to list the various dissociation constants of the substrates in terms of all the enzyme-substrate species (eqs. A.21-A.29).

$$E_D = \frac{E \text{ adp}}{K_D} \quad (\text{A.21})$$

$$E_{DD} = \frac{E \text{ adp}^2}{K_D^2} \quad (\text{A.22})$$

$$E_{DM} = \frac{E \text{ adp amp}}{K_D K_M} \quad (\text{A.23})$$

$$E_{TM} = \frac{E \text{ amp atp}}{K_M K_T} \quad (\text{A.24})$$

$$E_T = \frac{E \text{ atp}}{K_T} \quad (\text{A.25})$$

$$E_M = \frac{E \text{ amp}}{K_M} \quad (\text{A.26})$$

$$E_{MM} = \frac{E \text{ amp}^2}{K_M^2} \quad (\text{A.27})$$

$$E_i = \frac{E i}{K_i} \quad (\text{A.28})$$

$$(\text{A.29})$$

The rate of the reaction can be written as the following:

$$vAK_{spatio} = v_f [E_{DD}] - v_r [E_{TM}] \quad (\text{A.30})$$

By converting the enzyme-substrate complexes E_{DD} and E_{TM} to their respective fractional saturation ratios we get:

$$Y_{DD} = \frac{[E_{DD}]}{[E_{Tot}]} \quad Y_{TM} = \frac{[E_{TM}]}{[E_{Tot}]} \quad (\text{A.31})$$

By including eq. A.31 in A.30 :

$$vAK_{spatio} = v_f [E_{Tot}] Y_{DD} - v_r [E_{Tot}] Y_{TM} \quad (\text{A.32})$$

If $E_{DD} \rightarrow E_{Tot}$, $v_f \rightarrow V_f$. The same is true for the reverse reaction, therefore:

$$v_f [E_{Tot}] = V_f \quad v_r [E_{Tot}] = V_r \quad (\text{A.33})$$

Substituting eq. A.33 in A.32, we get:

$$vAK_{spatio} = V_f Y_{DD} - V_r Y_{TM} \quad (\text{A.34})$$

With the use of the fractional saturations (eq. A.31) we get a denominator term E_{Tot} :

$$vAK_{spatio} = \frac{V_f E_{DD} - V_r E_{TM}}{E_{Tot}} \quad (A.35)$$

By using the conservation of mass eq.A.20 and the dissociation constant eqs. A.21-A.29 we get:

$$vAK_{spatio} = \frac{V_f \frac{E adp^2}{K_D^2} - V_r \frac{E amp atp}{K_M K_T}}{E + \frac{E adp}{K_D} + \frac{E adp^2}{K_D^2} + \frac{E adp amp}{K_D K_M} + \frac{E amp atp}{K_M K_T} + \frac{E atp}{K_T} + \frac{E amp}{K_M} + \frac{E amp^2}{K_M^2} + \frac{E i}{K_i}} \quad (A.36)$$

Simplifying equation A.36 gives us the final rate equation for the iso random bi-bi binding schema in Figure 4.7:

$$vAK_{spatio} = \frac{V_f \frac{adp^2}{K_D^2} - V_r \frac{amp atp}{K_M K_T}}{1 + \frac{adp}{K_D} + \frac{adp^2}{K_D^2} + \frac{adp amp}{K_D K_M} + \frac{amp atp}{K_M K_T} + \frac{atp}{K_T} + \frac{amp}{K_M} + \frac{amp^2}{K_M^2} + \frac{i}{K_i}} \quad (A.37)$$

A.1.3 Iso-random spatio-temporal combination mechanism

The conservation of mass equation for the combination of the iso random and spatio-temporal mechanism is as follows:

$$E_{Tot} = {}^1 E + {}^2 E + {}^1 E_D + {}^1 E_{DM} + {}^1 E_M + {}^1 E_{MM} + {}^1 E_{DD} + {}^2 E_{MT} + {}^2 E_T + {}^2 E_M + {}^2 E_{MM} + {}^2 E_i \quad (A.38)$$

The next step is to list the various dissociation constants of the substrates in terms of all the enzyme-substrate species (eqs. A.39-A.51).

$${}^1E = K_E {}^2E \quad (\text{A.39})$$

$${}^2E = \frac{{}^1E}{K_E} \quad (\text{A.40})$$

$${}^1E_D = \frac{{}^1E \text{ adp}}{K_D} \quad (\text{A.41})$$

$${}^1E_M = \frac{{}^1E \text{ amp}}{K_M} \quad (\text{A.42})$$

$${}^1E_{MD} = \frac{{}^1E \text{ amp adp}}{K_M K_D} \quad (\text{A.43})$$

$${}^1E_{MM} = \frac{{}^1E \text{ amp}^2}{K_M^2} \quad (\text{A.44})$$

$${}^1E_{DD} = \frac{{}^1E \text{ adp}^2}{K_D^2} \quad (\text{A.45})$$

$${}^2E_{MT} = \frac{{}^2E \text{ amp atp}}{K_M K_T} = \frac{{}^1E \text{ amp atp}}{K_E K_M K_T} \quad (\text{A.46})$$

$${}^2E_T = \frac{{}^1E \text{ atp}}{K_E K_T} \quad (\text{A.47})$$

$${}^2E_M = \frac{{}^1E \text{ amp}}{K_E K_M} \quad (\text{A.48})$$

$${}^2E_{MM} = \frac{{}^1E \text{ amp}^2}{K_E K_M^2} \quad (\text{A.49})$$

$${}^2E_i = \frac{{}^1E i}{K_E K_i} \quad (\text{A.50})$$

$$(\text{A.51})$$

The rate of the reaction can be written as the following:

$$vAK_{\text{combo}} = v_f [{}^1E_{DD}] - v_r [{}^2E_{MT}] \quad (\text{A.52})$$

By converting the enzyme-substrate complexes ${}^1E_{DD}$ and ${}^2E_{MT}$ to their respective fractional saturation ratios we get:

$$Y_{DD} = \frac{[{}^1E_{DD}]}{[E_{\text{Tot}}]} \quad Y_{MT} = \frac{[{}^2E_{TM}]}{[E_{\text{Tot}}]} \quad (\text{A.53})$$

By including eq. A.53 in A.52 :

$$vAK_{\text{combo}} = v_f [E_{\text{Tot}}] Y_{DD} - v_r [E_{\text{Tot}}] Y_{TM} \quad (\text{A.54})$$

If ${}^1E_{DD} \rightarrow E_{\text{Tot}}$, $v_f \rightarrow V_f$. The same is true for the reverse reaction, therefore:

$$v_f [E_{Tot}] = V_f \quad v_r [E_{Tot}] = V_r \quad (\text{A.55})$$

Substituting eq. A.55 in A.54, we get:

$$vAK_{combo} = V_f Y_{DD} - V_r Y_{TM} \quad (\text{A.56})$$

With the use of the fractional saturations (eq. A.53) we get a denominator term E_{Tot} :

$$vAK_{combo} = \frac{V_f {}^1E_{DD} - V_r {}^2E_{TM}}{E_{Tot}} \quad (\text{A.57})$$

By using the conservation of mass eq.A.38 and the dissociation constant eqs. A.39-A.51 we get:

$$vAK_{combo} = \frac{V_f \frac{{}^1E \text{ adp}^2}{K_D^2} - V_r \frac{{}^1E \text{ amp atp}}{K_E K_M K_T}}{{}^1E + \frac{{}^1E}{K_E} + \frac{{}^1E \text{ adp}}{K_D} + \frac{{}^1E \text{ amp}}{K_M} + \frac{{}^1E \text{ amp adp}}{K_M K_D} + \frac{{}^1E \text{ amp}^2}{K_M^2} + \frac{{}^1E \text{ adp}^2}{K_D^2} + \frac{{}^1E \text{ amp atp}}{K_E K_M K_T} + \frac{{}^1E \text{ atp}}{K_E K_T} + \frac{{}^1E \text{ amp}}{K_E K_M} + \frac{{}^1E \text{ amp}^2}{K_E K_M^2} + \frac{{}^1E i}{K_E K_i}} \quad (\text{A.58})$$

Simplifying equation A.58 gives us the final rate equation for the iso random bi-bi binding schema in Figure 4.9:

$$vAK_{combo} = \frac{V_f \frac{\text{adp}^2}{K_D^2} - V_r \frac{\text{amp atp}}{K_E K_M K_T}}{1 + \frac{1}{K_E} + \frac{\text{adp}}{K_D} + \frac{\text{amp}}{K_M} + \frac{\text{amp adp}}{K_M K_D} + \frac{\text{amp}^2}{K_M^2} + \frac{\text{adp}^2}{K_D^2} + \frac{\text{amp atp}}{K_E K_M K_T} + \frac{\text{atp}}{K_E K_T} + \frac{\text{amp}}{K_E K_M} + \frac{\text{amp}^2}{K_E K_M^2} + \frac{i}{K_E K_i}} \quad (\text{A.59})$$

List of References

- [1] Hess, B. and Boiteux, A.: Oscillatory phenomena in biochemistry. *Annual review of biochemistry*, vol. 40, no. 1, pp. 237–258, 1971.
- [2] Goldbeter, A. *et al.*: Biochemical oscillations and cellular rhythms. *Biochemical Oscillations and Cellular Rhythms*, by Albert Goldbeter, Foreword by MJ Berridge, Cambridge, UK: Cambridge University Press, 1997, 1997.
- [3] Prigogine, I.I.: *Introduction to thermodynamics of irreversible processes*. 3rd edn. Wiley-Interscience, New York, N.Y., 1967. ISBN 0470699280.
- [4] Nicolis, G. and Prigogine, I.: *Self-organization in nonequilibrium systems : from dissipative structures to order through fluctuations*. Wiley, New York, N.Y., 1977. ISBN 0471024015.
- [5] Rastogi, R.P.: *Introduction to non-equilibrium physical chemistry towards complexity and non-linear science*. Elsevier, Amsterdam ; London, 2007. ISBN 0080551807.
- [6] Rapp, P.: An atlas of cellular oscillators. *Journal of Experimental Biology*, vol. 81, no. 1, pp. 281–306, 1979.
- [7] O’rourke, B., Ramza, B.M. and Marban, E.: Oscillations of membrane current and excitability driven by metabolic oscillations in heart cells. *Science*, vol. 265, no. 5174, pp. 962–966, 1994.
- [8] Halloy, J., Lauzeral, J. and Goldbeter, A.: Modeling oscillations and waves of camp in dictyostelium discoideum cells. *Biophysical chemistry*, vol. 72, no. 1-2, pp. 9–19, 1998.
- [9] Chou, H., Berman, N. and Ipp, E.: Oscillations of lactate released from islets of langerhans: evidence for oscillatory glycolysis in beta-cells. *American Journal of Physiology-Endocrinology And Metabolism*, vol. 262, no. 6, pp. E800–E805, 1992.
- [10] Reijenga, K.A., Snoep, J.L., Diderich, J.A., van Verseveld, H.W., Westerhoff, H.V. and Teusink, B.: Control of glycolytic dynamics by hexose transport in *saccharomyces cerevisiae*. *Biophysical Journal*, vol. 80, no. 2, pp. 626–634, 2001.
- [11] Reijenga, K.A., van Megen, Y.M., Kooi, B.W., Bakker, B.M., Snoep, J.L., van Verseveld, H.W. and Westerhoff, H.V.: Yeast glycolytic oscillations that are not

- controlled by a single oscillator: a new definition of oscillator strength. *Journal of Theoretical Biology*, vol. 232, no. 3, pp. 385–398, 2005.
- [12] du Preez, F.B., van Niekerk, D.D., Kooi, B., Rohwer, J.M. and Snoep, J.L.: From steady-state to synchronized yeast glycolytic oscillations i: model construction. *The FEBS journal*, vol. 279, no. 16, pp. 2810–2822, 2012.
- [13] Richard, P.: The rhythm of yeast. *FEMS microbiology reviews*, vol. 27, no. 4, pp. 547–557, 2003.
- [14] Richard, P., Bakker, B.M., Teusink, B., Van Dam, K. and Westerhoff, H.V.: Acetaldehyde mediates the synchronization of sustained glycolytic oscillations in populations of yeast cells. *European journal of biochemistry*, vol. 235, no. 1-2, pp. 238–241, 1996.
- [15] Ghosh, A., Chance, B. and Pye, E.: Metabolic coupling and synchronization of nadh oscillations in yeast cell populations. *Archives of biochemistry and biophysics*, vol. 145, no. 1, pp. 319–331, 1971.
- [16] Danø, S., Sørensen, P.G. and Hynne, F.: Sustained oscillations in living cells. *Nature*, vol. 402, no. 6759, p. 320, 1999.
- [17] Ashcroft, F.M. and Rorsman, P.: Electrophysiology of the pancreatic β -cell. *Progress in biophysics and molecular biology*, vol. 54, no. 2, pp. 87–143, 1989.
- [18] Kar, S. and Ray, D.S.: Sustained simultaneous glycolytic and insulin oscillations in β -cells. *Journal of theoretical biology*, vol. 237, no. 1, pp. 58–66, 2005.
- [19] Wierschem, K. and Bertram, R.: Complex bursting in pancreatic islets: a potential glycolytic mechanism. *Journal of theoretical biology*, vol. 228, no. 4, pp. 513–521, 2004.
- [20] Chance, B., Schoener, B. and Elsaesser, S.: Control of the waveform of oscillations of the reduced pyridine nucleotide level in a cell-free extract. *Proceedings of the National Academy of Sciences*, vol. 52, no. 2, pp. 337–341, 1964.
- [21] Madsen, M.F., Danø, S. and Sørensen, P.G.: On the mechanisms of glycolytic oscillations in yeast. *The FEBS journal*, vol. 272, no. 11, pp. 2648–2660, 2005.
- [22] Arcus, V.L., Prentice, E.J., Hobbs, J.K., Mulholland, A.J., Van der Kamp, M.W., Pudney, C.R., Parker, E.J. and Schipper, L.A.: On the temperature dependence of enzyme-catalyzed rates. *Biochemistry*, vol. 55, no. 12, pp. 1681–1688, 2016.
- [23] Richard, P., Teusink, B., Westerhoff, H.V. and van Dam, K.: Around the growth phase transition *s. cerevisiae*'s make-up favours sustained oscillations of intracellular metabolites. *FEBS letters*, vol. 318, no. 1, pp. 80–82, 1993.
- [24] Sel'Kov, E.: Self-oscillations in glycolysis. *European Journal of Biochemistry*, vol. 4, no. 1, pp. 79–86, 1968.

- [25] Garrett, H.R. and Grisham, M.C.: *Biochemistry*. 5th edn. Cengage Learning, 2012. ISBN 9781133108795.
- [26] Meyerhof, O.: The origin of the reaction of harden and young in cell-free alcoholic fermentation. *Journal of Biological Chemistry*, vol. 157, no. 1, pp. 105–120, 1945.
- [27] Walther, T., Mtimet, N., Alkim, C., Vax, A., Loret, M.-O., Ullah, A., Gancedo, C., Smits, G.J. and François, J.M.: Metabolic phenotypes of *saccharomyces cerevisiae* mutants with altered trehalose 6-phosphate dynamics. *Biochemical Journal*, vol. 454, no. 2, pp. 227–237, 2013.
- [28] Jonnalagadda, S.B., Becker, J.-U., Sel'kov, E. and Betz, A.: Flux regulation in glycogen-induced oscillatory glycolysis in cell-free extracts of *saccharomyces carlsbergensis*. *Biosystems*, vol. 15, no. 1, pp. 49–58, 1982.
- [29] Nakayama, A., Yamamoto, K. and Tabata, S.: Identification of the catalytic residues of bifunctional glycogen debranching enzyme. *Journal of Biological Chemistry*, vol. 276, no. 31, pp. 28824–28828, 2001.
- [30] Gustavsson, A.-K., Niekerk, D.D., Adiels, C.B., Kooi, B., Goksör, M. and Snoep, J.L.: Allosteric regulation of phosphofructokinase controls the emergence of glycolytic oscillations in isolated yeast cells. *The FEBS journal*, vol. 281, no. 12, pp. 2784–2793, 2014.
- [31] Su, S. and Russell, P.J.: Adenylate kinase from baker's yeast. ii. substrate specificity. *Biochimica et Biophysica Acta (BBA)-Enzymology*, vol. 132, no. 2, pp. 370–378, 1967.
- [32] Kuby, S.A., Hamada, M., Gerber, D., Tsai, W.-C., Jacobs, H.K., Cress, M.C., Chua, G.K., Fleming, G., Wu, L.H., Fischer, A.H. *et al.*: Studies on adenosine triphosphate transphosphorylases: Isolation and several properties of the crystalline calf atm-amp transphosphorylases (adenylate kinases) from muscle and liver and some observations on the rabbit muscle adenylate kinase. *Archives of biochemistry and biophysics*, vol. 187, no. 1, pp. 34–52, 1978.
- [33] King, E.L. and Altman, C.: A schematic method of deriving the rate laws for enzyme-catalyzed reactions. *The Journal of physical chemistry*, vol. 60, no. 10, pp. 1375–1378, 1956.
- [34] du Preez, F.B., van Niekerk, D.D. and Snoep, J.L.: From steady-state to synchronized yeast glycolytic oscillations ii: model validation. *The FEBS journal*, vol. 279, no. 16, pp. 2823–2836, 2012.
- [35] Olivier, B.G. and Snoep, J.L.: Web-based kinetic modelling using jws online. *Bioinformatics*, vol. 20, no. 13, pp. 2143–2144, 2004.
- [36] Teusink, B., Passarge, J., Reijenga, C.A., Esgalhado, E., Van der Weijden, C.C., Schepper, M., Walsh, M.C., Bakker, B.M., Van Dam, K., Westerhoff, H.V. *et al.*: Can yeast glycolysis be understood in terms of in vitro kinetics of the

- constituent enzymes? testing biochemistry. *European Journal of Biochemistry*, vol. 267, no. 17, pp. 5313–5329, 2000.
- [37] Ernst, O. and Zor, T.: Linearization of the bradford protein assay. *Journal of visualized experiments: JoVE*, , no. 38, 2010.
- [38] Bozdogan, H.: Model selection and akaike's information criterion (aic): The general theory and its analytical extensions. *Psychometrika*, vol. 52, no. 3, pp. 345–370, 1987.
- [39] Sheng, X.R., Li, X. and Pan, X.M.: An iso-random bi bi mechanism for adenylate kinase. *Journal of Biological Chemistry*, vol. 274, no. 32, pp. 22238–22242, 1999.
- [40] Abele, U. and Schulz, G.: High-resolution structures of adenylate kinase from yeast ligated with inhibitor ap5a, showing the pathway of phosphoryl transfer. *Protein Science*, vol. 4, no. 7, pp. 1262–1271, 1995.
- [41] Chiu, C.-S., Su, S. and Russell, P.J.: Adenylate kinase from baker's yeast. i. purification and intracellular location. *Biochimica et Biophysica Acta (BBA)-Enzymology*, vol. 132, no. 2, pp. 361–369, 1967.
- [42] Rao, B.N. and Cohn, M.: Asymmetric binding of the inhibitor di (adenosine-5') pentaphosphate (ap5a) to adenylate kinase. *Proceedings of the National Academy of Sciences*, vol. 74, no. 12, pp. 5355–5357, 1977.